



Technische Universität München

Institute for Diabetes and Obesity (IDO)

Helmholtz Zentrum München

Global gene regulation during T cell activation

Johannes Friedrich Lichti

Vollständiger Abdruck der von der Fakultät für Medizin der Technischen Universität München zur Erlangung des akademischen Grades eines

Doktors der Naturwissenschaften (Dr. rer. nat.)

genehmigten Dissertation.

Vorsitzender: Prof. Dr. Percy A. Knolle

Prüfer der Dissertation: 1. Prof. Dr. Matthias Tschöp

2. TUM Junior Fellow Dr. Matthias Heinig

Die Dissertation wurde am 23.10.2017 bei der Technischen Universität München eingereicht und durch die Fakultät für Medizin am 02.05.2018 angenommen.

Kurzfassung

T Zellen wachsen und reifen im Thymus, bilden ihren Antigenrezeptor und wandern in die Peripherie, um ihrer immunologischen Funktion nachzukommen. Dabei behalten Lymphozyten ihre RNA- und Proteinlevel auf basalem Niveau bis der Kontakt mit einem Antigen zu einer starken Immunantwort, einschließlich erhöhter mRNA und Proteinproduktion, sowie letztendlich einer Differenzierung in langlebige Gedächtniszellen führt. Die genauen molekularen Mechanismen, die hinter einer erfolgreichen Immunantwort stehen, sind jedoch noch immer unklar. Um globale Veränderungen der RNA Polymerase II (RNAPII)-Bindung, Transkription, Spleißen und Translation zu erforschen, wurde eine umfassende Kinetik, bestehend aus ChIP-seq, RNA-seq, 4sU-seq und ribosome profiling, während der Aktivierung von *in vitro* generierten Th1 Zellen durchgeführt. Diese erfasste die zeitliche Expression von 9420 Genen und identifizierte differentiell regulierte Gencluster, einschließlich schnell induzierter, sowie posttranskriptionell regulierter Gene. Dabei sind globale Veränderungen in Transkription und Translation stark gekoppelt und gehen mit konstanten Translationsraten einher. Obwohl eine pausierte RNAPII als möglicher Mechanismus vorgeschlagen wurde, um Gene schnell exprimieren zu können, vermittelt vor allem eine RNAPII Neurekrutierung transkriptionelle Veränderungen in aktivierten Th1 Zellen. Erstaunlicherweise zeigen kotranskriptionelle Spleißingraten genomweit eine vorübergehende Verlangsamung, welche auch auf polyadenylierte mRNAs am Chromatin zutrifft. Anschließend erfolgt eine Verbesserung, welche die Level unaktivierter Zellen übertrifft und mit einer zunehmenden Ser2 Phosphorylierung der carboxyterminalen Domäne (CTD) der RNAPII und Aktivierung des positiven Transkriptionselongationsfaktors b (pTEFb) korreliert. Zusammengefasst konnten wir zeigen, dass eine schnelle Neurekrutierung der RNAPII die Prozesse während der T Zell Aktivierung, insbesondere die Transkription, das Spleißen und letztendlich die Translation bestimmt. Am Ende der Arbeit wird unsere und andere genomweite Studien über Immunzellen in den Kontext gesetzt, um ein allgemeines Modell einer Immunantwort vorzuschlagen.

Abstract

Upon active proliferation and maturation in the thymus, T cells rearrange their antigen receptors, migrate to the periphery and wait to fulfill their immunological demands. Lymphocytes at this state maintain their RNA and protein levels at basal states until activation by contact with antigens leads to a drastic response including excessive mRNA and protein production, cell division and finally differentiation into long-lived memory cells. The exact molecular mechanisms that enable this shift to ensure a successful adaptive immune response however remain elusive. To visualize global changes in RNA polymerase II (RNAPII) binding, transcription, splicing and translation, a comprehensive kinetic study combining ChIP-seq, RNA-seq, 4sU-seq and ribosome profiling was performed during activation of *in vitro* generated Th1 cells. This illustrated temporal dynamics for 9,420 genes and identified differently regulated gene clusters, including rapidly induced genes and posttranscriptionally regulated genes. Global changes in transcription and translation were, however, highly coupled, consistent with constant translation rates over time. Although pausing of RNAPII was suggested as a key mechanism to keep genes highly responsive, recruitment of RNAPII primarily mediates transcriptional changes in activated Th1 cells. Surprisingly, cotranscriptional splicing rates show a genome-wide temporary slowdown, even for polyadenylated mRNAs at the chromatin. This is subsequently optimized, even beyond levels of unactivated cells and correlates with increasing Ser2 phosphorylation of the RNAPII CTD and activation of the positive transcription elongation factor b (pTEFb). We demonstrated that rapid *de novo* recruitment of RNAPII dictates the course of events during T cell activation, particularly transcription, splicing and consequently translation. Finally, our study and other genome-wide analyses of immune cells were set into context, to propose a general model of the immune response.

Table of contents

Kurzfassung	I
Abstract	II
1 Introduction.....	6
1.1 The role of T cells in adaptive immunity.....	7
1.2 T cell effector function	8
1.3 The central dogma of molecular biology: DNA → RNA → Protein	9
1.3.1 Transcriptional gene regulation.....	10
1.3.2 Cotranscriptional splicing.....	11
1.3.3 Posttranscriptional gene regulation	12
1.4 Methods to monitor changes in gene expression: Next generation sequencing	13
1.4.1 RNA sequencing to monitor transcriptional regulation.....	13
1.4.2 4sU sequencing to monitor <i>de novo</i> transcription.....	13
1.4.3 Ribosome Profiling to monitor translational regulation.....	15
1.4.4 ChIP sequencing to monitor DNA-protein interaction	17
1.5 Aim of the study	18
2 Materials	20
2.1 Antibodies and cytokines	20
2.2 Primers	21
2.3 Cell lines.....	22
2.4 Mouse strains.....	22
2.5 Chemicals and reaction kits	23
2.6 Buffers, solutions, media.....	25
2.7 Devices	27
2.8 Software	27
3 Methods	28
3.1 Cell Culture	28
3.1.1 Preparation and differentiation of primary Th1 cells.....	28
3.1.2 Activation of primary Th0/Th1 cells.....	28
3.1.3 Intracellular cytokine staining and flow cytometry	28
3.1.4 GFP spike-in assay.....	29
3.2 Handling of nucleic acids	29

3.2.1	RNA extraction.....	29
3.2.2	Subcellular fractionation	29
3.3	cDNA synthesis and qRT-PCR	30
3.4	Western Blot.....	30
3.5	4sU-labeling	31
3.5.1	Toxicity test of 4sU-labeling	33
3.5.2	Nuclear and cytoplasmic stress test for 4sU-labeling.....	33
3.6	Ribosome Profiling	33
3.7	Chromatin immunoprecipitation (ChIP)	37
3.8	Next generation sequencing.....	40
3.8.1	Library preparation for RNA-seq and 4sU-seq	40
3.8.2	Ribosome Profiling.....	40
3.8.3	Library preparation for ChIP-seq.....	40
3.8.4	Sequencing	41
3.9	Bioinformatics and statistical analysis	41
3.9.1	Adapter trimming and mapping	41
3.9.2	Gene expression and normalization	42
3.9.3	Turnover and translation rates	42
3.9.4	R.....	42
3.9.5	EnrichR	42
3.9.6	DAVID.....	42
4	Results	43
4.1	Establishment of methods	43
4.1.1	4sU-labeling – verify optimal conditions without perturbing cell physiology....	43
4.1.2	4sU-labeling – capture of newly transcribed RNA.....	45
4.1.3	4sU-seq – library preparation and verification of the results.....	47
4.1.4	Ribosome Profiling.....	48
4.1.5	Preliminary test for simultaneous analysis of transcriptional and translation control in activated Th1 cells	50
4.2	Simultaneous analysis of transcriptional and translational control in activated Th1 cells	51
4.2.1	Regulation of <i>Ifng</i>	52
4.2.2	Most upregulated genes.....	53
4.2.3	Transcriptional and translational gene response differ in time and magnitude.	54
4.2.4	Verification of downregulation.....	55
4.2.5	Hierarchical clustering of upregulated genes	56
4.2.6	Hierarchical clustering of downregulated genes	57
4.2.7	Global coupling of transcriptional and translational regulation.....	58
4.2.8	Transcriptional regulation dictates gene response.....	59
4.2.9	Turnover rates.....	60
4.2.10	Translation rates	62

4.2.11	Increased expression of transcriptional but not translational machinery	63
4.2.12	Enrichment analysis for transcription factor targets	64
4.2.13	Reduction of cotranscriptional splicing rates early after activation	66
4.3	RNA polymerase II ChIP-seq	68
4.3.1	Rapid recruitment of RNAPII mediates transcriptional upregulation.....	68
4.3.2	Paused RNAPII is not the main mechanism to allow rapid transcriptional upregulation.....	69
4.4	Further analysis of cotranscriptional splicing and rapid recruitment of RNAPII	71
4.4.1	Shift in exon/intron ratio for polyadenylated nuclear RNA and polyadenylated chromatin RNA	71
4.4.2	Phosphorylation states of the CTD of RNAPII correlate with fluctuations in splicing rates.....	73
4.4.3	Changes in splicing rate reflect distance to TSS.....	74
4.4.4	Interaction of splicing factors with phosphorylated CTD and activation of pTEFb 75	
4.5	H3K36me ChIP-seq.....	76
5	Discussion	78
5.1	Transcriptional regulation	78
5.2	Coupled changes in transcription and translation	79
5.3	Cotranscriptional splicing	81
5.4	Global pausing of RNAPII is not the main mechanism to keep genes responsive	83
5.5	Rapid recruitment of RNAPII dictates transcriptional changes	85
5.6	The emerging picture of a global immune response	86
6	Conclusion	90
7	Contributions and Acknowledgments	91
8	Literature	93
9	Supplements	101
9.1	List of tables	101
9.2	List of figures.....	102
9.3	List of abbreviations	104
10	Publications	106
11	Erklärung	107
12	Lebenslauf.....	108

1 Introduction

Mammals are under constant exposure to viruses, bacteria or other microbes. They have to tolerate those that are beneficial (probiotics) but face and fight the pathogenic ones. As extensively described by Janeway *et al.*, protection against harmful pathogens is ensured through the interplay between the innate and the adaptive immune system with both depending upon the activities of leukocytes (Figure 1) (Janeway *et al.*, 2005). The innate immune system, especially macrophages and neutrophils, provide a first line of defense against many common microorganisms. But they only recognize pathogens comprising of certain molecular patterns (PAMPs, i.e. pathogen associated molecular patterns) or those, which induce interferons. The recognition of PAMPs through pattern recognition receptors (PRRs) and subsequent innate immune response activates the complement system and leads to phagocytosis of the pathogen, as well as activation of the adaptive immune system. The latter confers lifelong protection and prevents from reinfection with the same pathogen.(Janeway *et al.*, 2005)

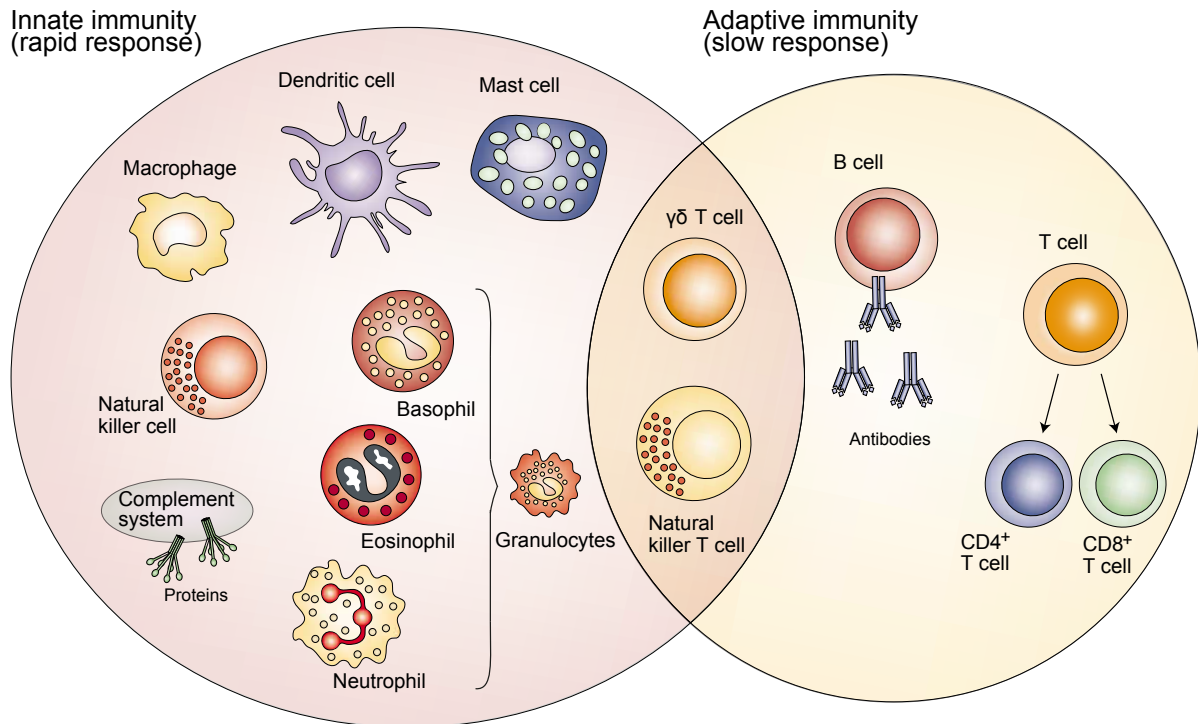


Figure 1: The innate and adaptive immune response (modified from Dranoff, 2004)

The innate immune system (left) serves as the first line of defense against infection. It consists of soluble factors (complement proteins) and many cellular components (mast cells, dendritic cells, macrophages, natural killer cells and granulocytes (basophils, eosinophils, neutrophils)). The adaptive immune system (right) responds slower, but provides protection against subsequent reinfection. It consists of B cells and CD4⁺ and CD8⁺ T cells. Natural killer T cells and γδ T cells are cytotoxic lymphocytes, which exert biological function of both innate and adaptive immunity.

1.1 The role of T cells in adaptive immunity

While the evolutionary highly conserved innate immune system is an ancient but still the dominant defense strategy for plants, fungi, insects and primitive organisms, the highly specific adaptive immune system arose later – also not fully enlightened yet - by the event of somatic gene rearrangement in ‘higher vertebrates’ (and jawed fish) as summarized by Janeway *et al.* (Janeway *et al.*, 2005). Lymphocytes of the adaptive immune system are able to recognize a great variety of different antigens from viruses, bacteria and other microbes. B cells and T cells are the main types of lymphocytes and derive from hematopoietic stem cells. Whereas B cells mature in the bone marrow and produce antibodies, T cells mature in the thymus. Although there are several subsets of T cells and each has a distinct function they share a common feature, the T-cell receptor (TCR) a complex of membrane proteins that express a large repertoire of antigen receptors by site-specific somatic recombination. T

cells can be classified into T helper cells (Th cells), also termed CD4⁺ (cluster of differentiation) T cells because they express the CD4 glycoprotein on their surface and cytotoxic (CD8⁺) T cells. Naïve CD4⁺ T cells, which have not yet encountered a specific antigen migrate with the blood stream through the lymphoid tissue and enter lymph nodes. They are not activated until the first time they encounter a specific antigen in the form of a peptide:MHCII (major histocompatibility complex II) complex on the surface of an activated antigen-presenting cell (APC). (Janeway *et al.*, 2005)

Depending on the cytokine milieu naïve CD4⁺ T cells can differentiate into various types of T cell lineages, such as Th1, Th2, Th3, Th9, Th17 or follicular T helper cells (Tfh). Each lineage secretes specific cytokines but flexibility and plasticity of Th cells, which can change their profile of cytokine expression is now widely accepted (O'Shea and Paul, 2010; Janeway *et al.*, 2005).

1.2 T cell effector function

To activate a naïve CD4⁺ T helper cell to proliferate and differentiate into an effector cell two signals are required. The first signal is provided by a specific antigen bound to an MHC protein on the surface of an APC and involves the TCR and its associated proteins (Janeway *et al.*, 2005). The second signal is provided by costimulatory proteins on the membrane of APCs, especially the B7 proteins CD80 and CD86, which are recognized by the co-receptor protein CD28 on the surface of a T cell (Alberts, 2015). Differentiation of naïve CD4⁺ T cells into one of the various types of T cell lineages – also termed priming - is accompanied by clonal expansion of the cell (Murphy and Reiner, 2002). Upon a second encounter with an antigen, primed T cells become fully activated to suppress or regulate immune responses by releasing large amounts of T cell cytokines. In line with this, Scheu *et al.* could show that *in vitro* priming of CD4⁺ T helper type 2 cells induces the transcription of *Il4* mRNA, whereas these transcripts were not translated until the cells were engaged by a second encounter (Scheu *et al.*, 2006).

Two key features mainly define a T helper cell lineage: expression of a signature cytokine and a “master regulator transcription factor”. Despite this clear definition of each T cell lineage, it is well known that T helper cells are much more diverse and plastic (e.g. Th17 cells can produce interferon- γ (IFN γ)) than previously assumed (Boniface *et al.*, 2010; Hegazy *et al.*, 2010). Thus, many mechanisms and features come into play when defining the fate of

a T cell lineage. The master regulator that is necessary for Th1 differentiation is the T-box transcription factor (T-bet), which is also important in suppressing the differentiation of Th2 and Th17 cells (Djuretic *et al.*, 2007; Lazarevic *et al.*, 2011; Szabo *et al.*, 2000). T-bet expression is also dependent on signal transducer and activator of transcription 1 (STAT1), which is in turn activated by IFN γ (Afkarian *et al.*, 2002). STAT4 is a further important transcription factor involved in the Th1 cell differentiation and in inducing IFN γ production (Thierfelder *et al.*, 1996). Th1 cells are mainly characterized by the release of their signature cytokine IFN γ and tumor necrosis factor- α (TNF- α). They primarily activate macrophages and B cells to ensure protection against intracellular microorganisms (Reiner and Locksley, 1995).

1.3 The central dogma of molecular biology: DNA \rightarrow RNA \rightarrow Protein

The central dogma of molecular biology, postulated years ago by Francis Crick, described the detailed residue-by-residue transfer of sequential information and stated that the transfer of information from protein to either DNA or RNA is not possible. But, simply spoken he concluded that DNA makes RNA makes protein (Crick, 1970; Crick, 1958). Of course, by now we know that gene expression is a concerted process of many factors and regulation can be exerted at multiple steps including transcription, mRNA degradation, translation and protein degradation (Figure 2). Each of these steps contributes to the repertoire of expressed proteins and thus has to be tightly regulated. In immunology, most global studies have focused on transcriptional control but especially regarding Th1 cell activation, certain posttranscriptional control mechanisms have been proposed to regulate gene expression (Chang *et al.*, 2013; Scheu *et al.*, 2006). But, despite numberless possibilities to study genome-wide gene regulation most existing studies so far focused on single mechanisms and there is still a gap in comprehensive global and dynamic analyses.

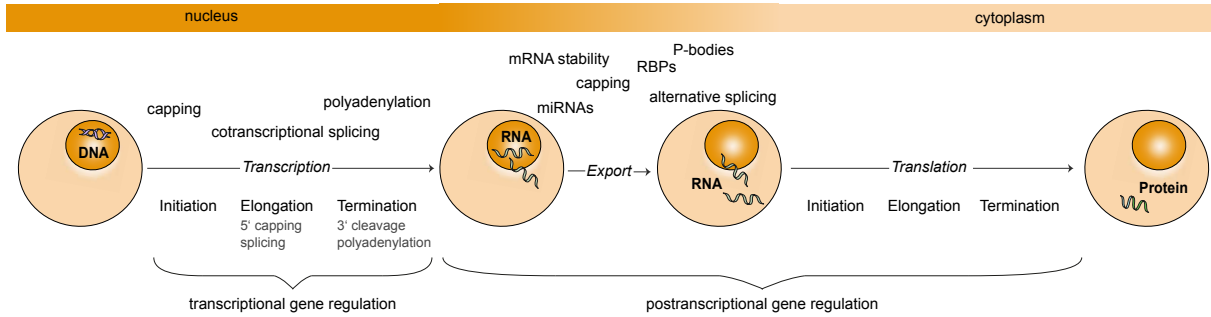


Figure 2: The central dogma of molecular biology (from today's view)

Schematic drawing illustrating the flux of information from DNA to RNA and protein as formerly described in the central dogma of molecular biology. The process of transformation is shown (transcription, translation) as well as their main steps (below) and the main gene regulatory processes taking place during both steps (above).

1.3.1 Transcriptional gene regulation

Regulation of gene activity is a pivotal mechanism to maintain vital processes and adapt to changes we encounter at nearly every moment in life. As summarized by Cooper and Hausman, gene expression is primarily controlled at the level of transcriptional initiation and orchestrated by transcription factors (TFs) which turn genes on or off by binding to DNA regulatory sequences (Cooper and Hausman, 2013). They are even responsible for binding of the RNA polymerase II (RNAPII), which synthesizes mRNAs. Synthesis of mRNA is divided into initiation, elongation and termination and each of these steps can be regulated independently. First, the RNAPII specifically binds to the chromosome of a gene and forms a preinitiation complex. DNA strands are separated and the RNA polymerase accesses single-stranded nucleotide bases which serve as a template for transcription of nascent RNA. This process transcribes an average of 20 - 30 nucleotides per second until the complete gene has been transcribed. After the polymerase recognizes the signal for termination, the nascent transcript dissociates from the elongating RNA polymerase, which is free to start initiation at the next promoter. (Cooper and Hausman, 2013)

In the last decades there have been many significant contributions to our understanding of gene regulation in immune cells. The discovery of dozens of transcription factors shown to be important for development and function of T cells as well as elucidating signaling pathways were achievements that laid the foundation for upcoming experiments. But it was also shown that T cells are even more complex and flexible than previously thought. For example the initially as Th1-specific defined TF T-bet (encoded by the *Tbx21* gene) was later

proven to be expressed in other cells like CD8⁺ T cells, natural killer T (NKT) cells or B cells, too (Lazarevic *et al.*, 2013).

Classically, global studies in the field of immunology were centered on transcriptional gene regulation, but its impact in determining the abundance of proteins is still under heavy debate. Schwanhäusser *et al.* conducted one of the first global studies showing that mRNA and protein abundance are better correlated than previously thought (Schwanhausser *et al.*, 2011; Schwanhausser *et al.*, 2013). When analyzing the response of dendritic cells to LPS, Jovanovic *et al.* determined that changes in mRNA levels even accounted for ~90 % of changes in protein abundance (Jovanovic *et al.*, 2015). Recently it was shown that mRNA superinduction, which describes a massive and sustained production of cytokine transcripts, mediates host response during an infection with an intracellular bacterial pathogen (Barry *et al.*, 2017).

Upon activation, T cells massively and rapidly increase cytokine and effector molecule transcription. These short-term changes are defined by *de novo* transcription, which can be determined using metabolic RNA labeling with 4sU (see 1.5.2) (Dolken *et al.*, 2008). Applying 4sU-labeling to study the response of mouse dendritic cells to LPS, major principles of temporal RNA regulation in mammalian cells could be discovered (Rabani *et al.*, 2011). Changes in transcription rates are highly correlated with changes in RNA levels and dynamic changes in degradation rates seem to have minimal effect on most RNA profiles. Furthermore, degradation and processing rates differ between genes rather than over time. (Rabani *et al.*, 2011)

1.3.2 Cotranscriptional splicing

Splicing describes the removal of introns from pre-mRNA and is spatially and temporally coupled to transcription (Bentley, 2014). It was shown years ago that it can take place either after transcription termination (posttranscriptionally) or even during the process of transcription (cotranscriptionally) (Beyer and Osheim, 1988). Cotranscriptional splicing takes place while the RNA is still attached to the DNA by the elongating RNAPII and is mediated by the spliceosome, which is a large multicomponent complex composed of five small nuclear ribonucleoproteins (snRNPs) and non-snRNP proteins, including members of the SR protein family (Tarn and Steitz, 1997; Manley and Tacke, 1996). The mammalian RNAPII, in contrast to the other RNA polymerases, consists of a conserved C-terminal domain (CTD), which is made up of 52 heptad repeats (YSPTSPS) (Corden, 1990; Barron-

Casella and Corden, 1992). This heptapeptide repeat contains five potential amino acids for phosphorylation. The predominant sites of phosphorylation are the serines at position 2 (Ser2) and 5 (Ser5) (Zhang and Corden, 1991). While Ser5 is phosphorylated at the initiation of transcription by the transcription factor TFIIF, Ser2 is phosphorylated during transcriptional elongation by the positive transcriptional elongation factor b (pTEFb) (Lin *et al.*, 2008; Barboric *et al.*, 2009; Buratowski, 2009). Based on the phosphorylation status, two forms of the RNAPII can be distinguished. The hypophosphorylated IIA form preferentially enters the preinitiation complex at the promoter, whereas the hyperphosphorylated IIO form is associated with the elongation complex (Dahmus, 1996).

1.3.3 Posttranscriptional gene regulation

Posttranscriptional control of gene expression is a well-studied and accepted mechanism for the regulation of protein abundance. Changes in the proteome are induced without changing (*de novo*) transcription, e.g. when rapid adaptation to environmental changes is required. As described by Cooper and Hausman, it can be directed amongst others through the regulation of splicing, the export of mRNA from the nucleus to the cytosol, mRNA stability and mRNA translation (Cooper and Hausman, 2013). Similar to mRNA synthesis, translation can be separated into initiation, elongation, termination and a recycling step. First the small subunit of a ribosome attaches to the mRNA, assembles at the start codon AUG and forms the complete ribosome by joining its large subunit. The ribosome moves one triplet after another with a new tRNA and amino acid entering the ribosome each time, elongating the protein. When the ribosome reaches one of three possible stop codons, termination proteins bind and the ribosome dissociates from the mRNA. (Cooper and Hausman, 2013)

Scheu *et al.* could show that after differentiation of naïve T helper cells, they express cytokine mRNA but do not secrete cytokine protein without additional TCR stimulation (Scheu *et al.*, 2006). These data suggest that naïve T cells primed by the engagement of the T cell receptor are initially restricted in cytokine translation, but that translation takes place after a further activation of the T cell. According to their study T lymphocytes require components of the integrated stress response to release the cell from restricting cytokine production. Another study suggesting posttranscriptional control in T cells was performed by Chang *et al.* and showed that the switch of T effector cells to aerobic glycolysis upon activation is necessary for increased IFN γ production (Chang *et al.*, 2013). Furthermore, they

conclude that glyceraldehyde-3-phosphate dehydrogenase (GAPDH) directly regulates IFN γ translation and thus has posttranscriptional control over it.

1.4 Methods to monitor changes in gene expression: Next generation sequencing

In 1977, Sanger *et al.* and Maxam and Gilbert developed new methods for sequencing DNA by chain termination and by fragmentation of labeled DNA, respectively (Maxam and Gilbert, 1977; Sanger *et al.*, 1977). Especially the technique by Sanger (also termed Sanger-Sequencing) became widely used and led to the decipherment of entire genomes. Further developments enabled the Human Genome Project to publish 90 percent of the human genome DNA sequence in 2001 (Venter *et al.*, 2001; Lander *et al.*, 2001) and finally complete the project in 2006 with the annotation of the last chromosome (Gregory *et al.*, 2006). This did not only reveal that the human genome consists of far less protein-coding genes than previously expected, but also that new methods and technologies are needed to fasten, facilitate and reduce costs of genome sequencing. Next-generation sequencing fulfills these requirements although it is still pushed to its limits.

1.4.1 RNA sequencing to monitor transcriptional regulation

To understand the functional elements of the whole genome, sequencing of the transcriptome is generally applied. Although direct RNA sequencing is possible, RNA-seq is still mainly performed through the conversion into cDNA (Ozsolak *et al.*, 2009). In general, a poly(A)-selected or rRNA-depleted pool of RNA is converted into a cDNA library with adaptors attached to one or both ends. The cDNA library is sequenced to obtain short sequences from one end (single-end sequencing) or both ends (paired-end sequencing) (Wang *et al.*, 2009). In principle, any sequencing technology can be applied but most commonly used are platforms by Illumina (Bentley *et al.*, 2008), Ion Torrent (Rothberg *et al.*, 2011) and PacBio (Eid *et al.*, 2009). To reveal the diversity of the transcriptome, which is much more complex than previously thought, strand-specific sequencing was introduced, which enables the detection of antisense regulatory transcripts (Levin *et al.*, 2010).

1.4.2 4sU sequencing to monitor *de novo* transcription

Cells rapidly adapt in response to environmental changes accompanied by an altered gene expression. Since short-term changes in RNA transcription can hardly be measured by total

RNA-seq, as changes of total RNA additionally depend on e.g. RNA half-lives, total RNA represents a poor template for reflecting rapid adaptation of cells. For instance, Schwalb *et al.* determined that human cells have a median mRNA half-life of ~50 min (Schwalb *et al.*, 2016) whereas it was previously reported to be ~139 min in mice dendritic cells (Rabani *et al.*, 2014). Nuclear transcription run-on assays (Birse *et al.*, 1997) and their modifications (Garcia-Martinez *et al.*, 2004) have long been used for the detection of *de novo* transcription. The major drawback of these methods is, however, that they are cell-invasive and are not compatible with current technologies like next-generation sequencing.

Hence, new strategies have been described for the analysis of nascent transcripts, like global run-on sequencing (GRO-seq), native elongating transcript sequencing (NET-seq), factory RNA-seq, nascent-/chromatin-seq, transient transcriptome sequencing (TT-seq) and 4sU-seq. While GRO-seq is a further development of nuclear run-on assays that maps and quantifies transcriptionally engaged polymerase density genome-wide (Core *et al.*, 2008) NET-seq determines the position of actively elongating RNAP (Core *et al.*, 2008; Churchman and Weissman, 2012). Nascent-/chromatin-seq and factory RNA-seq rely on fractionation and subsequent sequencing of chromatin associated RNA transcripts or transcription factories, respectively (Bhatt *et al.*, 2012; Caudron-Herger *et al.*, 2015). TT-seq, a method published in 2016, is based on 4sU-labeling but uniformly maps the transient transcriptome without a 5' bias due to RNA fragmentation before isolation of labeled RNA fragments (Schwalb *et al.*, 2016).

4-thiouridine (4sU) is a natural occurring uridine derivate that was chemically synthesized in 1908 and isolated from soluble ribonucleic acid of *Escherichia coli* in 1965 (Lipsett, 1965). It was first used in 1978 for labeling endogenous RNA which provides access to newly transcribed RNA since it is very rapidly and efficiently incorporated by the growing RNA chain in place of uridine (Melvin *et al.*, 1978). Nevertheless this approach was not broadly applied until 2007 when 4sU incorporated RNA was isolated by affinity-chromatographic isolation (Kenzelmann *et al.*, 2007). Another amendment was performed by Dölken *et al.* who used thiol-specific biotinylation and affinity purification using streptavidin-coated magnetic beads to separate total RNA into newly transcribed and pre-existing RNA, as eukaryotic mRNAs normally do not contain thiol-groups (Dölken *et al.*, 2008). All three fractions (total RNA, pre-existing RNA, newly transcribed RNA) could be used for further downstream analysis (e.g. RNA-seq). Thus, it enables short-term labeling and detection of newly synthesized transcripts but also determination of RNA half-lives (Windhager *et al.*, 2012). A

main advantage is its minimal adverse effect on gene expression, RNA decay, protein stability and cell viability (Dolken *et al.*, 2008). Nevertheless, it can inhibit the production and processing of rRNA and induce cytoplasmic as well as nuclear stress when high doses or prolonged labeling times are used (Burger *et al.*, 2013).

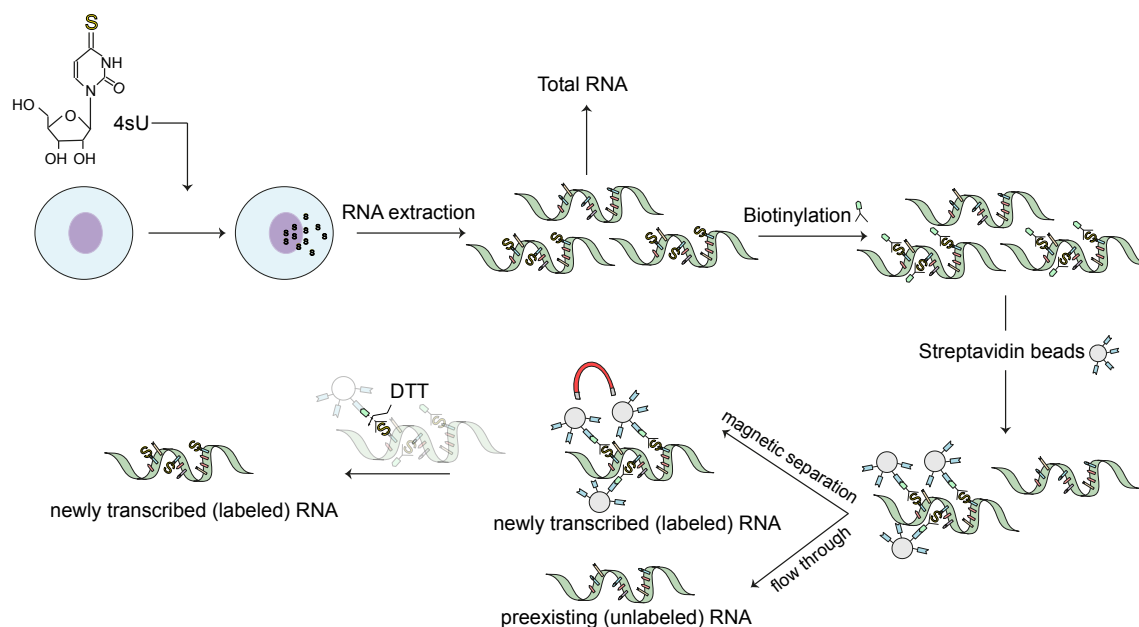


Figure 3: Work-flow for 4sU-labeling

A schematic drawing of 4sU-labeling is depicted. 4sU is added to the cells for a defined time, followed by RNA extraction. Labeled RNA (can additionally be used as total RNA) is biotinylated and incubated with magnetic streptavidin beads. RNA can then be magnetically separated into newly transcribed (labeled) RNA and preexisting (unlabeled) RNA. A reducing agent (DTT) is added to cleave the disulfide bond and recover the newly transcribed RNA from the beads.

1.4.3 Ribosome Profiling to monitor translational regulation

Until recently, detailed monitoring of translation was quite challenging. Hence, in 2009 a method termed ribosome profiling (RP) was developed that was able to precisely reveal locations of ribosomes on each mRNA at single codon level (Ingolia *et al.*, 2009). Ribosome profiling, which is an improved version of ribosome footprinting, is based on sequencing of ribosome protected mRNA fragments and thus enables global monitoring of *in vivo* translation. It creates a snapshot of all ribosomes present at the mRNA at a specific moment but does not distinguish paused ribosomes from those engaged in active elongation. In general, the translating ribosome which protects ~28 - 30 nt mRNA from nuclease activity is chemically stopped and ribosome protected mRNA fragments (RPFs) are generated. The RPF abundance is quantified by sequencing. Mapping the distribution at the genome and

analyzing its abundance reveals the exact position and density of the ribosome occupation. To immobilize initiating ribosomes and define translation start sites, cells can initially be pretreated with harringtonine, which enriches ribosomes specifically on initiation sites before finally stalling ribosomes on the transcripts with cycloheximide treatment.(Ingolia *et al.*, 2012)

Cycloheximide is a commonly used protein synthesis inhibitor, originally isolated from *Streptomyces griseus*, which blocks the translocation step during elongation (Schneider-Poetsch *et al.*, 2010). Initially developed to monitor translational changes in yeast under stress conditions (Ingolia *et al.*, 2009), ribosome profiling was further adapted for the use of mammalian cells (Guo *et al.*, 2010) and a kit is now commercially sold by Illumina (TruSeq Ribo Profile).

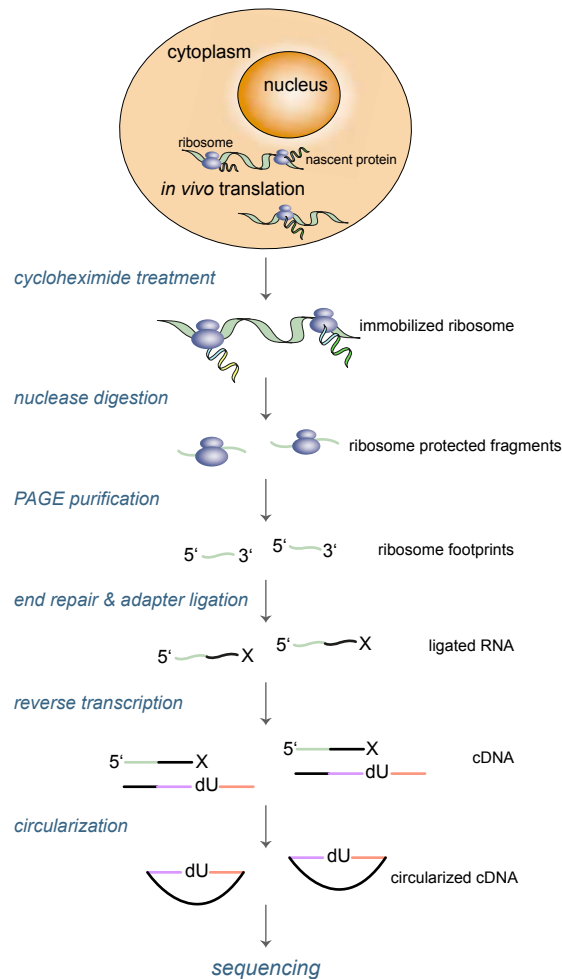


Figure 4: Work flow for Ribosome Profiling

A schematic drawing of Ribosome Profiling is depicted. Cycloheximide is added to the cell to stop the translating ribosome. Ribosome protected fragments are protected from nuclease digestion and can be further purified by gel purification. After RNA end repair and 3' adapter ligation reverse transcription takes place and cDNA is circularized. Following cDNA amplification, samples are suitable for sequencing.

1.4.4 ChIP sequencing to monitor DNA-protein interaction

In 1984, chromatin immunoprecipitation (ChIP), which detects protein-DNA interactions *in vivo*, was presented in *Escherichia coli* (Gilmour and Lis, 1984). This method covalently crosslinks proteins to DNA and was improved over the years. In short, the crosslinked chromatin is lysed, fragmented and an immobilized antibody of interest enriches DNA attached to protein. After reversing the crosslink, DNA can be further analyzed to determine where the protein is binding to the genome. To perform genome-wide assays, immunoprecipitated DNA was first hybridized to microarray chips (ChIP-chip) (Ren *et al.*, 2000). The next major progress came by the advent of next-generation sequencing, which

directly enables sequencing of immunoprecipitated fragments (ChIP-seq) to profile protein-DNA occupancy on a genome-wide basis, thus facilitating resolution of promoter targets (Johnson *et al.*, 2007). This provides nearly infinite possibilities of ChIP to profile for instance the distribution of transcription factors, histone modifications or RNA polymerase across entire genomes (Mahony and Pugh, 2015). Meanwhile, advances in sequencing but also in the ChIP protocol allow for high-throughput analysis of large-scale *in vivo* studies (Blecher-Gonen *et al.*, 2013). It is known that the dynamic binding of proteins to DNA regulates gene function and transcription factors are key regulatory elements of gene expression. This regulation can be either short-term, such as the response to environmental stimuli or long-term, such as during development and differentiation. With the help of ChIP-seq it was revealed that upon activation of Th1 cells, expression of many Th1 specific genes largely depends on the presence of T-bet (Thieu *et al.*, 2008). Furthermore, T-bet, which was originally described as a transcription factor regulating Th1 cell lineage commitment, was also shown to have a fundamental role in coordinating immune response even for other immune cells (Lazarevic *et al.*, 2013).

1.5 Aim of the study

Gene regulation takes place at different molecular levels, ranging from epigenetic changes to transcriptional and translational regulation each comprising of many regulatory levels. Within the last years posttranscriptional control of gene regulation became a highly investigated field of research, especially in the field of immunology. Scheu *et al.* showed that after initial priming of naïve T cells, primed T helper cells express cytokine mRNA but do not secrete cytokine protein without an additional stimulation via the TCR (Scheu *et al.*, 2006). These data let the authors speculate that cytokine release might be controlled at the level of translation. Additionally, Chang *et al.* showed that T cells do not rely on aerobic glycolysis for proliferation but it is necessary for optimal *Ifng* production in T cells, regulated by binding of GAPDH to *Ifng* mRNA (Chang *et al.*, 2013). Among others, these studies support the idea of a major impact of posttranscriptional gene regulation in T cells, especially during T cell activation. Besides, it is still unclear to which extent transcription and translation determine protein abundance genome-wide. While it was previously thought that differences in translation rates predominate (Schwanhausser *et al.*, 2011; Kristensen *et al.*, 2013), recent studies suggest that transcriptional control dominates (Jovanovic *et al.*,

2015; Li *et al.*, 2014). Nevertheless, comprehensive analyses in T cells are still missing and genome-wide mechanism are insufficiently described, since most studies addressing these questions were performed under steady state conditions or in cell lines.

To display multiple layers of gene regulation during the process of T cell activation, we simultaneously performed 4sU-seq, RNA-seq, Ribosome profiling and ChIP-seq over time. Combining these methods enabled us to display the genome-wide course of action in detail.

2 Materials

2.1 Antibodies and cytokines

All antibodies were either generated in collaboration with Elisabeth Kremmer or purchased. Cytokines were purchased.

Table 1 Anti-mouse antibodies and cytokines for T cell differentiation

<i>Antibody or cytokine</i>	<i>Manufacturer</i>
Anti-CD3 (145-2C11)	In-house by E. Kremmer
Anti-CD28 (37N)	In-house by E. Kremmer
Anti-Il4 (IIB11)	In-house by E. Kremmer
Recombinant Il-12	R&D Systems
Goat anti-hamster immunoglobulin G	MP Biomedicals
Proleukin S	Novartis

Table 2 Western Blot antibodies

<i>Antibody</i>	<i>Manufacturer</i>
Anti-Actin (C4)	Merck Chemicals
Anti-CDK9 (H-169)	Santa Cruz Biotechnology
Anti-Cyclin T1 (C-20)	Santa Cruz Biotechnology
Anti-GAPDH (1A7)	In-house by E. Kremmer
Anti-p53 (ab26)	Abcam
Anti-Phospho 4E-BP1 (Thr37/46)	Cell Signaling Technology
Anti-Phospho CDK9 (Thr-186)	Cell Signaling Technology
Anti-Phospho eIF2 α (Ser51)	Cell Signaling Technology
Anti- eIF2 α	Cell Signaling Technology
Anti-RNAPII (phospho S2) (H5)	Abcam
Anti-RNAPII (phospho S5) (3E8)	Provided by D. Eick
Anti-Rpb1 (Pol3.3) (M-G1)	Provided by D. Eick
Anti-SC35	BD Bioscience
Anti-SNRP70 (ab83306)	Abcam
Anti-Tubulin (B-5-1-2)	Santa Cruz Biotechnology
Anti-U2AF65 (MC3)	Santa Cruz Biotechnology

Table 3 ChIP antibodies

<i>Antibody</i>	<i>Manufacturer</i>
anti-RNA Pol II [8WG16]	abcam
anti-Histon H3K36me3	abcam

Table 4 FACS antibodies

<i>Antibody</i>	<i>Manufacturer</i>
7-AAD	BD Biosciences
Annexin V	BD Biosciences
IFN γ	eBioscience

2.2 Primers

Primers were purchased from Metabion.

Table 5 Primers for detection of gene expression

<i>Gene</i>	<i>Direction</i>	<i>Sequence (5' → 3')</i>
Ifng	Fw	CTTCAGCAACAGCAAGGCGA
	Rev	CATTGAATGCTTGGCGCTGG
Il3	Fw	TCAATCAGTGGCCGGGATAAC
	Rev	TTGAGTTCAGGTTCTGGGAGC
Tnf	Fw	CATCTTCTCAAAATTCGAGTGACAA
	Rev	TGGGAGTAGACAAGGTACAACCC
Gapdh	Fw	GGGTCCCAGCTTAGGTTTCAT
	Rev	CCCAATACGGCCAAATCCGT
Hprt	Fw	AGCAGTACAGCCCCAAAATG
	Rev	ATCCAACAAAGTCTGGCCTGT
Gfp	Fw	AACGATCTGGATGGCAGCTT
	Rev	TCCACCACGGAGCTGTAGTA
18S rRNA	Fw	GTAACCCGTTGAACCCCAT
	Rev	CCATCCAATCGGTAGTAGCG

Table 6 Primers for splicing

<i>Gene</i>	<i>Exon/intron</i>	<i>Direction</i>	<i>Sequence</i>
Ifng	Exon 1-2	Fw	TCATGGCTGTTTCTGGCTGT
		Rev	ACATCTATGCCACTTGAGTTAAAAT
	Intron 1-2	Fw	TCATGGCTGTTTCTGGCTGT
		Rev	GGTCAACCAACCACAAGCATT
Il3	Exon 1-2	Fw	TCAATCAGTGGCCGGGATAAC
		Rev	TTGAGTTCAGGTTCTGGGAGC
	Intron 1-2	Fw	TCAATCAGTGGCCGGGATAAC
		Rev	GCCAACCTCAGCCAGTTACTC
Ccl3	Exon 2-3	Fw	TACAGCCGGAAGATTCCACG
		Rev	TCAGGAAAATGACACCTGGCT
	Intron 2-3	Fw	TACAGCCGGAAGATTCCACG

	Rev	AGCACGAGAACAGAACTTACA
--	-----	-----------------------

Table 7 Primers for detection of downregulated genes

<i>Gene</i>	<i>Direction</i>	<i>Sequence</i>
Ccng2	Fw	AGGCTACCCCGGAGAATGAT
	Rev	ATGCAGGACAGGTGTTTCGG
Pik3ip1	Fw	GTTGCCCAGAGACCACTTCC
	Rev	CCTGTGCCTCCTTGTCACCT
S1pr1	Fw	AGCTCAGGGAACCTTTGCGAG
	Rev	GAGAAACAGCAGCCTCGCTC
Vipr1	Fw	TCAGCCGTAACCTGCACTGAA
	Rev	TCTGTTGCTGCTCATCCATACT

Table 8 Primers for ChIP

<i>Gene</i>	<i>Direction</i>	<i>Sequence</i>
Ifng	Fw	CGTAATCCCGAGGAGCCTTC
	Rev	GTGTCTTCTCTAGGTCAGCCG
Il3	Fw	TCACACATTCTGGTTTGGAGTGA
	Rev	ACATCACATGCGGCTACACA
Fos	Fw	CTGGGGCGTAGAGTTGACG
	Rev	GCCGGCTCTATCCAGTCTTC
Ins (neg)	Fw	TGTCAAACAGCATCTTTGTGG
	Rev	CACTTGTGGGTCCCTCACTT
Sox9 (neg)	Fw	GTGCAGCACAAGAAAGACCAC
	Rev	AGCGCCTTGAAGATAAGCATTAG

2.3 Cell lines

The murine EL4 cell line was provided by Dr. Heissmeyer. It was originally established from a lymphoma induced in a C57BL/6N mouse (Gorer, 1950).

2.4 Mouse strains

Balb/c DO11.10 TCR transgenic mice and C57BL/6J were purchased from Jackson Laboratory and bred in a specific pathogen-free barrier facility. DO11.10 is a transgenic TCR specific for MHCII loaded ovalbumin OVA323-339 peptide. These mice can be used for antigen specific T cell activation, which was not used in these studies. Mice were used at 8 – 12 weeks of age

in accordance with the Helmholtz Zentrum München institutional, state and federal guidelines.

2.5 Chemicals and reaction kits

Table 9 Chemicals

<i>Chemical</i>	<i>Manufacturer</i>
100 bp Plus Marker	Thermo Scientific
4-thiouridine (100 mg)	Carbosynth
Agarose	Biozym
Agencourt RNAClean XP beads	Beckman Coulter
β -mercaptoethanol	Sigma-Aldrich
BH3I-1	Sigma-Aldrich
Chloroform	Sigma-Aldrich
Dimethylformamide	Sigma-Aldrich
Dithiothreitol (DTT)	Roth
DNA low bind microcentrifuge tubes	Eppendorf
DETAChAbeAD	Thermo Scientific
Dynabeads Mouse CD4	Thermo Scientific
Dynabeads Protein G	Invitrogen
E-Gel EX 1% agarose precast gels	Invitrogen
ECL prime western blot detection reagent	GE Healthcare Life Sciences
EDTA (UltraPure, 0.5M, pH 8.0)	Thermo Scientific
Ethanol	Merck
EZ-Link Biotin-HPDP (50 mg)	Pierce
Fetal bovine serum (FBS)	Sigma-Aldrich
Formaldehyde (16 %)	Thermo Scientific
GlutaMAX	Life Technologies
Glycine	Sigma-Aldrich
GlycoBlue Coprecipitant	Thermo Scientific
Glycogen	Roche
HEPES buffer (1M)	Life Technologies
Illustra MicroSpin S-400 HR Columns	GE Healthcare
Ionomycin	Santa Cruz Biotechnology
Isopropanol	Merck
μ Macs Streptavidin MicroBeads	Miltenyi
MEM vitamin solution	Life Technologies
NaCl (5M)	Sigma-Aldrich
Non-essential amino acids	Life Technologies
Nuclease-free EDTA (500 mM), pH 8.0	Invitrogen
Nuclease-free H ₂ O	Sigma-Aldrich
Nuclease-free Tris HCl (1M), pH 7.4	Lonza
Paraformaldehyde (PFA)	Sigma-Aldrich
PBS tablet	Thermo Scientific

Penicillin-streptomycin	Life Technologies
Phase Lock Gel Heavy tubes (2.0 ml)	5Prime
Phosphatase Inhibitor (PhosStop)	Roche
Phorbol-12-myristate-13-acetate (PMA)	Sigma
Power SYBRgreen Master mix	Thermo Scientific
Protease Inhibitor (cOmplete, EDTA-free)	Roche
Proteinase K	Invitrogen
Qiagen RLT Buffer	Qiagen
QIAzol Lysis Reagent	Qiagen
Rnase, DNase free	Roche
RPMI 1640	Thermo Scientific
Salmon sperm	Sigma-Aldrich
Saponin	VWR chemicals
Skimmed milk powder	Roth
Sodium citrate	Sigma-Aldrich
Sodium pyruvate	Lonza
SYBR Gold nucleic acid gel stain	Thermo Scientific
Thapsigargin	Sigma-Aldrich
Tris-EDTA (TE) pH 8.0	Sigma-Aldrich
Tris-HCl (10 mM, pH 8.0)	Sigma-Aldrich
Tween 20	Sigma-Aldrich

Table 10 Kits

<i>Kit</i>	<i>Manufacturer</i>
ARTseq™ Ribosome Profiling Kit	Epicentre
BCA protein assay kit	Thermo Fisher
ChIP library preparation kit	KapaBiosystems
DynaMag-96 side skirted magnet	Thermo Scientific
High Sensitivity DNA Kit	Agilent Technologies
µMacs Streptavidin Kit	Miltenyi
MinElute PCR Purification Kit	Qiagen
Mouse T Cell Nucleofector Kit	Lonza
NEBNext® Ultra™ RNA Library Prep Kit for	New England BioLabs
PE Annexin V Apoptosis Detection Kit I	BD Biosciences
QuantiTect Reverse Transcription Kit	Qiagen
Qubit dsDNA HS Assay kit	Invitrogen
Qubit RNA HS assay kit	Life Technologies
Ribo-Zero Gold rRNA Removal Kit	Illumina
RNA 6000 Nano kit	Agilent Technologies
RNA Clean & Concentrator-25 kit	Zymo Research
RNA Clean & Concentrator-5 kit	Zymo Research
RNeasy MinElute Cleanup Kit	Qiagen
TruSeq Ribo Profile kit (Mammalian)	Illumina
TruSeq stranded total RNA library prep kit	Illumina
µMacs Streptavidin Kit	Miltenyi

2.6 Buffers, solutions, media

Table 11 Composition of buffers, solutions and media

<i>Buffer, solution, media</i>	<i>Composition</i>
4sU Biotinylation Buffer (10x)	100 mM Tris/HCl pH 7.4, 10 mM EDTA in nuclease-free water; make aliquots of 1 ml; store at 4°C
4sU RNA precipitation buffer	1.2 M NaCl, 0.8 M sodium citrate in nuclease free water. Prepare in advance under nuclease-free conditions. Store at room temperature in 50 ml falcon tubes.
4sU Washing Buffer for streptavidin capture	100 mM Tris/HCl pH 7.4, 10 mM EDTA, 1 M NaCl, 0.1% Tween 20 in nuclease-free H ₂ O
ChIP Binding/Blocking buffer	PBS with 0.5 % BSA and 0.5 % Tween 20
ChIP Cell-Lysis buffer	5 mM Pipes (pH 8.0), 85 mM KCl, and 0.5 % NP40
ChIP Elution buffer	10 mM Tris-HCl (pH 8.0), 5 mM EDTA (pH 8.0), 300 mM NaCl and 0.5 % SDS
ChIP IP buffer	0.01 % SDS, 1.1% Triton X-100, 1.2 mM EDTA, 16.7 mM Tris-HCl, pH 8.1, 16.7 mM NaCl
ChIP Nuclei-Lysis buffer	50 mM Tris [pH 8.0], 10 mM EDTA, 1 % SDS
ChIP Wash buffer I	0.1 % SDS; 1 % Triton X-100; 2 mM EDTA; 20 mM Tris-HCL pH 8.1; 150 mM NaCl
ChIP Wash buffer II	0.1 % SDS; 1 % Triton X-100; 2 mM EDTA; 20 mM Tris-HCL pH 8.1; 500 mM NaCl
ChIP Wash buffer III	0.25 M LiCl; 1% NP-40; 1 mM EDTA; 10 mM Tris-HCl, pH 8.1
FACS buffer	PBS (pH 7.4), FCS (1 %), sodium acid (0.01 %), 2 mM EDTA
FACS buffer (intracellular)	PBS (pH 7.4), FCS (1 %), sodium acid (0.01 %), saponin (0.5 %), 2 mM EDTA

Materials

Fractionation cytoplasmic lysis buffer	0.05% NP-40, 10mM Tris (pH 7.5), 150 mM NaCl
Fractionation glycerol buffer	20 mM Tris (pH 7.9), 75 mM NaCl, 0.5 mM EDTA, 50 % glycerol, 0.85 mM DTT
Fractionation nuclei lysis buffer	20 mM HEPES (pH 7.6), 7.5 mM MgCl ₂ , 0.2 mM EDTA, 0.3 M NaCl, 1 M urea, 1 % NP-40, 1 mM DTT
Fractionation sucrose buffer	10 mM Tris pH7.5, 150 mM NaCl, 24% sucrose
Laemmli sample buffer (4x)	200 mM Tris-HCl pH 6.8, 8 % SDS, 0.1 % bromophenol blue, 40 % glycerol, 10 % β -mercaptoethanol (fresh)
PBS	1 PBS tablet dissolved in 500 ml Milli-Q
RIPA lysis buffer	20 mM Tris-HCl pH 7.5, 250 mM NaCl, 10 mM MgCl ₂ , 1 % NP40, 0.1 % SDS, 0.5 % sodium deoxycholate
SDS buffer	200 mM Tris-HCl pH 6.8, 8 % SDS, 0.1 % bromphenol blue, 4 % glycerol, 10 % β-mercaptoethanol (fresh)
T cell media	RPMI medium supplemented with 10 % (vol/vol) FBS, β-mercaptoethanol (0.05 mM), penicillin-streptomycin (100 U/ml), sodium pyruvate (1 mM), non-essential amino acids (1x), MEM Vitamin Solution (1x), Glutamax (1x), HEPES pH 7.2 (10 mM)
TBS (1x)	10 mM Tris/HCl pH 8.0, 150 mM NaCl
TBST	TBS (1x), 0.05 % Tween 20
Western blot buffer	25 mM Tris-Base, 192 mM glycine, 20 % methanol (pH 8.4) in H ₂ O

2.7 Devices

Table 12 Devices

<i>Device</i>	<i>Company</i>
2100 Bioanalyzer instrument	Agilent
Bioruptor sonication device	Diagenode
Bioruptor TBX microtubes 1.5 ml	Diagenode
Blotting chamber	Bio-Rad
DynaMag-2 Magnet	Life Technologies
E-Gel iBase Power System	Invitrogen
FACS AriaIII Flow Cytometer	BD Bioscience
GelDoc-It TS Imaging System	UVP
HERA cell 150i CO ₂ incubator	Thermo Scientific
High-speed centrifuge	Thermo Scientific
High-speed rotor	Thermo Scientific
HiSeq 4000	Illumina
MACS multistand	Miltenyi Biotec
Microscope	Zeiss
Nanodrop 2000	Thermo Scientific
Neubauer chamber (hemocytometer)	Carl Roth
Qubit 2.0 Fluorometer	Thermo Scientific
PHERASTAR microplate reader	BMG Labtech
Protein gel chamber	BioRad
Refrigerated table-top centrifuge	Eppendorf
RNA 6000 Nano Kit	Agilent
RNA 6000 Pico Kit	Agilent
RNaseZap	Sigma
Thermocycler	Eppendorf
Ultra-fine scale	Mettler Toledo
UV/VIS spectrophotometer	Thermo Scientific
ViiA 7 real-time PCR system	Thermo Fisher

2.8 Software

Table 13 Software

<i>Software</i>	<i>Version</i>
Bioconductor packages for R	Diverse
DAVID	6.8
FeatureCounts	1.5.0-p1
FlowJo	9.7.6
RStudio	0.98.1091 and 1.0.136

3 Methods

Parts of the following protocol were published under the title “Real-time Analysis of Transcription Factor Binding, Transcription, Translation and Turnover to Display Global Events During Cellular Activation” in the Journal of Visualized Experiments (JoVE)(Lichti, Davari *et al.*, in revision).

3.1 Cell Culture

3.1.1 Preparation and differentiation of primary Th1 cells

Peripheral CD4⁺ T cells were isolated from spleen and lymph nodes with CD4 Dynabeads (Invitrogen) and kept in T cell medium (chapter 2.6). Naïve CD4⁺ T cells were stimulated for 36 – 48 h under Th1 conditions (on surfaces coated with goat anti-hamster immunoglobulin G) with soluble anti-CD3 (0.1 µg/ml) and anti-CD28 (1 µg/ml), anti-interleukin 4 (10 µg/ml) and recombinant IL-12 (10 ng/ml). Stimulation of naïve CD4⁺ T cells under Th0 conditions was done with soluble anti-CD3 (0.1 µg/ml) and anti-CD28 (1 µg/ml) on surfaces coated with goat anti-hamster immunoglobulin G. Cells were normally kept in an incubator adjusted to 5 % CO₂ and 37 °C. After being stimulated for at least 36 h cell populations were expanded in T cell media supplemented with Proleukin S (200 IE/ml, IL2-analog) for additional 2 or 3 days. One day before activation, cells were cultured in T cell media (without Proleukin S).

3.1.2 Activation of primary Th0/Th1 cells

T cells were activated with plate-bound goat anti-hamster immunoglobulin G or plate-bound anti-CD3 (5 µg/ml) and/or soluble anti-CD3 (1 µg/ml) and anti-CD28 (2.5 µg/ml). T cells were also activated with PMA (25 ng/ml) and ionomycin (1 µg/ml) if indicated.

3.1.3 Intracellular cytokine staining and flow cytometry

For intracellular cytokine staining, cells were fixed in 4 % PFA for 10 min at room temperature (RT), permeabilized in FACS buffer (intracellular) and stained with antibodies against e.g. IFN γ . Flow cytometry was all recorded with FACSAriaIII and analyzed with Flow Jo software.

3.1.4 GFP spike-in assay

The GFP control plasmid of the Mouse T Cell Nucleofector Kit was transfected into expanding Th1 cells 12 – 15 h after differentiation according to manufacturer's instructions. The cells were activated and RNA was taken at indicated time points for qRT-PCR. Genes of interest were normalized to GFP expression.

3.2 Handling of nucleic acids

3.2.1 RNA extraction

For RNA isolation samples were lysed with QIAzol lysis reagent by pipet mixing and incubated for 5 min. Lysed cells were frozen or immediately proceeded by addition of chloroform (200 μ l / ml Qiazol lysis reagent). Samples were shaken vigorously, incubated at RT for 2 min and centrifuged at 12,000 g for 15 min at 4 °C. The aqueous phase was transferred to a new 1.5 ml vial and precipitated with 500 μ l isopropanol and 1 μ l coprecipitant (e.g. GlycoBlue). The solution was centrifuged at 12,000 g for 10 min at 4 °C. The RNA pellet was washed with 1 ml freshly prepared ethanol (75 %) and by centrifuging for 7,600 g and 5 min at 4 °C. The supernatant was removed completely and the air-dried for ~5 min. RNA was eluted in nuclease-free water at 60 °C for 5 min.

3.2.2 Subcellular fractionation

40 - 60 x 10⁶ T cells were washed once in ice cold phosphate-buffered saline (PBS) in 15 ml conical tubes (250 rpm, 6 min, 4 °C). The cell pellets were resuspended in 250 μ l ice cold cytoplasmic lysis buffer using wide orifice tips and incubated on ice for 5 min. The lysate was layered on top of 1 ml cold sucrose buffer, and centrifuged in microfuge tubes at 10,000 rpm for 2 min at 4 °C. 10 % of the supernatant volume (\cong cytoplasmic fraction) was used for immunoblot analysis.

The nuclear pellet was gently resuspended in 250 μ l ice cold glycerol buffer using wide orifice tips. An additional 250 μ l of ice cold nuclei lysis buffer was added to the samples, followed by a pulsed vortexing and incubation on ice for 1 min. Samples were spun in microfuge tubes for 2 min at 14,000 rpm and 4 °C. The supernatant represented the nucleoplasmic fraction and 10 % of supernatant was kept for immunoblot analysis.

50 μ l of ice cold PBS was added to the remaining chromatin pellet and vortexed vigorously to fully resuspend. The solution was centrifuged and 5 μ l of the supernatant was collected for

immunoblot analysis. The pellet was lysed in 500 μ l QIAzol lysis reagent and vigorously vortexed to resuspend the chromatin. Chromatin-associated RNA was extracted by adding 100 μ l chloroform and incubated at room temperature for 5 min. The chromatin samples were then centrifuged in microfuge tubes for 15 min at 13,000 rpm at 4 °C. The resulting upper aqueous layer was then added to 3.5 x volumes QIAGEN RLT buffer from the RNeasy MinElute Cleanup Kit.

RNA purification was performed according to the manufacturer's instructions.

3.3 cDNA synthesis and qRT-PCR

For all RNAs, except fractionated RNAs, cDNA was synthesized with QuantiTect Reverse Transcription Kit with genomic wipeout according to the manufacturer's instructions. For nuclear RNA random hexamer and oligo d(T) primer were used and for chromatin associated RNA only oligo d(T) primer were used. Complete removal of genomic DNA was confirmed with primer pairs for genes that are not expressed. Amount of introns was normalized to exons (Δ ct-method) per gene at each time point and fold change was calculated.

All primer pairs were tested for efficiency and qRT-PCR was performed by the SYBR green method on a ViiA 7 real-time PCR system. Primer pairs are given in chapter 2.2.

3.4 Western Blot

For western blot analysis, cells were washed once with PBS and resuspended in RIPA lysis buffer with freshly added DTT (1 mM), protease inhibitor and if required phosphatase inhibitor. Cells were incubated for 15 min on ice and centrifuged at 10.000 rpm. One part of the supernatant was transferred to a tube for determining protein concentration (BCA assay) and the other part to a tube containing 4 x Laemmli sample buffer and heated at 95 °C for 5 min. Equal amounts of protein lysate were loaded on a 8 % - 12 % SDS polyacrylamide gel, depending on the protein size. Samples were run for ~100 min at 100 V to separate proteins according to their molecular weight and proteins were blotted on a polyvinylidenfluoride (PVDF) membrane at 20 V and 4 °C over night in blotting buffer. Membranes were blocked with 5 % milk dissolved in TBS for 1 h at room temperature on a shaker. Afterwards the membrane was washed twice with water (Milli-Q) and once with TBST. The primary antibody (dissolved in 1 % milk in TBST) was incubated for 90 min at room temperature. The membrane was washed twice with TBST for 10 min, each. Secondary antibody (horseradish

peroxidase coupled, dissolved in 1 % TBS in milk) was incubated for 45 min at room temperature and washed for 5 min with TBST, TBS and water (Milli-Q), each. The membrane was stained with ECL prime western blotting detection reagent and chemiluminescence was detected by photosensitive films.

3.5 4sU-labeling

The protocol for 4sU-labeling of T cells was modified from Rädle, *et al.* (Rädle *et al.*, 2013). Fast and gentle handling during the experiment was important to ensure identical labeling times and time points for comparison with the replicate, ribosome profiling and CHIP-seq.

Start of labeling:

4sU was thawed just before use, added at each time point directly to the medium containing the cells ($\geq 20 \times 10^6$ cells per sample) and mixed gently. At the end of labeling cells were centrifuged at 330 x g for 5 min at 4 °C in polypropylene tubes (which resist high g forces) and Qiazol was added (≥ 1 ml per 3×10^6 cells) to each tube. The pellet was fully resuspended, incubated for 5 min at room temperature and samples were frozen at -20 °C. Those samples can be stored at -20 °C for at least 1 month.

RNA preparation using modified Qiazol protocol:

0.2 ml chloroform per 1 ml Qiazol was added and thoroughly mixed by shaking for 15 s. RNA preparation was performed as mentioned in the metabolic labeling protocol (step 1-12, 2. RNA preparation using modified trizol protocol) from Rädle *et al.* (Rädle *et al.*, 2013). RNA concentration was measured on a Nanodrop 2000, according to manufacturer's instructions. This RNA was also used for total RNA-seq and stored at -80 °C for at least 1 month.

Thiol-specific biotinylation of newly transcribed RNA:

Between 30 μ g - 60 μ g of total cellular RNA were used for thiol-specific biotinylation. Whenever possible biotinylation was performed using 60 μ g RNA to recover sufficient yields of newly transcribed RNA.

Labeling reaction was prepared by pipetting in the following order (per μ g RNA):

1 μ l 10x Biotinylation Buffer

7 μ l RNA (containing 1 μ g RNA diluted in nuclease-free H₂O)

2 μ l biotin-HPDP (1 mg/ml)

Biotin-HPDP was added last, mixed immediately by pipetting and incubated at room temperature for 1.5 h with rotation. 2 ml Phase Lock Gel (PLG) tubes were centrifuged at 15,000 x g for 2 min. The total amount of biotinylated RNA was pipetted into the pre-spun 2 ml PLG tube, an equal volume of chloroform was added and mixed vigorously. Samples were incubated for 2 - 3 min until the phases begun to separate and bubbles started to disappear. The samples were centrifuged at 15,000 x g for 15 min at 4 °C and the upper aqueous phase was transferred into a new tube. This chloroform extraction step using a PLG tube was repeated once. Next, 10 % the volume of NaCl (5 M) and an equal volume of isopropanol was added to the aqueous phase. The sample was centrifuged at 20,000 x g for 20 min at 4 °C and supernatant was discarded afterwards. An equal volume freshly prepared 75 % ethanol was added, centrifuged at 20,000 x g and the supernatant discarded. After briefly spinning and removing remaining ethanol, RNA was fully resuspended in 30 - 100 μ l H₂O (~1 μ l per 1 μ g input RNA) by pipette mixing. At this step an aliquot was taken to verify RNA integrity by electrophoretical analysis on a Bioanalyzer.

Separation of newly transcribed (labeled) and preexisting (unlabeled) RNA:

Since there was no interest in small RNAs like miRNAs purification of newly transcribed RNA was performed with Solid Phase Reversible Immobilization (SPRI) beads (Agencourt RNACleanXP). To ensure proper purification, beads were removed from 4 °C storage and let stand for at least 30 min to bring them at room temperature. 4sU Washing Buffer (3 ml per sample) was heated to 65 °C and 100 mM dithiothreitol (DTT) solution was prepared. DTT (always prepared fresh) was weighted on an ultra-fine scale and required amount of nuclease-free water added. Biotinylated RNA samples were heated to 65 °C for 10 min to denature and immediately placed on ice. 100 μ l streptavidin beads were added to biotinylated RNA and incubated at room temperature for 15 min with rotation. Next, a μ Macs column per sample was placed into the magnetic stand and each μ Macs column was pre-equilibrated with 1 ml room temperature 4sU Washing Buffer. The RNA/beads mix was now applied to the columns. The flow-through was discarded unless there was interest in the recovery of unlabeled RNA. If so, the flow-through and the first wash were collected, since this contains the majority of unlabeled RNA. Recovery of unlabeled RNA was performed with RNAClean XP beads according to the manufacturer's guideline. The RNA/bead mix was washed three times with 0.9 ml preheated 4sU Washing Buffer and three

times with 0.9 ml room temperature 4sU Washing Buffer. For recovery of newly transcribed RNA 400 μ l of well-dispersed room temperature RNACleanXP beads were pipetted in a tube per sample and placed each underneath a μ Macs column. Newly transcribed RNA was eluted with 100 μ l 100 mM DTT. After 3 min a second elution with 100 μ l 100 mM DTT was performed. The newly transcribed RNA/beads solution was thoroughly mixed by pipette mixing 10 times and processed according to the manufacturer's guideline. RNA was first eluted in 32 μ l and later in 11 μ l nuclease-free H₂O. RNA was quantified using a Qubit 2.0 fluorometer. This RNA was stored at -80 °C for at least 1 month.

3.5.1 Toxicity test of 4sU-labeling

Cells were treated with 4sU for indicated time points and BH3I-1 (500 ng/ μ l) for 1h or heat shock for 5 min at 95 °C was used to induce apoptosis. Apoptotic cells were determined by Annexin V/7-AAD staining and analyzed by flow cytometry. Nuclear stress was determined by p53 accumulation, cytoplasmic stress by eIF2 α phosphorylation and thapsigargin (0.5 μ M) was used as positive control.

3.5.2 Nuclear and cytoplasmic stress test for 4sU-labeling

To determine nuclear and cytoplasmic stress upon 4sU treatment, western blot analysis was performed as described in chapter 3.4. Nuclear stress was determined by p53 accumulation, cytoplasmic stress by eIF2 α phosphorylation and thapsigargin was used as a positive control for the latter.

3.6 Ribosome Profiling

Ribosome Profiling was performed according to the TruSeq Ribo Profile Library Prep Kit from Illumina (Mammalian), with little modifications.

Preparation and isolation of ribosome protected fragments (RPFs):

Cells of each time point ($\geq 20 \times 10^6$) were collected and pooled into one polypropylene tube, each. Final concentration was adjusted to 1×10^6 cells per ml of T cell media. Cycloheximide was added to a final concentration of 0.1 mg/ml, mixed by inverting the polypropylene tube and incubated for 1 min. Cells were centrifuged for 5 min at 330 x g at 4 °C. The medium was aspirated and cells were washed with at least 10 ml PBS supplemented with cycloheximide (final concentration of 0.1 mg/ml). Cells were centrifuged for 5 min at 330 x g at 4 °C. The

medium was aspirated and 100 μ l Mammalian Lysis Buffer per 10×10^6 cells was added. The solution was mixed by pipetting and expelled through a sterile 22 - 25 gauge needle to lyse the cells completely.

The cell lysate was transferred to a precooled tube and incubated for 10 min on ice with periodic inversions. After centrifuging for 10 min at 20,000 g at 4 °C to clarify the lysate, the supernatant was transferred to a precooled tube. A 1:10 dilution of the lysate was prepared with nuclease-free water and an A_{260} reading recorded using the Nanodrop 2000. Nuclease-free water was used as blank and a 1:10 dilution of Mammalian Lysis Buffer as standard. The A_{260} /ml concentration of the lysate was calculated according to the following equation:

$$(A_{260} \text{ cell lysate} - A_{260} \text{ Mammalian Lysis Buffer}) \times 10 \text{ dilution factor} = A_{260}/\text{ml}$$

200 μ l aliquots of the lysate were created on ice. This was immediately followed by nuclease treatment.

Ribosome footprinting with TruSeq Ribo Profile Nuclease:

Nuclease treatment was performed immediately without freezing the lysate. 7.5 units of TruSeq Ribo Profile Nuclease were added for each A_{260} of lysate.

For example: 80 A_{260} /ml lysate x 0.2 ml lysate x 7.5 U/ A_{260} TruSeq Ribo Profile Nuclease = 120 U TruSeq Ribo Profile Nuclease. The nuclease reaction was incubated for 45 min at room temperature with gentle mixing. 200 μ l aliquots of the lysate were frozen with liquid nitrogen and either stored them at -80 °C or directly stopped the nuclease reaction by adding 15 μ l RNase Inhibitor to each 200 μ l aliquot.

Purification of RPFs:

In case of freezing the cells immediately after the nuclease reaction, nuclease digested RPFs were unfrozen and 15 μ l RNase Inhibitor was added on ice. RPFs were purified according to Illumina's TruSeq Ribo Profile (Mammalian) Kit User Guide. Column purification was performed (step 1-7, MicroSpin S-400 Columns). RNA concentration was measured on a Nanodrop 2000.

rRNA depletion:

For rRNA depletion, best results were achieved when 5 μ g of purified RPFs were used. rRNA depletion was performed according to Illumina's TruSeq Ribo Profile (Mammalian) Kit User

Guide (step 1-2, Primary rRNA depletion) and RNA concentration was measured on a Nanodrop 2000.

PAGE purification of RPFs:

500 ng of rRNA depleted RPFs were used for PAGE purification. If less than 500 ng of RPFs were recovered, rRNA depletion was repeated and purified RPFs were pooled with RNA Clean & Concentrator-5 columns. Alternatively, they were loaded next to each other on the gel and gel slices were pooled during RNA elution from the gel.

TruSeq Ribo Profile RNA Control, samples and ladder for PAGE purification were prepared as follows:

- a) 5 μ l TruSeq Ribo Profile RNA Control and 5 μ l denaturing gel loading dye were mixed in a 0.5 ml microcentrifuge tube.
- b) 10 μ l of each RPF were mixed with 10 μ l of denaturing gel loading, respectively.
- c) A ladder aliquot (4 μ l 20/100 ladder, 1 μ l nuclease-free water, 5 μ l denaturing gel loading dye) was prepared and loaded between each sample and control to prevent cross-contamination.

Samples and ladder were denatured by incubating at 95 °C for 5 min and immediately placed on ice. 20 μ l of each sample separated by 10 μ l of prepared ladder were loaded onto a 12 % or 15 % urea-polyacrylamide gel. Additionally, 10 μ l of TruSeq Ribo Profile RNA Control were loaded. The gel was run until the bromphenol blue band reached bottom of the gel (180 V, ~70 min) and stained with pre-chilled SYBR Gold at 4 °C. We used a UVP GelDoc Imager to visualize the RNA. Gel slices for each sample corresponding to ~28 and 30 nt in length were excised. Since RPFs were hardly visible we excised slices at the size indicated by the Ribo Profile RNA Control, which we excised, too. To elute RNA, a hole was punched in the bottom of 0.5 ml microcentrifuge tubes with a sterile 20 gauge needle. Afterwards, each gel slice was transferred into a separate tube and placed capped tubes in a 1.5 ml tube. The samples were centrifuged for 2 min at 12,000 g. This step was repeated if gel slices were not completely shred into the 1.5 ml tube. The RNA was eluted from disrupted gel slices with 400 μ l nuclease-free water, 40 μ l ammonium acetate (5 M) and 2 μ l SDS (10 %) each overnight at 4 °C. Afterwards, the slurry was transferred to 1.5 ml filter tubes (provided by Illumina) with a 1 ml pipette tip (wide-bore tip or self-made 1 ml tip with cut end) and centrifuged for 3 min at 2,000 g to separate eluted RNA from gel slices. The aqueous solution was gently pipetted into a 1.5 ml tube. 2 μ l glycogen (provided by Illumina) and 700 μ l 100 %

isopropanol were added and the tubes were stored at -20 °C for at least 1 h. Next, samples were centrifuged at 4 °C for 20 min at 13,000 g and the supernatant was discarded. The pellet was washed with pre-chilled freshly prepared 80 % ethanol at 4 °C for 10 min at 13,000 g. The supernatant was discarded and air-dried. Each sample was resuspended in 20 µl and the Ribo Profile RNA Control in 8 µl of nuclease-free water. These samples were stored at -20 °C.

Fragmentation, end repair, 3' adaptor ligation and reverse transcription:

These steps were performed as described by Illumina's TruSeq Ribo Profile (Mammalian) Kit User Guide (Fragmentation and end repair, 3' adapter ligation, reverse transcription).

PAGE purification of cDNA:

Samples, TruSeq Ribo Profile RNA Control and ladder for PAGE purification were prepared as follows:

- a) 10 µl of each sample and RNA Control were mixed with 10 µl denaturing gel loading dye, respectively.
- b) A ladder aliquot (4 µl 20/100 ladder, 1 µl nuclease-free water, 5 µl denaturing gel loading dye) was prepared and loaded between each sample and control to prevent cross-contamination.

To denature samples and ladder both were incubated at 95 °C for 5 min and immediately placed on ice. 20 µl of each sample separated by 10 µl of prepared ladder were loaded onto a 10 % polyacrylamide/7-8 M urea/TBE gel. Additionally, 10 µl of TruSeq Ribo Profile RNA Control were loaded. The gel was run until the bromphenol blue completely migrates out of the gel (180 V, ~60 min) and stained with pre-chilled SYBR Gold at 4 °C. A UVP GelDoc Imager was used to visualize the RNA and excised the gel slices for each sample corresponding to ~70 - 80 nt. Afterwards, RNA elution from gel slices was performed as described above and each sample was resuspended in 10 µl nuclease-free water.

cDNA circularization:

CircLigase mastermix was prepared for all reactions by combining the following reagents for each sample on ice:

4.0 µl TruSeq Ribo Profile CL Reaction Mix

2.0 µl ATP

2.0 μ l MnCl₂

2.0 μ l CircLigase

10 μ l of the mastermix were added to each sample. They were mixed gently and centrifuged briefly. Samples were incubated at 60 °C for 2 h and immediately placed on ice.

PCR amplification and library verification:

PCR amplification was performed according to Illumina's TruSeq Ribo Profile (Mammalian) Kit User Guide (step 1-3, PCR amplification). For primary T cells best results were achieved when 4 μ l of circularized cDNA was used for amplification with 9 PCR cycles.

Libraries were purified and their size distribution was checked according to Illumina's TruSeq Ribo Profile (Mammalian) Kit User Guide (step 4-8, PCR amplification). The expected size of the amplified cDNA library is 140 - 160 bp (see Figure 10).

3.7 Chromatin immunoprecipitation (ChIP)

To perform ChIP, a modified protocol from Blecher-Gonen *et al.* was used (Blecher-Gonen *et al.*, 2013).

Crosslinking and harvesting the cells:

At least 20 x 10⁶ cells for each time point were crosslinked with a final concentration of 1 % formaldehyde in T cell medium for 10 min at room temperature with gentle rocking. Crosslinking reaction was stopped by the addition of glycine to a final concentration of 0.125 M. Cells were centrifuged at 330 x g for 5 min at 4 °C and the supernatant was discarded. Cells were washed in ice-cold PBS and repeated the last two steps for a total of three washes. Afterwards, the cell pellet was frozen at -80 °C. Frozen pellets can be stored for at least 6 months.

Cell lysis and sonication:

During all cell lysis and sonication steps, samples were kept on ice or at 4 °C to minimize crosslink reversal and protein degradation. The cell pellets were resuspended in 1 ml ice-cold cell lysis buffer with freshly added protease inhibitors to isolate the nuclei (phosphatase inhibitors were added if necessary). The lysate was incubated for 10 min on ice and centrifuged at 5,000 rpm for 5 min at 4 °C. The supernatant was aspirated and the nuclei

pellet resuspended in 1 ml ice-cold nuclei lysis buffer with freshly added protease inhibitors (phosphatase inhibitors were added if necessary). Samples were incubated for 10 min on ice. Cells were sonicated to generate a mean DNA size fraction of 0.2 - 1.0 kb using a bioruptor sonication device. 20 - 25 cycles (30 s on, 30 s at high) were performed in two 1.5 ml bioruptor microtubes with 500 µl each tube. 20 - 50 µl aliquot were taken of the sheared chromatin and heated for 10 min at 95 °C and 1,000 rpm shaking to perform a fast reverse crosslink and verify chromatin size. 2 - 5 µl Proteinase K were added and incubated for 20 min at 56 °C and 1,000 rpm shaking. Heat inactivation was performed for 10 min at 95 °C and 1,000 rpm shaking. Chromatin was purified with the MinElute PCR Purification Kit and chromatin size verified on a 1 % agarose gel using a 100 bp Plus Marker. The sheared chromatin with a mean DNA size fraction of 0.2 - 1.0 kb was centrifuged for 10 min at 14,000 rpm and 4 °C to pellet insoluble chromatin and debris. The supernatant was transferred to a new tube and kept on ice. 5 - 10 % of the sonicated chromatin was kept as input and frozen at -20 °C until needed.

Couple antibody to beads:

10 µg antibody (e.g. anti-RNAPII) were coupled in 220 µl PBS (with 0.5 % BSA and 0.5 % Tween 20) to 80 µl Dynabeads protein G for at least 1 h at room temperature with rotation. Afterwards, tubes containing coupled beads were placed on a magnet and waited until all beads were bound to the magnet. The supernatant was removed and beads further blocked with 6 µl sonicated salmon sperm DNA in PBS (with 0.5 % BSA and 0.5 % Tween 20) for 30 min at room temperature with rotation. The tubes were placed on a magnet and we waited until all beads were bound to the magnet. The clear supernatant was removed and beads were washed with ChIP IP buffer three times.

Chromatin immunoprecipitation:

Chromatin was diluted to 1 ml total volume in nuclei lysis buffer with freshly added protease inhibitors (phosphatase inhibitors were added if necessary). Next, ChIP IP buffer, freshly supplied with protease inhibitors (phosphatase inhibitors were added if necessary) was added to a final volume of 3 ml. The solution was kept on ice or at 4 °C while antibody is coupled to the beads. Afterwards, the diluted chromatin was added to the antibody coupled beads and incubated over night at 4 °C with gentle rotation.

Afterwards the chromatin/beads solution was washed with following buffers (1 ml each) at room temperature for 5 min with rotation:

- Buffer I (0.1 % SDS; 1 % Triton X-100; 2 mM EDTA; 20 mM Tris-HCL pH 8.1; 150 mM NaCl)
- Buffer II (0.1 % SDS; 1 % Triton X-100; 2 mM EDTA; 20 mM Tris-HCL pH 8.1; 500 mM NaCl)
- Buffer III (0.25 M LiCl; 1% NP-40; 1 mM EDTA; 10 mM Tris-HCl, pH 8.1)
- 2x TE pH 8.0

After each wash, the tubes were placed back on the magnet and the supernatant was removed. Supernatant was discarded and air-dried for ~ 5 min.

Reverse crosslinking:

To elute protein-DNA complexes from the beads, samples were removed from the magnet, 50 µl elution buffer was added and mixed by pipetting. From now on, the input sample(s) from above was included. Elution buffer was added to input sample(s) for a final volume of 50 µl (to keep the buffer composition similar to the ChIP samples) and processed together with the ChIP samples. 3 µl of elution buffer and 2 µl of RNase (DNase free) were mixed. 5 µl of the mix were added to each sample and incubated for 30 min at 37 °C. Next, 2.5 µl proteinase K, 1 µl glycogen and 1.5 µl elution buffer were mixed (per sample). 5 µl of the mix was added to each sample (1 U proteinase K and 20 µg glycogen per sample) and incubated for 2 h at 37 °C. Afterward, the samples were incubated at 65 °C overnight (at least 4 h) with shaking to perform reverse crosslinking. The tubes were placed on the magnet for at least 30 s and transferred the supernatant to a new tube. Samples can be frozen at -20 °C for up to 12 months.

DNA purification and verification:

140 µl of well-dispersed room-temperature SPRI beads were added to 60 µl of sample (2.3x ratio) and carefully pipetted up and down 25 times to mix thoroughly until the liquid in each tube was homogenous. Samples were incubated at room temperature for 2 min and placed on the magnet until all beads were bound to the magnet. The supernatant was discarded and 200 µl of freshly prepared 70 % ethanol were added with tubes left on the magnet. Samples were incubated for 30 s without disturbing the beads. Afterwards, the supernatant was discarded and the washing step with ethanol repeated once more. Finally, ethanol was

aspirated completely and the SPRI beads air-dried for 4 min. The tubes were removed from the magnet and 20 μ l 10 mM Tris-HCl (pH 8.0) was added. The entire volume was gently pipetted up and down 25 times to mix thoroughly. Samples were incubated for 2 min at room temperature. Next, the tubes were placed back on the magnet for 4 min and the supernatant was transferred to another tube. The amount of DNA was quantified with a Qubit 2.0 fluorometer. Successful ChIP was verified by qPCR (1 μ l diluted in 100 μ l H₂O; 2 - 5 μ l were used for qPCR). Specific primers for a positive (known binding site of your protein) and negative control (e.g. a gene that is silent and/or not a target of your protein of interest) were used.

3.8 Next generation sequencing

Library preparation was performed with specific kits for each sequencing method. While appropriate kits for total RNA, 4sU RNA and ChIP library preparation had to be chosen, library preparation for ribosome profiling was included in the kit.

3.8.1 Library preparation for RNA-seq and 4sU-seq

For both total and 4sU RNA samples, library preparation and rRNA depletion was performed using the TruSeq Stranded Total RNA Library Prep Kit (Illumina) starting with 400 ng RNA as input for each sample and creating a strand specific library. Only 11 cycles were used for PCR amplification to minimize PCR bias. Amplified cDNA libraries were further purified using Agencourt RNAClean XP Beads and quality control of cDNA libraries were performed using Agilent Bioanalyzer with High Sensitivity DNA Reagents.

3.8.2 Ribosome Profiling

Illumina's TruSeq Ribo Profile (Mammalian) Kit generates a cDNA library suitable for sequencing.

3.8.3 Library preparation for ChIP-seq

Library preparation was performed with 2 ng of ChIP DNA using Kapa's ChIP library preparation kit according to the manufacturer's instructions.

3.8.4 Sequencing

Barcoded libraries were sequenced on a HiSeq 4000 with paired-end, 100 bp reads at the HelmholtzZentrum München, Neuherberg according to the manufacturer's guidelines. Pooled RNA-seq and 4sU-seq samples were sequenced, yielding $\sim 40 \times 10^6$ reads, Ribosome Profiling samples, yielding $\sim 80 \times 10^6$ reads and ChIP-seq samples, yielding $\sim 40 - 60 \times 10^6$ reads.

3.9 Bioinformatics and statistical analysis

Prof. Dr. Caroline Friedel performed analysis described in 3.9.1 - 3.9.3 as well as parts of further analysis (3.9.4. - 3.9.6).

3.9.1 Adapter trimming and mapping

Sequencing quality was assessed with FastQC (<https://www.bioinformatics.babraham.ac.uk/projects/fastqc/>) and sequencing adapters were trimmed using cutadapt (Martin, 2011). Reads were mapped against the mm10 mouse reference genome and rRNA sequences using ContextMap version 2.5.2, except data from 4.1.3, which was mapped against the mm9 mouse reference genome using TopHat (Bonfert *et al.*, 2015; Trapnell *et al.*, 2009). For 4sU and total RNA, reads were mapped in paired-end mode. For ribosome-associated mRNA, the sequence of the ~ 30 nt ribosome-protected mRNA was determined first as the consensus sequence from both mates of a read pair and then mapped in single-end mode to the coding sequence of a gene. ChIP-Seq reads were aligned to the mouse mm10 reference genome using BWA-MEM version 0.7.13 and PCR duplicates removed using Picard Tools version 1.119 (Li and Durbin, 2009)(<https://broadinstitute.github.io/picard/>). For visualization, mapped reads were converted to bedGraph using the HOMER software suite version 4.8.3 (Heinz *et al.*, 2010). Peaks were called over input using MACS2 version 2.1.0 with an FDR threshold of 0.05. RNAPII promoter and gene body FPKM was determined as for RNA-Seq by counting reads with featureCounts on the promoter ($TSS \pm 500nt$) or the gene body (including exons and introns) and normalizing to promoter/gene length and sequencing depth (Zhang *et al.*, 2008). For visualization of mapped reads, the UCSC genome browser and the integrative genomics viewer (IGV) were used (Kent *et al.*, 2002; Robinson *et al.*, 2011).

3.9.2 Gene expression and normalization

To calculate FPKM (Fragments Per Kilobase Of Exon Per Million Fragments Mapped) values, fragment counts per gene were calculated using the `featureCounts` program from the `subread` package version 1.4.6-p3. For ribosome-associated mRNA, only fragments mapped to the coding sequence were counted. FPKM values were additionally normalized by the median fold changes of ~3,400 housekeeping genes according to a recent publication (Eisenberg and Levanon, 2013).

Evaluation was restricted to genes that fulfill the following criteria. The FPKM has to be ≥ 1 for at least one sample of 4sU RNA, RP or total RNA, respectively. The gene has further to be annotated as protein-coding without being a pseudogene or a predicted gene. Finally, each coding sequence of all RP samples has to be covered by at least 15 % unique reads or unique reads of all RP samples have to be at least 40 % of the overall reads of the coding sequence. All in all, this resulted in a total of 9.420 protein-coding genes that were included for subsequent analysis.

3.9.3 Turnover and translation rates

For calculation of RNA turnover rates from ratios of 4sU- to total RNA, normalization is based on median turnover rates (e.g. assuming an RNA half-life of 5h) (Friedel and Dolken, 2009).

3.9.4 R

Downstream analysis with normalized sequencing data was performed in R (Team, 2016). Tools provided by the Bioconductor project were used to generate plots (Huber *et al.*, 2015).

3.9.5 EnrichR

Enrichment analysis for experimentally-determined transcription factor binding was performed using EnrichR (Chen *et al.*, 2013).

3.9.6 DAVID

Functional enrichment analysis was performed using the DAVID webserver (Huang *et al.*, 2009).

4 Results

The presented experiments were performed in cooperation with the co-author of the publications in Cell Reports and JoVE, Dr. Kathrin Davari (HelmholtzZentrum München) and results in this chapter have been published to some extent in both journals (Lichti, Davari *et al.*, 2017; Lichti, Davari *et al.*, in revision). This may include figures and argumentation. The contribution of collaborators to the presented data is fully depicted in chapter 7.

4.1 Establishment of methods

4.1.1 4sU-labeling – verify optimal conditions without perturbing cell physiology

To test optimal conditions for 4sU labeling it was inevitable to perform some preliminary tests, although it was previously suggested that 4sU shows minimal interference to cell growth and gene expression (Dolken *et al.*, 2008; Kenzelmann *et al.*, 2007). Nevertheless, it was observed that elevated concentrations of 4sU could influence cellular processes, inhibit rRNA synthesis and cause a nucleolar stress response (Burger *et al.*, 2013). Since this would ultimately alter the results of the sequencing data, 4sU-labeling conditions were carefully validated. First, cell apoptosis was analyzed by FACS analysis. For this purpose, *in vitro* generated Th0 cells were activated and treated with 4sU for 0.5 h, 1 h and 2 h, respectively. After personal correspondence with Prof. Dr. Dölken, we decided to label T cells for 0.5 h with 500 μ M 4sU and for longer time points with 200 μ M 4sU to exclude stress response. The cells were stained for Annexin V (ANXA5), which is used to determine cells undergoing apoptosis and for 7-aminoactinomycin D (7-AAD) which detects nonviable cells (Zimmermann and Meyer, 2011). ANXA5 binds to the membrane phospholipid phosphatidylserine (PS) which is translocated to the cell surface upon loss of plasma membrane, an early feature of apoptosis (Lecoeur *et al.*, 1997). 7-AAD binds GC regions of the DNA accessible in late apoptotic cells and necrotic cells that lost cell membrane integrity (Schmid *et al.*, 1994). Different concentrations of the apoptosis inducer BH3I-1 were used as a positive control for cells that become apoptotic, whereas heat exposure for 5 min at 95 °C lead to rapid cell death indicated by Annexin V and 7-AAD double positive

cells. As shown in Figure 5A even 2 h exposure of Th0 cells with 200 μ M 4sU does not induce apoptosis compared to untreated cells.

Furthermore, we wanted to rule out the possibility of a nucleolar stress response in 4sU labeled cells. It was shown that the nucleolar phosphoprotein nucleoplamin (NPM1) translocates to the nucleoplasm upon stress, which stabilizes p53 and blocks cell cycle progression (Kurki *et al.*, 2004; Chan *et al.*, 1996). Although elevated 4sU concentrations can strongly induce p53, as shown by others (Burger *et al.*, 2013) and us (Figure 5B), it is not induced upon 0.5 h as well as 1 h treatment and just mildly upon 2 h treatment.

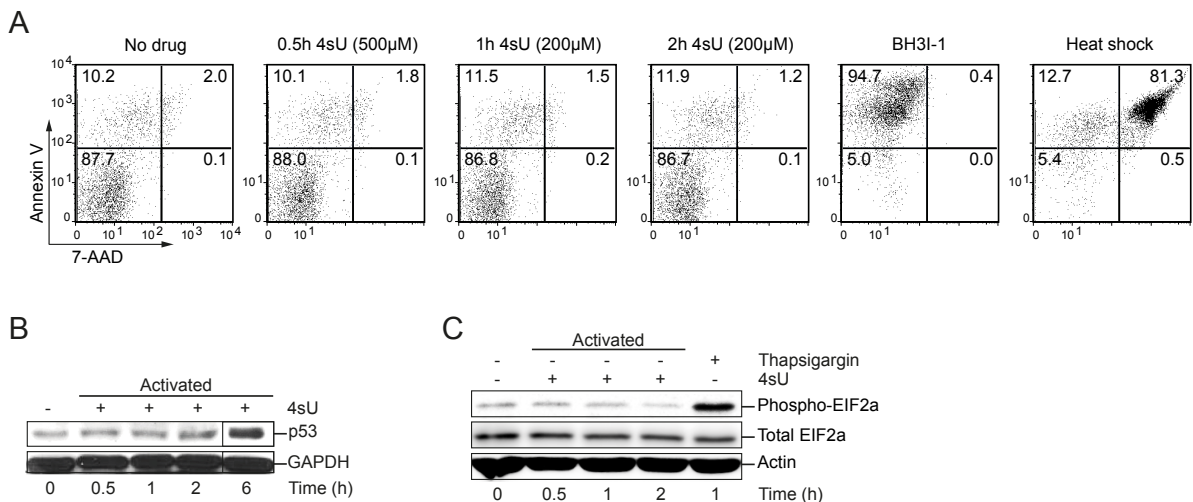


Figure 5: Verification of optimal 4sU-labeling conditions without perturbing cell physiology (Lichti, Davari *et al.*, 2017)

(A) Detection of cell apoptosis by FACS analysis. *In vitro* generated Th0 cells were treated with different concentrations of 4sU (indicated in brackets) for 0.5 h, 1 h and 2 h, respectively. BH3-1 treatment was used to induce apoptosis determined by Annexin V, whereas heat shock (5 min at 95 $^{\circ}$ C) was used to induce cell death determined by 7-AAD. (B) Western blot analysis for p53 of 4sU treated and activated T cells. Cells were labeled with 200 μ M 4sU for the indicated time of activation, except the 0.5 h time point, which was labeled with 500 μ M 4sU. (C) Western blot analysis of phospho-eIF2 α and total eIF2 α in activated T cells with the same labeling conditions as in (B). Thapsigargin was used as a positive control.

Phosphorylation of the eukaryotic translation initiation factor 2 α (eIF2 α) restricts the activity of the guanine nuclear exchange factor eIF2B, which is responsible for the formation of the GTP-eIF2-tRNA^{iMet} ternary complex (Kimball, 1999). Since this complex promotes translation of mRNAs, phosphorylation of eIF2 α is an indicator of a cellular stress response leading to diminished global protein synthesis (Kimball, 1999). Phosphorylation of eIF2 α was verified for defined time points and labeling concentrations by western blot analysis and did not lead to any increase with total eIF2 α levels remaining unchanged (Figure 5C).

Thapsigargin, a known inducer of endoplasmic reticulum (ER) stress response (Thastrup *et al.*, 1990), was used as a positive control and provoked elevated levels of p $\text{eIF2}\alpha$.

All in all, we could verify that we neither induced a nucleolar or cellular stress response nor apoptosis for the conditions of 4sU that were planned to apply.

4.1.2 4sU-labeling – capture of newly transcribed RNA

To test the feasibility of 4sU-labeling for our approach a preliminary test with EL4 cells, a murine tumor cell line, initially isolated from a chemically induced lymphoma (Gorer, 1950), was performed. These cells can – like T cells – be activated by phorbol myristate acetate (PMA) and calcium ionophore ionomycin (Hashimoto *et al.*, 1991). Cells were activated with PMA and ionomycin for 0.5 h or 2 h and labeled with 500 μM or 200 μM 4sU, respectively. To test specific capture of 4sU RNA, cells were also activated with PMA and ionomycin for 2 h without being 4sU labeled (unlabeled control). After isolation of RNA the original protocol recommends to use 60 - 80 μg total RNA for the biotinylation reaction (Radle *et al.*, 2013). This is mainly because lower amounts are hard to see when precipitating RNA. Anyway, we decided to start biotinylation with both, 30 μg and 60 μg for each sample, except the unlabeled control (30 μg). After biotinylating the labeled RNA for 1.5 h, followed by the removal of unbound biotin and RNA precipitation, RNA integrity was verified on an Agilent Technologies 2100 Bioanalyzer using a RNA Nano Chip, which calculates an RNA integrity number (RIN). An algorithm integrating the 28S to 18S ribosomal RNA (rRNA) ratio of electrophoretical measurements calculates the RIN. It assigns a value of 1 to 10 to each RNA sample and higher numbers indicate less degradation (Schroeder *et al.*, 2006). Although intact biotinylated RNA would implement that the respective total RNA is also not degraded, we decided to verify both samples. Figure 6 depicts a representative example of all RNAs which show no traces of RNA degradation, indicated by a RIN of 10. For further processing of the RNA, RIN for eukaryotic samples should be ≥ 8 .

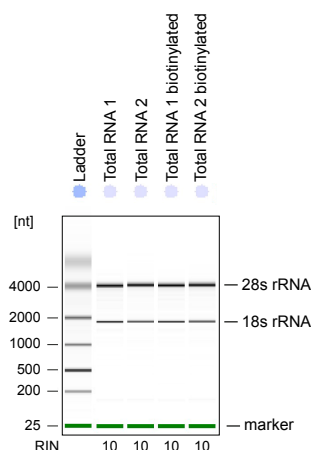


Figure 6: RNA integrity of 4sU labeled RNA (Lichti, Davari *et al.*, in revision)

Representative Bioanalyzer electropherogram showing total RNA (4sU labeled) and biotinylated RNA (4sU labeled) analyzed with an RNA nano chip. 18S rRNA and 28S rRNA are shown and RIN is calculated by the instrument to determine integrity of the RNA. The green line indicates the lower marker.

After proceeding as described in the protocol, newly transcribed RNA was separated from preexisting RNA and eluted in 32 μ l of nuclease-free water (Radle *et al.*, 2013). For library preparation the NEBNext Ultra RNA Library Prep Kit for Illumina was used first, because its applicable starting amount is not restricted to low volumes. Since later on we switched to Illumina's TruSeq Stranded Total RNA Library Prep Kit, which just allows to start with a maximum of 10 μ l, the elution volume had to be decreased. Hence, for all upcoming experiments newly transcribed RNA was recovered with Agencourt RNAClean XP beads and eluted in 11.5 μ l.

It was shown that newly transcribed RNA represents about 1 – 4 % of total RNA upon 1 h of 4sU labeling (Radle *et al.*, 2013). This would result in a maximum of 150 ng/ μ l RNA in our sample which is hard to detect by the absorption based Nanodrop 2000 present in our laboratory. Since at that time no Qubit fluorometer was yet available, recovery of newly transcribed RNA was further validated by qPCR before sequencing the samples. For upcoming experiments, recovery of newly transcribed RNA was quantified by a Qubit 2.0 fluorometer. Reverse transcription was performed with 5 μ l (\cong 21.875 %) of the whole amount of each newly transcribed RNA, including the negative control. The percentage of recovered *Hprt* and *18S rRNA* of each newly transcribed RNA sample, including the negative control, was calculated and compared to biotinylated RNA (Figure 7). As expected, there is hardly any amount of mRNA detectable in the unlabeled control, whereas newly transcribed *Hprt* and *18S rRNA* was measured for the labeled samples. Consistent with prolonged

labeling time and higher starting amounts of biotinylated RNA, recovery of *Hprt* and *18S rRNA* was increased. Afterwards, we proceeded in generating a cDNA library suitable for sequencing.

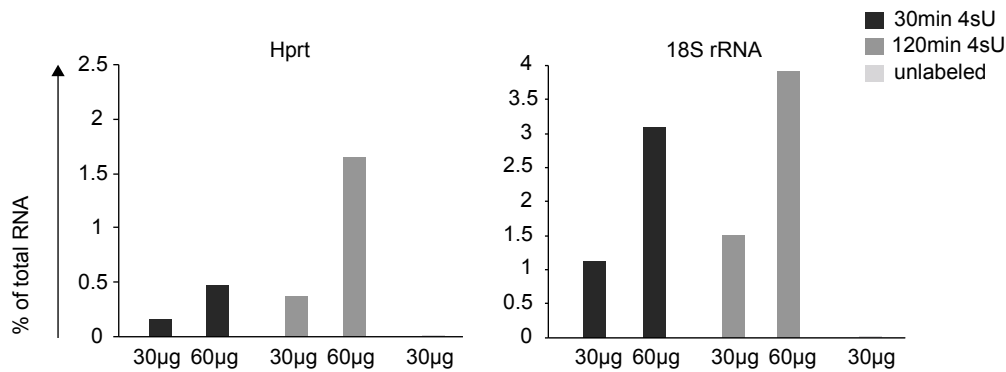


Figure 7: Recovery of *Hprt* and *18S rRNA* in newly transcribed RNA samples

qRT-PCR results of *HPRT* (left) and *18S rRNA* (right) for newly transcribed RNA samples compared to biotinylated RNA. The percentage of recovered newly transcribed RNA is depicted. EL4 cells were activated with PMA and ionomycin and treated with 4sU for the indicated time points. Biotinylation of 4sU-labeled samples was performed with 30 µg and 60 µg, respectively.

4.1.3 4sU-seq – library preparation and verification of the results

The newly transcribed RNA samples, including unlabeled control and total RNA samples were used for library preparation. The prepared cDNA libraries, each marked with a unique single index adapter, were pooled and 2 nm of pooled library was loaded onto a lane of a flow cell. To verify the specificity of the newly transcribed RNA separation, sequenced samples were mapped to the mouse genome and mapping was quantified. The percentage of reads mapped to the mouse genome ranged between 89 - 97 % for all samples except the unlabeled control, which was 1.5 % (Figure 8). These results confirmed the outcome from qPCR, confirming that the pulldown of newly transcribed RNA was specific for 4sU-labeled RNA. We further wanted to verify differences in labeling time. Therefore, the ratio of intronic rate / exonic rate was calculated by simply analyzing reads mapped to intronic regions or exonic regions in the genome. Enhanced labeling time clearly correlated with increased exonic reads consistent with enhanced splicing of short-lived intronic regions over time (Figure 8). Furthermore, we proved that it is also possible to start biotinylation with 30 µg RNA since there are hardly any differences in ratios of intronic rate / exonic rate between samples with same labeling time but different starting amounts of RNA. All in all,

we established 4sU-seq for T cells even for less starting amounts than suggested from the original protocol.

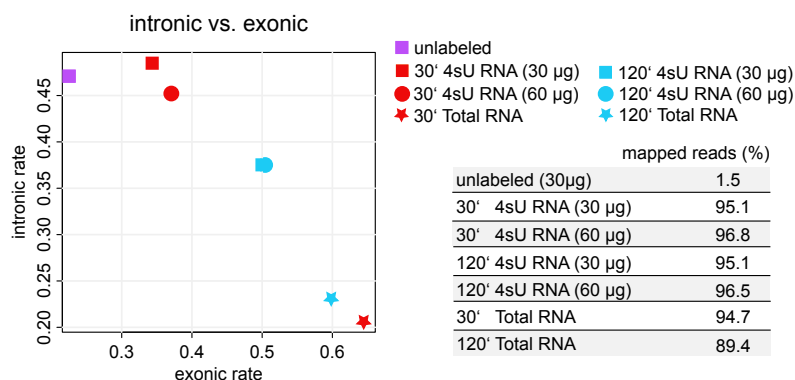


Figure 8: Differences in exonic/intronic rate and mapping statistics for sequenced samples

Exonic and intronic rate is shown for 4sU RNA and Total RNA of EL4 cells activated with PMA and ionomycin for 0.5 h (red) and 2 h (blue) including different amounts of biotinylated RNA, respectively. An unlabeled control (purple) is also shown. Percentage of reads mapped to the genome is given for all samples.

4.1.4 Ribosome Profiling

To establish ribosome profiling, EL4 cells were cultured and either left untreated or activated for 0.5 h with CD3/CD28. Both samples were subsequently treated with cycloheximide to block translational elongation and ribosome profiling was performed as described in the manufacturer's protocol (Illumina's TruSeq Ribo Profile (Mammalian) Kit User Guide). The first main issue that arose when performing ribosome profiling was, that RPFs were hardly visible after PAGE purification so they had to be cut according to the positive control (Figure 9). At this point, it was quite important to cut bands as close as possible to the 28 nt and 30 nt bands indicated by the positive control to exclude short fragments from digested rRNAs and tRNAs. Otherwise these unwanted fragments could become part of the sequencing library and reduce reads for the RPFs. An aggravating factor was that a distinct band at the respective height in the lane of the samples was not visible. We speculated that this could be improved by increasing the amount of nuclease 1.5 times than suggested which should guarantee proper digestion. Also no adverse effects have been reported with increased amounts of nuclease unless starting with degraded RNA. Ribosome profiling was proceeded as recommended in the manufacturer's protocol. This included RNA elution, fragmentation, 3' adapter ligation and reverse transcription (chapter 3.6).

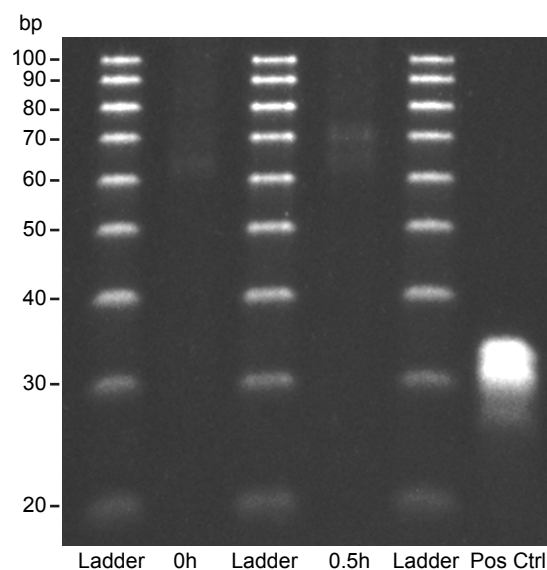


Figure 9: PAGE purification of RPFs

SYBR Gold staining of PAGE purified RPFs. Ladder, RPFs (0h/0.5h) and positive control (Pos Ctrl) are shown. The positive control indicates 28 nt and 30 nt bands.

After amplifying the PAGE purified cDNA as recommended, samples were analyzed by Bioanalyzer (Figure 10). Although cDNA samples had the expected size and the positive control resembled a perfect library, some changes had to be implemented to improve further ribosome profiling experiments and library preparation.

Besides the mentioned improvements, we also speculated that we could increase the yield of the PCR amplified library and decrease undesired products by increasing the amount of the sample. Other than stated in the protocol we decided to load the whole sample (and not just half of it) at both PAGE purification steps. All these changes further improved the result of the ribosome profiling cDNA library. Moreover, excessive amounts of adapters and adapter dimers can be purified by PAGE purification or Agencourt RNA CleanXP beads.

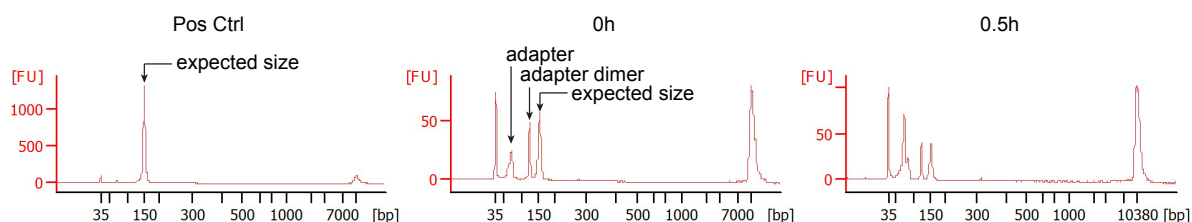


Figure 10: Amplified Ribosome Profiling library

Final ribosome profiling library showing a positive control, as well as non-activated (0h) and 0.5 h activated EL4 cells. The expected size of a good library is indicated, as well as adapter and adapter dimer peaks.

4.1.5 Preliminary test for simultaneous analysis of transcriptional and translation control in activated Th1 cells

Since the main goal was to simultaneously perform 4sU-seq, RNA-seq and ribosome profiling over time during activation of Th1 cells, we decided to perform a preliminary test. For this purpose, *in vitro* generated Th1 cells were activated with CD3/CD28 and samples were labeled with 500 μ M 4sU for 0.5 h. The non-activated sample was labeled for 1 h with 200 μ M 4sU. Ribosome profiling was performed simultaneously for non-activated and 0.5 h activated cells. To directly compare results for newly transcribed and translated RNAs and exclude differences in the starting material, cells were pooled before the treatment. One part of the pooled cells was taken away for the untreated control, while the remaining part was activated and further divided into cells used for 4sU-labeling and ribosome profiling. To verify the activation of the cells, a small aliquot was left in the incubator for 4 h followed by IFN γ detection by FACS analysis. This indicated effective activation of Th1 cells. After library preparation, total RNA (from 4sU labeled RNA samples), newly transcribed RNA and ribosome profiling samples, were pooled and sequenced 100 bp paired-end with 40×10^6 reads per sample. Since mapping statistics for all samples were fine further analysis of the data was performed, including gene expression of each sample. The integrative genomics viewer (IGV) was used to visualize the regulation of genes over time (Robinson *et al.*, 2011). Of course, expression of the Th1 cell cytokine *Ifng* was verified first and revealed a strong increase in newly transcribed RNA, even 0.5 h upon activation. This also applied for the activated ribosome profiling sample.

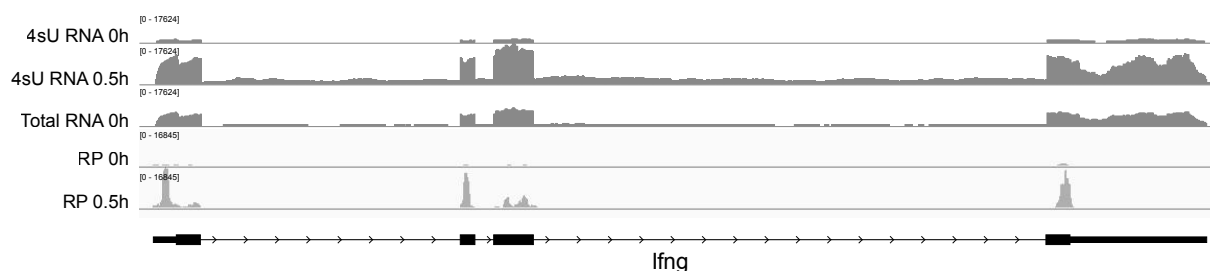


Figure 11: Mapped reads for *Ifng* of the preliminary test

Mapped sequencing reads for non-activated and 0.5 h activated Th1 cells are shown for newly transcribed (4sU) RNA and translated RNA (RP) and for non-activated Th1 cells of total RNA. Gene annotation is indicated below, with exons depicted as boxes (smaller boxes depict untranslated regions) and introns depicted as lines. For each sample, the range of read counts is shown in square brackets.

After mapping reads of all samples, ribosome profiling samples showed significantly less total numbers of mapped reads than total and 4sU RNA samples. The main reason for this was that these samples are just ~29 nt in size, which makes them hard to map to exonic regions. Besides, rRNA content was higher than expected, although rRNA depletion was performed. Therefore, we decided to sequence from now on 80×10^6 reads per ribosome profiling samples. Since there were no further issues with the gathered data, we decided to perform the final assay as described implementing the mentioned modifications.

4.2 Simultaneous analysis of transcriptional and translational control in activated Th1 cells

After establishing simultaneous analysis of 4sU-seq and ribosome profiling in *in vitro* generated T cells, the experimental setup was designed (Figure 12). The exact procedure of combining the methods is published in JoVE (Lichti, Davari *et al.*, in revision).

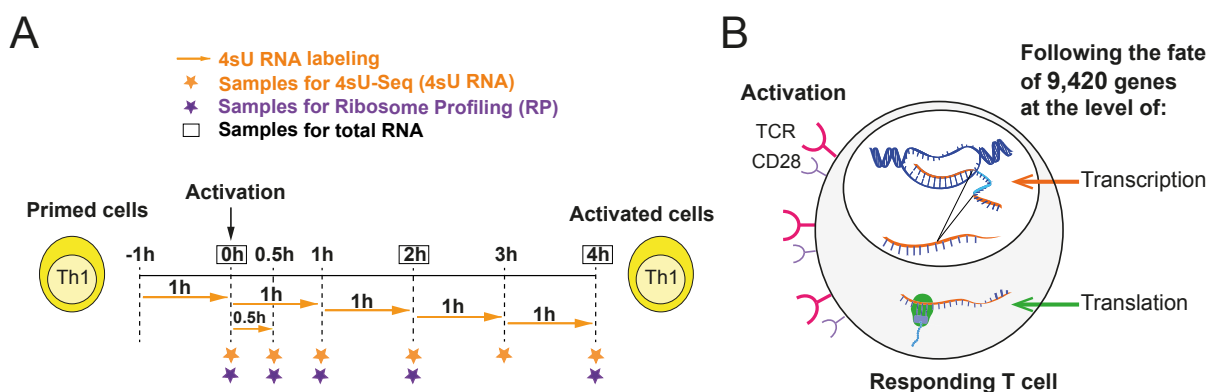


Figure 12: Experimental setup (Lichti, Davari *et al.*, 2017)

(A) Experimental setup. Th1 cells were activated at $t = 0$ h with anti-CD3 and anti-CD28 antibodies. 4sU labeling was performed in 1 h intervals (indicated by orange arrows) for 4 h of activation followed by sequencing (4sU-seq; orange asterisks). Ribosome profiling (RP; purple asterisks) and sequencing of total RNA (black boxes) were performed at indicated time points.

To follow changes in transcription and translation, 4sU-seq, total RNA-seq and ribosome profiling was performed during 4 h of Th1 activation, since FACS analysis showed that $\text{IFN}\gamma$ levels are decreased at later time points (data not shown). Total RNA was sequenced at time points when translation and/or turnover rates should be calculated. For all time points of 4sU-seq and ribosome profiling, samples were collected from the same starting pool of cells. Therefore, all cells were pooled in one flask just prior to treatment. The required amount of

cells for the untreated control was taken away and the remaining cells were activated with CD3/CD28. Samples for 4sU-seq were labeled at indicated time points, for 1 h, each, except the 0.5 h time point which was labeled for 0.5 h. All further bioinformatical analysis was performed for the defined set of 9,420 genes (chapter 3.9.1). A biological replicate of 4sU-seq, RNA-seq and ribosome profiling in activated *in vitro* generated Th1 cells was performed for 0 h, 1 h and 4 h. This revealed high correlation ($\text{cor} \geq 0.94$) between expression levels, quantified as fragments per kilobase of transcript per million mapped reads (FPKM), for each method 4 h upon activation (Figure 13). All findings depicted below were proven for both replicates.

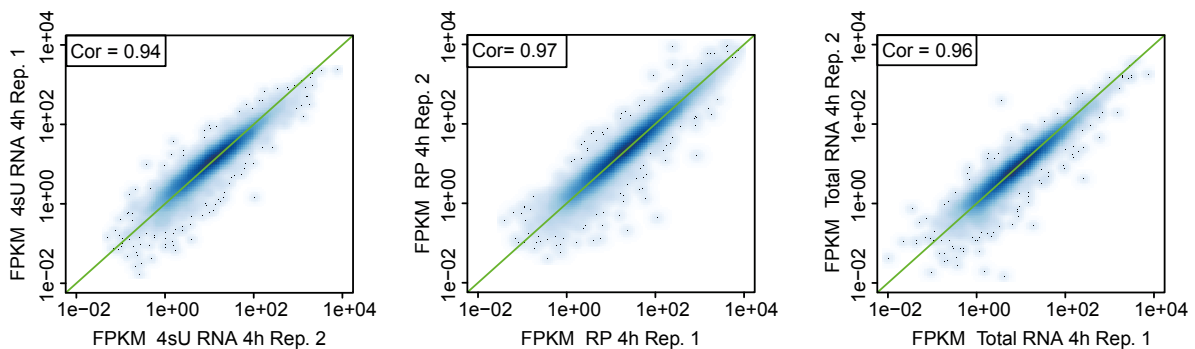


Figure 13: Replicates are highly correlated (Lichti, Davari *et al.*, 2017)

Scatter plots comparing expression values (FPKM) between newly transcribed RNA (4sU RNA), translated RNA (RP) and total RNA at 4 h upon activation of the two replicates. The green line indicates equal FPKM values and rank correlation is indicated in each plot.

4.2.1 Regulation of *Ifng*

To verify the activation of Th1 cells *de novo* transcription (4sU RNA) and translation (RP) of *Ifng* was analyzed. Since gene expression was also verified by qPCR and protein expression by FACS analysis, sequencing data was compared with data gathered from these classical molecular methods (Figure 14). *Ifng* was ~100 times induced after 1 h of activation as determined by qRT-PCR. Sequencing data likewise showed strong induction for both, total RNA and 4sU RNA, depicted as increase in FPKM over time. IFN γ protein expression was rapidly increased as shown for FACS analysis and RP data. Interestingly, transcription and translation seemed to be coupled for *Ifng*.

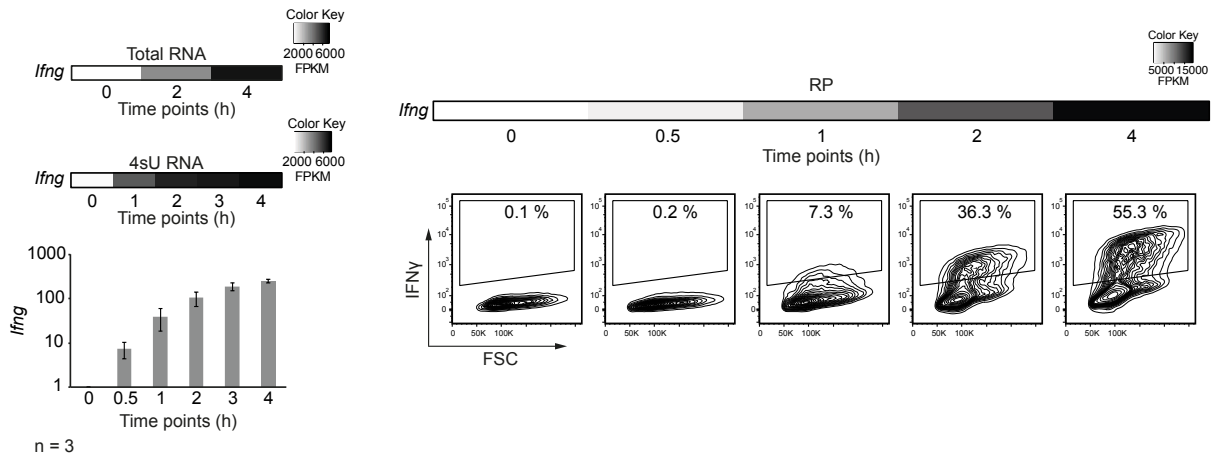


Figure 14: Analysis of *Ifng* expression over time (Lichti, Davari *et al.*, 2017)

Top left: Expression values (FPKM) of *Ifng* in sequencing data (total and newly transcribed (4sU) RNA). Bottom left: qRT-PCR results for *Ifng* (normalized to *Hprt*). The mean and standard deviation (error bars) of three independent experiments is represented. Top right: Expression value of *Ifng* (FPKM) in ribosome profiling (RP) for each time point. Bottom right: Representative FACS plots for IFN γ production. The percentage of IFN γ producing cells is indicated above for each time point.

4.2.2 Most upregulated genes

Th1 response is not exclusively determined by *Ifng* expression, but by a comprehensive interplay of many factors. Nevertheless, genes that were most extensively upregulated 1 h upon activation in 4sU RNA shared same molecular functions (Figure 15). Besides, most of these genes belonged to the same superfamily like the nuclear hormone receptor family genes *Nr4a1*, *Nr4a2* and *Nr4a3* or the early growth receptor family genes *Egr1*, *Egr2* and *Egr3*. Classifying the 15 transcriptionally most upregulated genes 1 h upon activation clearly depicted the molecular activity of a T cell response. Regarding GO terms, genes could be grouped into (1) cytokine activity (*Il3*, *Il10*, *Il21*, *Ccl3*, *Ccl4*, *Tnfsf14*, *Ifng*) and (2) transcription factor activity (*Egr1*, *Egr2*, *Egr3*, *Nr4a1*, *Nr4a2*, *Nr4a3*, *Fos*, *Fosb*). Although these genes might have even more molecular functions (like chemokine function for *Ccl3* and *Ccl4*), this lead to a first global view of the gene response. The early T cell response focuses on the differentiation and effector function of the cell as well as activation and increase of transcription from the RNAPII promoter. Consistently, the list of the 15 most upregulated genes in newly transcribed RNA and in translation show a clear overlap. 12 of the 15 most transcriptionally upregulated genes were also determined in the group of most translationally upregulated genes within 1 h upon activation. Furthermore, all of these genes belonged to the group of the top 20 most upregulated genes in translation at this time point.

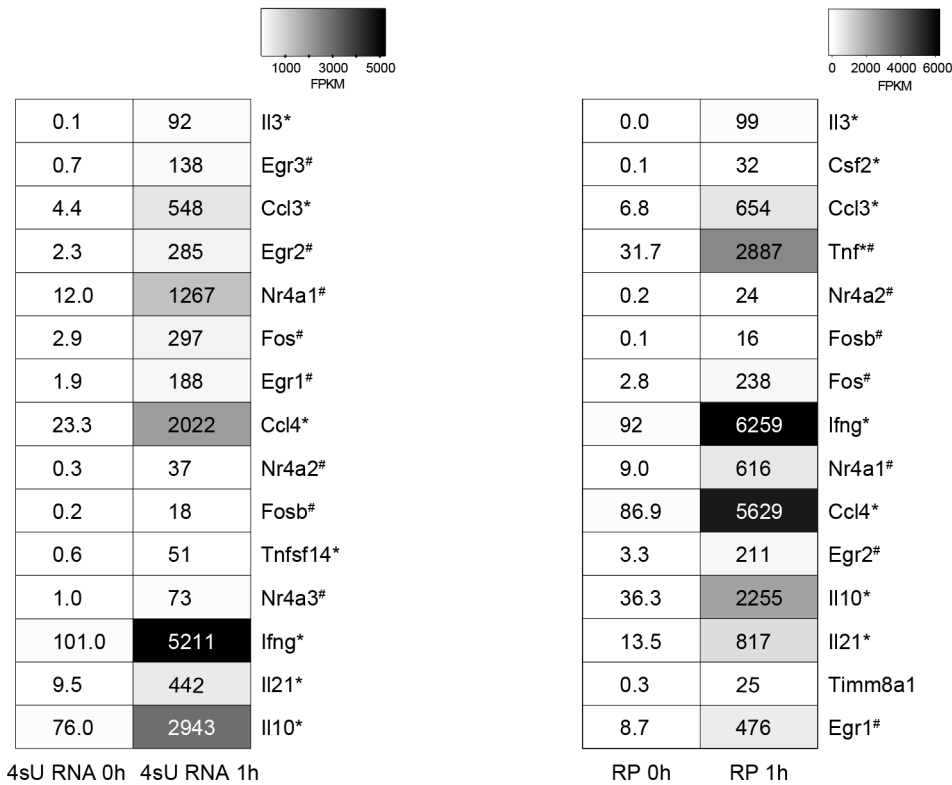


Figure 15: Most upregulated genes (Top 15)

Expression values (FPKM) of most upregulated genes 1h upon activation for newly transcribed (4sU) RNA (left) and translated RNA (RP, right) ordered by fold change. Genes belonging to the GO term ‘cytokine activity’ are highlighted by an asterisk and genes belonging to the GO term ‘transcription factor activity’ are marked by a hash key.

4.2.3 Transcriptional and translational gene response differ in time and magnitude

The experimental setup of the kinetic study allowed a comparative analysis of global gene regulation in time and magnitude. Interestingly, for most time points upon activation numbers of downregulated genes (< -2-fold) were higher than those of upregulated genes (> 2-fold) (Figure 16). This applied especially for 4sU RNA, while for RP this was not observed before 2 h. Analyzing this in more detail considering the magnitude of regulation could explain this observation. Although total numbers of upregulated genes were lower for most time points, the magnitude of upregulation exceeded the downregulation. Hence, downregulation of a high number of genes might be important to compensate for the intense upregulation of genes.

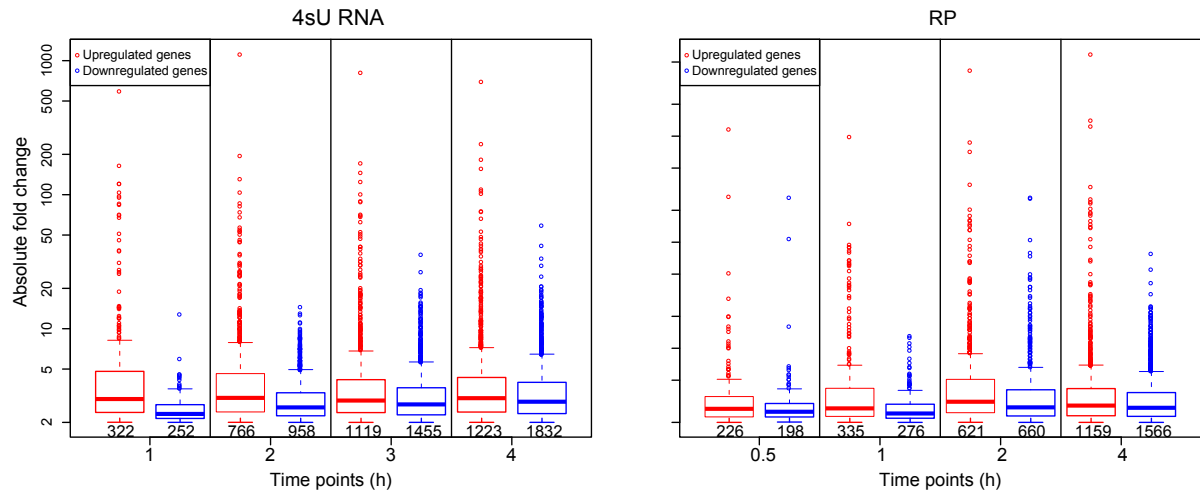


Figure 16: Gene regulation differs in speed and magnitude for up- and downregulated genes
 Fold changes for 4sU RNA and RP is given for all genes. Numbers of regulated genes are indicated below each boxplot.

4.2.4 Verification of downregulation

Although our data was additionally normalized on a global set of housekeeping genes (chapter 3.9.2), the possibility of a global transcriptional amplification as shown by Lin *et al.* could not be neglected (Lin *et al.*, 2012). The fact that c-Myc was also discovered as a key regulator for transcriptional regulation (chapter 4.2.12) prompted us to further validate downregulated genes. Therefore, a GFP plasmid that is not integrated into the genome was transfected into Th1 cells. The expression of a selected set of genes, which were defined as downregulated due to our sequencing analysis, was determined over time via qRT-PCR and normalized to GFP expression. Results showed that the selected “downregulated” genes are indeed downregulated upon activation (Figure 17) similar to results from our sequencing data. This most likely applies to all genes that have been defined as downregulated.

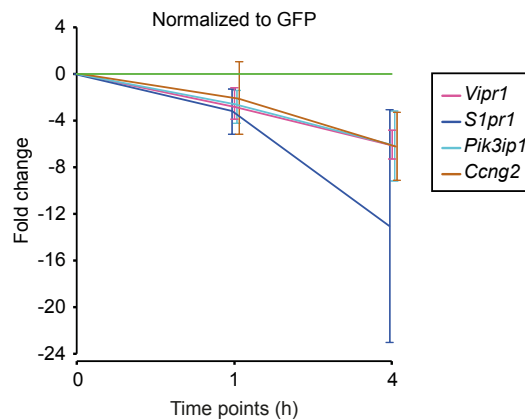


Figure 17: Validation of downregulated genes via GFP plasmid (Lichti, Davari *et al.*, 2017)

Fold changes of selected genes that were defined as downregulated based on the RNA-seq data were determined by qRT-PCR at 1 h and 4 h upon activation. Samples are normalized to spiked-in GFP plasmids (indicated by the green line). The mean and standard deviation (indicated by error bars) of three independent experiments is shown.

4.2.5 Hierarchical clustering of upregulated genes

To investigate global gene regulation in more detail, clusters of genes with similar regulation were defined by means of hierarchical clustering. Genes were defined as either up- or downregulated when they changed >2 -fold until 4 h in at least two consecutive time points in *de novo* transcription (4sU RNA) and translation (RP) at 1, 2 and 4 h upon activation. The six largest upregulated clusters contained 95 % of all 1,185 upregulated genes and are depicted in Figure 18. These clusters could be further classified into three distinct types of gene regulation. First, an immediate-early response, characterized by a strong and immediate transcriptional upregulation followed by a slight decrease which can also be observed in translation, although delayed (cluster 3 & 5). Second, a gradual increase in transcription followed by an increase in translation (cluster 1, 2, 4). Third, a very mild transcriptional regulation but a certain translational upregulation (cluster 6). To assess whether genes of each cluster share common features, functional enrichment analysis was performed. Cluster 5, consisting of immediate early genes (IEGs), was consistently associated with the term cytokine activity. Interestingly, cluster 5 contained many immunological genes such as *Ifng*, *Il3*, *Fos* and *Junb*, but also many genes that are unstudied in the immunological context. Cluster 3 likewise included immunological genes (*Irf8*, *Traf1/4*, *Batf*) but was just enriched for the term receptor. Cluster 2, which was functionally enriched for cytokines, contained e.g. *Il4*, *Irf4* and *Il2*. Noteworthy in terms of

posttranscriptional regulation were the 39 genes of cluster 6 which were not functionally enriched. These genes were translationally upregulated although they discover just a mild transcriptional regulation. In line with this, promoter analysis determined that cluster 6 genes have in average longer 3' UTRs (data not shown) and thus might be more prone to posttranscriptional regulation by RNA binding proteins. Cluster 1, consisting of the largest set of genes, was enriched for many terms that were all related to translation. This was first surprising but led us to further analyses regarding this finding.

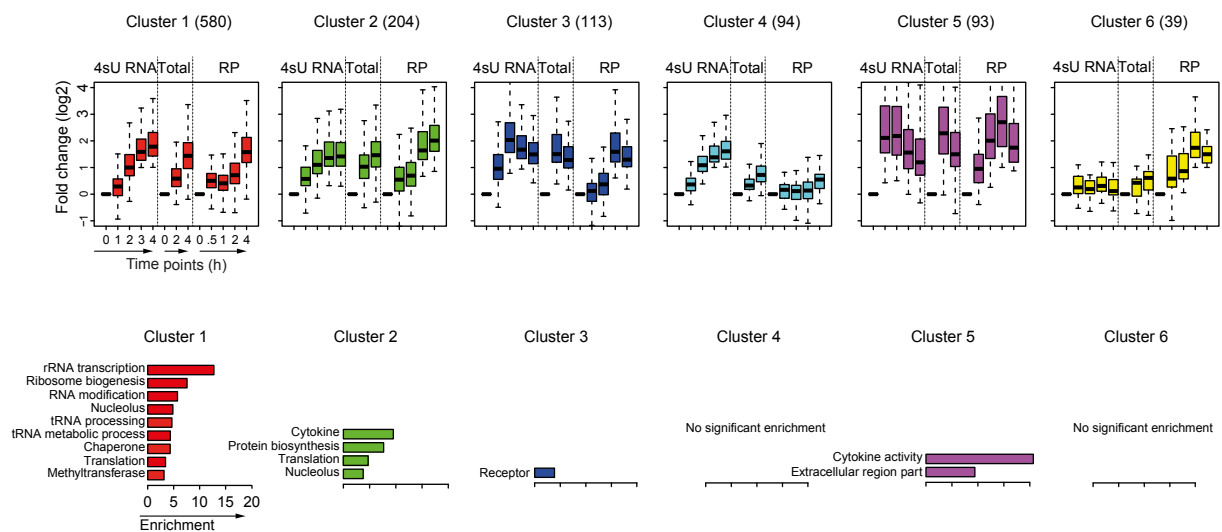


Figure 18: Gene response for upregulated genes differ in time and magnitude on the transcriptional and translational level (Lichti, Davari *et al.*, 2017)

Top: Hierarchical clustering of all upregulated genes based on log₂ fold changes in *de novo* transcription (4sU RNA) and translation (RP) at 1, 2, and 4 h upon activation. Boxplots illustrating the distribution of log₂ fold changes for the six largest clusters are shown and the number of genes in each cluster is indicated in brackets. Bottom: Enriched gene ontology (GO) terms ($p < 0.001$) and protein keywords (from SwissProt and Protein Information Resource [PIR] for the functional enrichment analysis performed with DAVID are shown for each cluster, ordered according to their enrichment value. Redundant terms were removed with DAVID's clustering option.

4.2.6 Hierarchical clustering of downregulated genes

Similar to the upregulated genes, hierarchical clustering was performed for downregulated genes. 4 clusters were determined which contained 97 % of all 1,574 downregulated genes (Figure 19). Cluster 1 was the largest cluster containing 78 % of all downregulated genes. Again, three types of regulation could be observed. First, an immediate early response in *de novo* transcription followed by a delayed translational response (cluster 3). Second, a continuous downregulation (cluster 1). Third, a cluster of genes experiencing a rather mild transcriptional downregulation but a certain extent of translational regulation (cluster

2 & 4). While cluster 2 and 3 did not show any functional enrichment, functionally enriched terms for cluster 1 displayed a rather low enrichment score. Nevertheless, most terms were related to cell cycle or chromosome organization, leading to the assumption that mainly cell division processes were downregulated. Cluster 4 was highly enriched for the term nucleosome core, which basically reflects that it mainly consists of histones (e.g. *Hist2h2aa2*, *Hist1h2bk*, *Hist1h4b*).

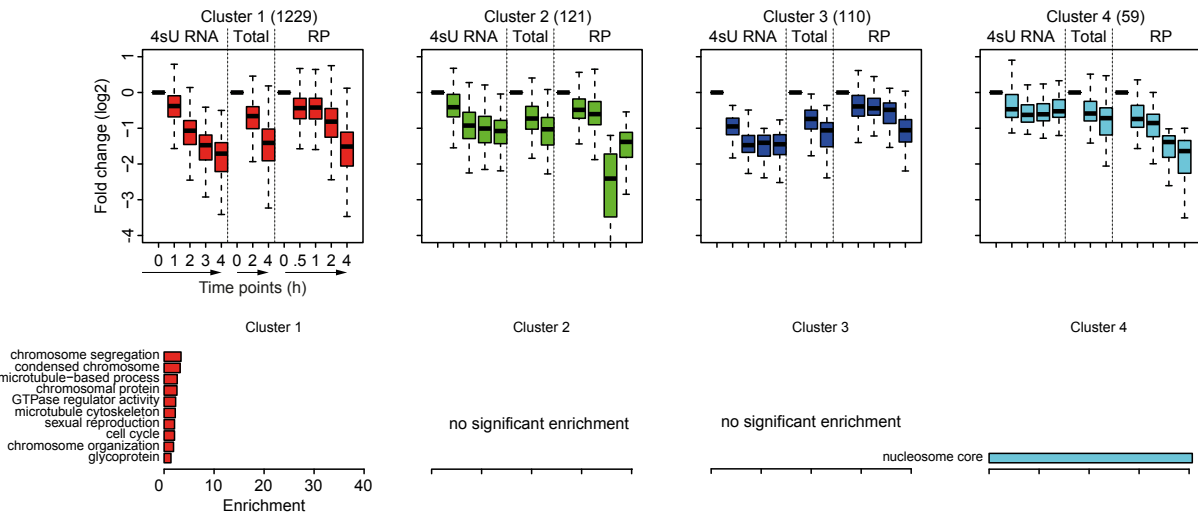


Figure 19: Gene response for downregulated genes differs in time and magnitude on the transcriptional and translational level (in part from Lichti, Davari *et al.*, 2017)

Top: Hierarchical clustering of all downregulated genes with the same criteria as in Figure 18. Boxplots illustrating the distribution of log₂ fold changes for the four largest clusters are shown and the number of genes in each cluster is indicated in brackets. Bottom: Enriched GO terms with the same criteria as in Figure 18.

4.2.7 Global coupling of transcriptional and translational regulation

Besides distinct types of regulation and functional enrichment for different clusters, comparison of 4sU RNA with RP let us speculate whether transcription and translation are globally coupled and which role potential exceptions, as there might be for cluster 6 (upregulated genes) or cluster 4 (downregulated genes), might play. A global correlation analysis of all fold changes between all samples demonstrated a strong correlation for nearly all time points and methods (Figure 20). In detail, 4 h upon activation fold changes in translation highly correlated to fold changes in both, total RNA (0.88) and *de novo* transcribed RNA (0.85). Furthermore, correlation tended to be higher among each type of measurement (4sU RNA, RP, Total RNA) at the same time points, compared to different time points of each type of measurement.

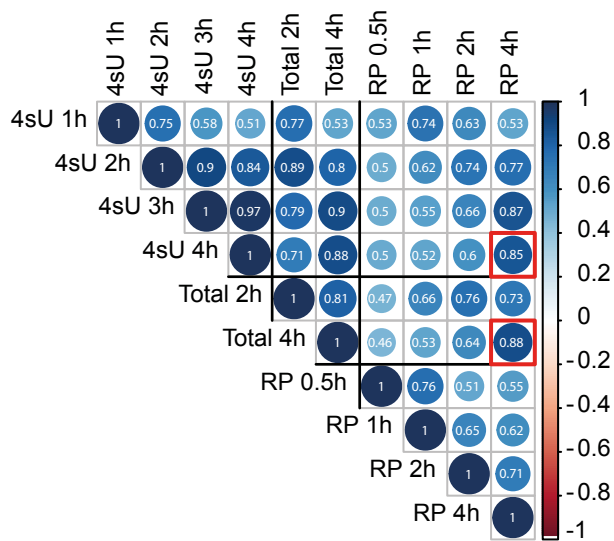


Figure 20: Global correlation analysis shows highly coupled changes in transcription and translation (Lichti, Davari *et al.*, 2017)

Global correlation analysis of fold changes among all samples at all time points of newly transcribed (4sU), total and translated RNA (RP) for all genes. Rank correlation is indicated for each time point. The high correlation at 4 h between translated (RP) and total or 4sU RNA, respectively, is highlighted with red boxes.

4.2.8 Transcriptional regulation dictates gene response

Fold changes of all genes were directly compared to each other to determine differences in regulation in more detail. While changes in translation and total RNA 4 h upon activation mainly resembled each other (Figure 21A), changes in total RNA tended to be smaller than changes in 4sU RNA (Figure 21B). We hypothesized that this might be due to changes in turnover rates and calculated them in terms of the ratio of newly transcribed to total RNA levels in non-activated cells. Indeed, there was a strong negative correlation. Whereas low turnover rates (<5 %) were reflected by higher fold changes of newly transcribed RNA than of total RNA, genes with high turnover rates (>10 %) showed nearly equal fold changes (Figure 21C).

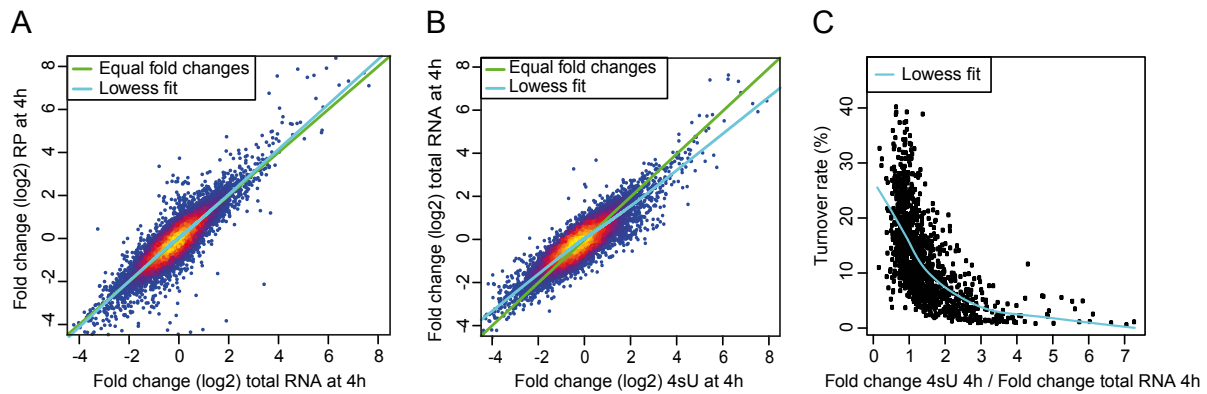


Figure 21: Changes in translation are mainly determined by changes in total RNA (Lichti, Davari *et al.*, 2017)

(A) Scatterplot comparing fold changes (log₂) at 4 h in translation (RP) and total RNA. Local regression fit using locally weighted scatterplot smoothing (Lowess) and equal fold changes are indicated by a cyan and green line, respectively. (B) Scatterplot comparing fold changes (log₂) at 4 h in total RNA and newly transcribed (4sU) RNA. Lowess and equal fold changes are indicated by a cyan and green line, respectively. (C) Scatterplot of RNA turnover rates against the fold change observed in 4sU RNA at 4 h compared to the fold change in total RNA at the same time point. Lowess is indicated by a cyan line.

All in all, most changes (>92 %) in translation that happened during Th1 activation were determined by changes in total RNA levels, which mostly followed alterations in *de novo* transcription with a delay depending on basal RNA turnover rates.

4.2.9 Turnover rates

We wondered whether differences between the up- and downregulated clusters from chapter 4.2.5 and 4.2.6 could be explained by RNA turnover rates. Calculation of turnover rates for each cluster depicted clear differences (Figure 22). For instance, upregulated cluster 3 and 5, which were characterized by a high coupling between 4sU RNA, RP and total RNA, displayed significant higher turnover rates. In contrast, cluster 1 and 4 had lower turnover rates which is reflected by a delayed translational regulation. Similarly, differences between downregulated cluster 1 and 3 may be explained by different turnover rates. However, upregulated cluster 6 and especially downregulated cluster 2 and 4 do not show a consistent behavior, which favors the suggestion that these genes are indeed translationally regulated.

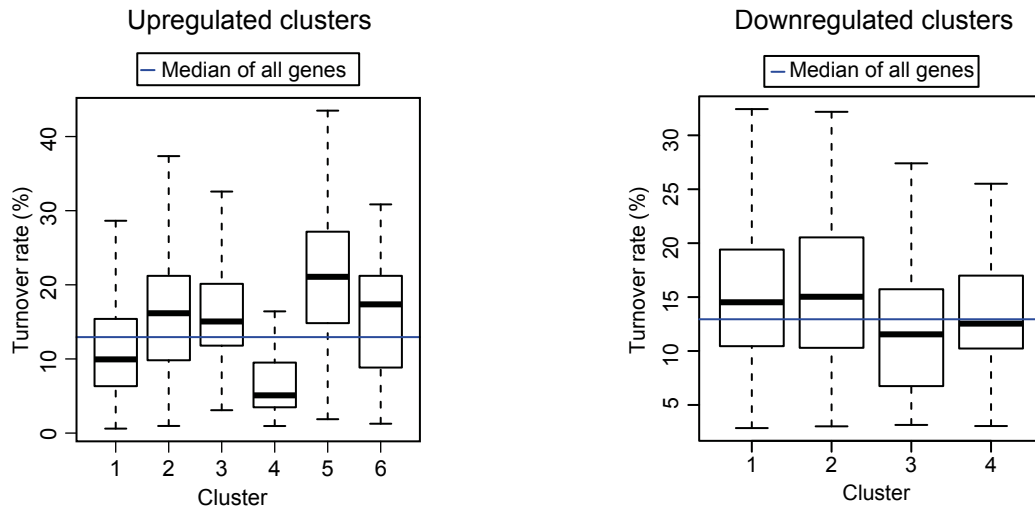


Figure 22: Turnover rates determine correlation between transcription and translation (Lichti, Davari *et al.*, 2017)

Distribution of RNA turnover rates for each cluster of upregulated (left) and downregulated (right) genes are represented as boxplots (horizontal blue line illustrates the median RNA turnover rate over all genes).

Since turnover rates differed between genes we were wondering whether the induction of genes correlates with distinct levels of turnover rate. Indeed, the highest expressed immunological genes showed significantly higher turnover rates, probably to restrict expression to the time of the response (data not shown).

To analyze whether there was a link between gene function and turnover rate, all genes were divided into 5 equally sized groups according to their turnover rates and gene ontology analysis was performed by DAVID (Figure 23) (Huang *et al.*, 2009). This indicated that genes with average turnover rates (group 2 & 3) were hardly enriched for a distinct gene function, while genes with low (group 1) and genes with high turnover rates (group 4 & 5) were. Genes belonging to group 1 were highly enriched for functions in the extracellular compartment and antigen processing, indicating a role for cell proliferation, migration and intercellular communication. Genes belonging to group 4 and 5 were mainly enriched for the terms zinc finger and RNA processing. Since both groups consisting of the highest turnover rates were enriched for zinc finger protein encoding genes, these genes might ensure cell maintenance before activation. Moreover, a low half-life might prevent degradation or regulation of target proteins during the immune response, since zinc finger proteins are known for their diverse functions including transcriptional and translational regulation (Laity *et al.*, 2001).

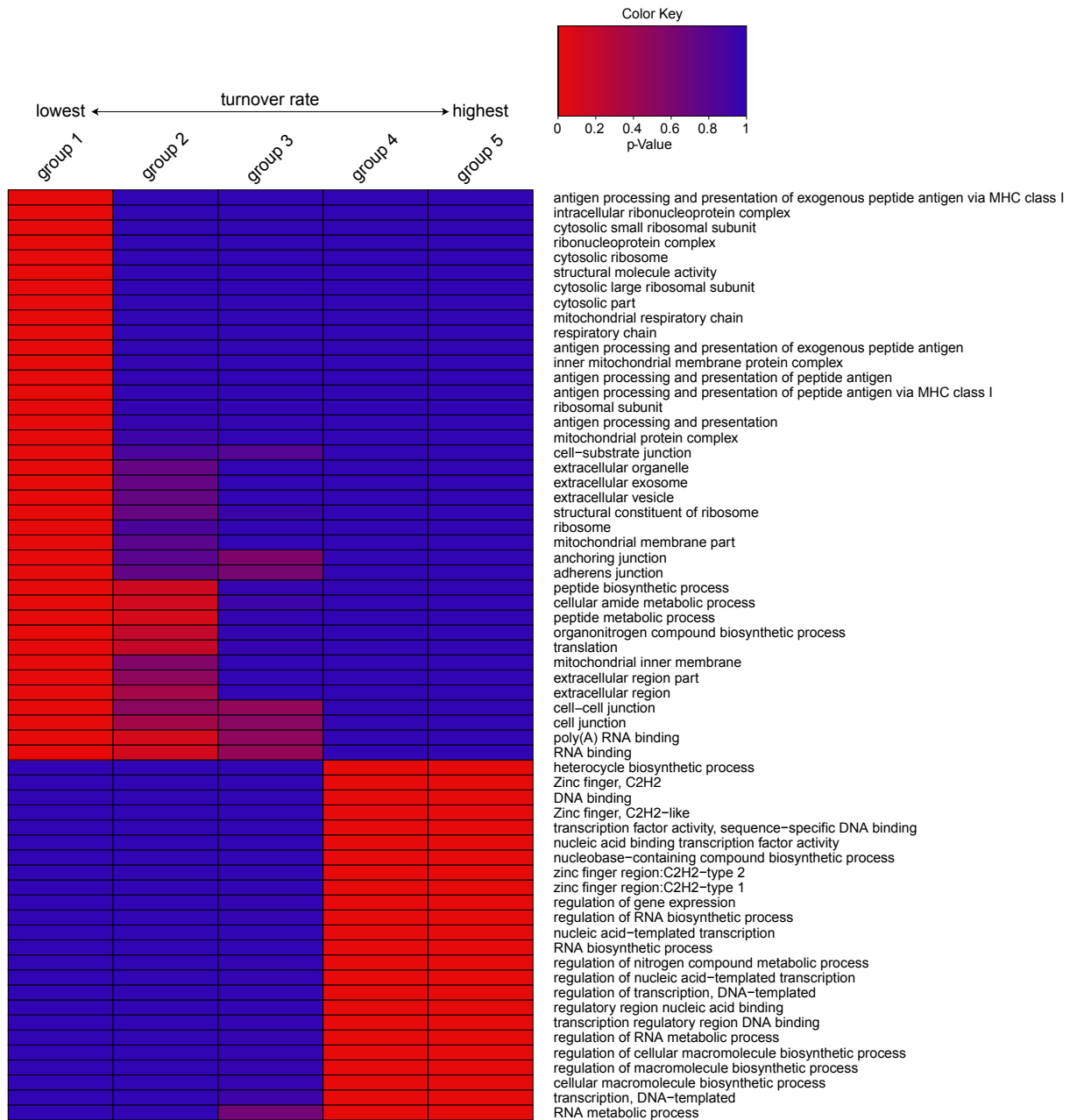


Figure 23: Functional characteristics of gene groups with different turnover rates

The most enriched GO terms and protein families (from InterPro) of each group are shown for the functional enrichment analysis performed with DAVID and are clustered according to their p-value. Groups were equally sized according to their turnover rates and 5 groups were generated (group 1 has the lowest and group 5 has the highest turnover rate).

4.2.10 Translation rates

To further investigate posttranscriptional regulation translation rates (FPKM RP / FPKM Total RNA) were calculated (Figure 24). This allowed a quantitative analysis of the effect of translation on each gene and subsequently determined translational regulation.

Consistently, global translation rates did not change over time supporting our finding that most changes in gene expression are defined by transcription.

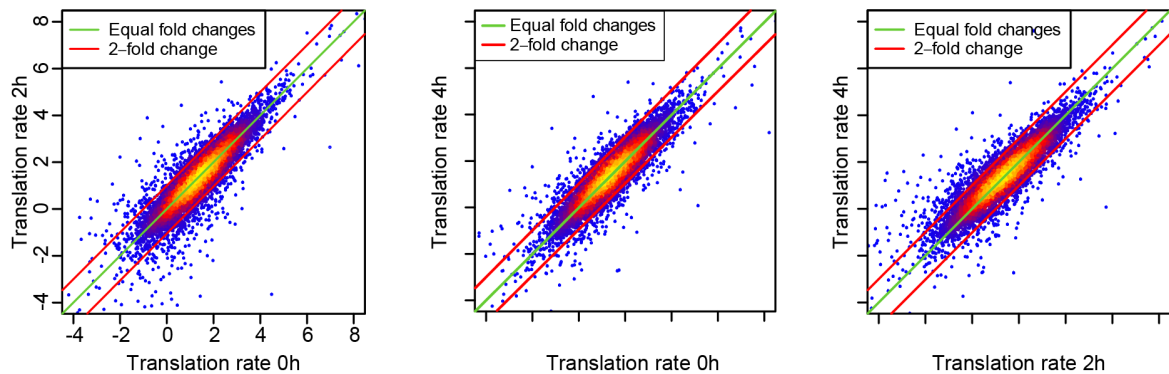


Figure 24: Global translation rates do not change (Lichti, Davari *et al.*, 2017)

Scatter plot comparing translation rates between different time points. Translation rates were determined as the ratio of translated RNA (FPKM in RP) to total RNA (FPKM in total RNA). The green line indicates equal fold changes and the red lines 2 fold changes.

To further analyze posttranscriptionally regulated genes of cluster 6 (upregulated genes) and cluster 2 and 4 (downregulated genes) they were ordered according to their fold changes in translation rates 2 h and 4 h upon activation, respectively (data not shown). Upregulated cluster 6 showed particularly high fold changes in translation rate, but predominantly for histone family members and ribosomal proteins. No distinct gene family could be related to elevated changes in translation rates proofing that even though posttranscriptional control might occur, it does not apply to a specific set of genes.

4.2.11 Increased expression of transcriptional but not translational machinery

Functional enrichment analysis of upregulated clusters (chapter 4.2.5) showed enrichment of cytokines but also for terms related to translation (cluster 1). To analyze this in more detail, an enrichment analysis for selected GO terms and SP-PIR keywords was performed which means that fold changes for selected terms at each time point were calculated (Figure 25). Once more, cytokines were massively and rapidly upregulated in both, 4sU RNA and RP. Factors involved in the process of translation and protein folding were also consistently upregulated, albeit less than cytokines, in *de novo* transcription and translation. This was consistent with an overall increase in rRNA synthesis (data not shown). Surprisingly, neither the terms transcription factor activity nor transcription seemed to be regulated. Figure 25B showed that although individual genes involved in transcriptional processes were regulated

there was no distinct global regulation as observed for translational processes. Hence, the transcription machinery seemed to be poised for the rapid transcriptional response in contrast to the translational machinery.

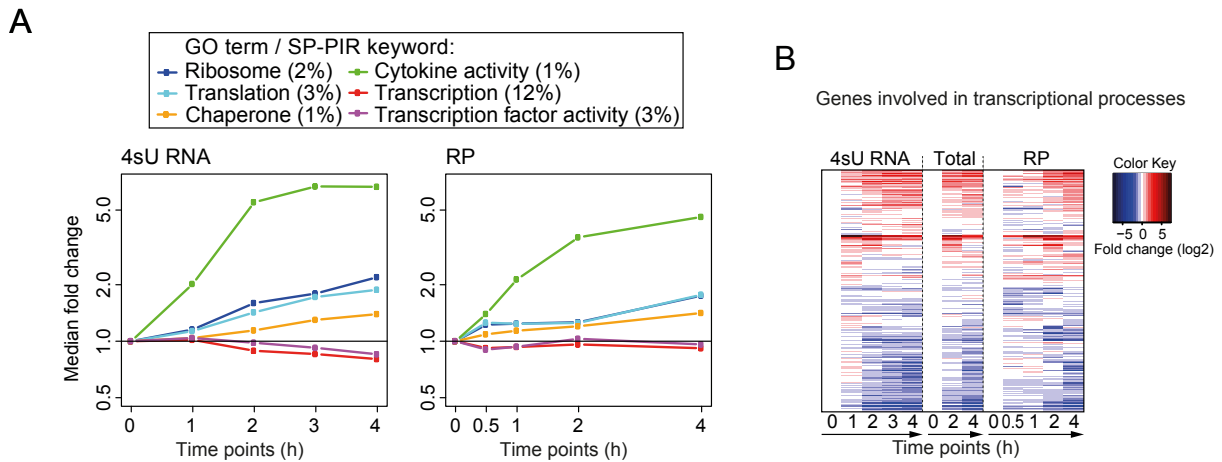


Figure 25: Increased expression of the translational but not of the transcriptional machinery (Lichti, Davari *et al.*, 2017)

(A) Median fold changes in newly transcribed (4sU) RNA and translated RNA (RP) over time compared to non-regulated Th1 cells are shown for selected GO terms and SP-PIR keywords. Numbers in brackets indicate which percentage of analyzed genes is annotated with this GO term or keyword. (B) Heatmap of fold changes (log₂) for genes annotated with a function in transcription.

4.2.12 Enrichment analysis for transcription factor targets

To identify transcription factors with enriched targets among upregulated genes an enrichment analysis was performed with EnrichR (Chen *et al.*, 2013). This tool determines transcription factor targets from published ChIP-seq or ChIP-Chip experiments (annotated in the ChEA database (Lachmann *et al.*, 2010)). The analysis identified c-Myc as the main regulator for cluster 1, 2 and 3. STAT3, STAT4 and RelA were identified as the main regulators for cluster 3 and 5 (Figure 26). For cluster 6, consisting of potentially posttranscriptionally regulated genes, different transcription factors were found. Our data showed no upregulation of RelA, Stat3, Stat4 over the whole time course and no upregulation of c-Myc until 1 h upon activation (data not shown).

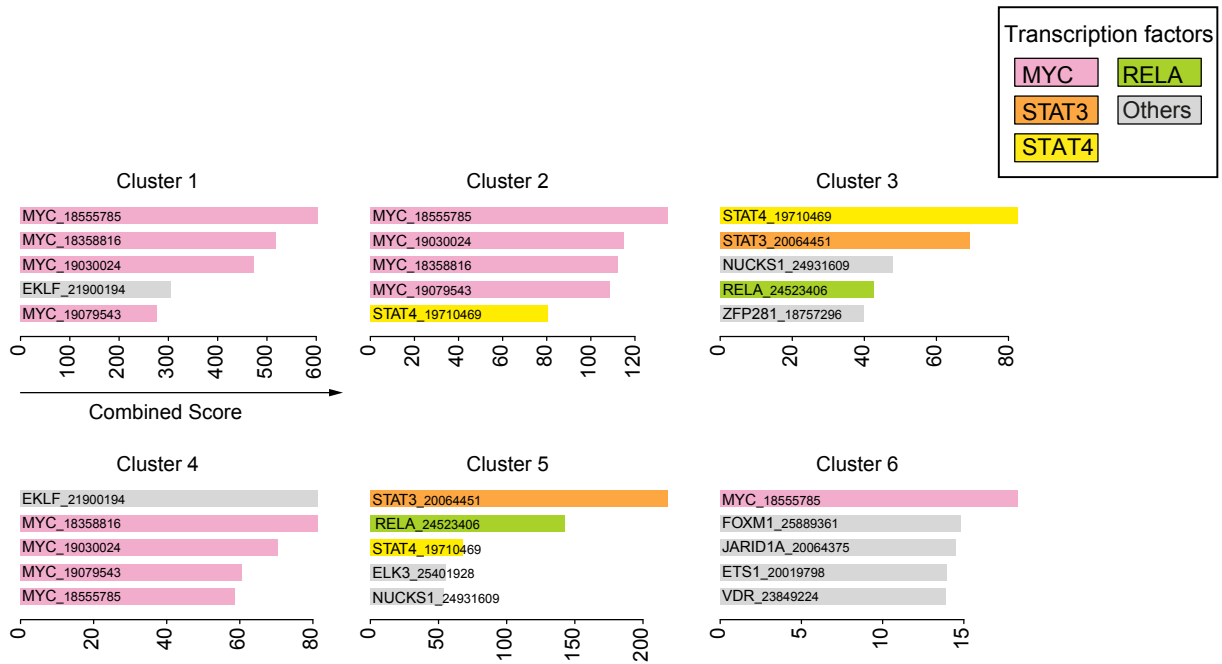


Figure 26: Enriched transcription factor targets (modified from Licht, Davari *et al.*, 2017)

Enrichment analysis with EnrichR for transcription factor targets identified experimentally using ChIP-seq or ChIP-chip for each upregulated cluster. Bars indicate the combined score determined by EnrichR (calculated from the p value and a rank-based score) and are annotated with both the transcription factor and the PubMed identifier (ID) for the corresponding publication. Results are shown for the top five datasets with $p < 0.001$.

To further validate the role of c-Myc for our defined upregulated genes in general and mentioned clusters in particular c-Myc binding sites determined with ChIP-seq in CD8⁺ T cells (Chou *et al.*, 2014) were verified for our set of genes. Indeed, c-Myc binding sites were enriched among both, all upregulated genes as well as genes from upregulated clusters 1, 2 and 4 (Figure 27). Hence, it is suggested that c-Myc was responsible for the downstream response whereas STATs and RelA mediated the early and rapid response.

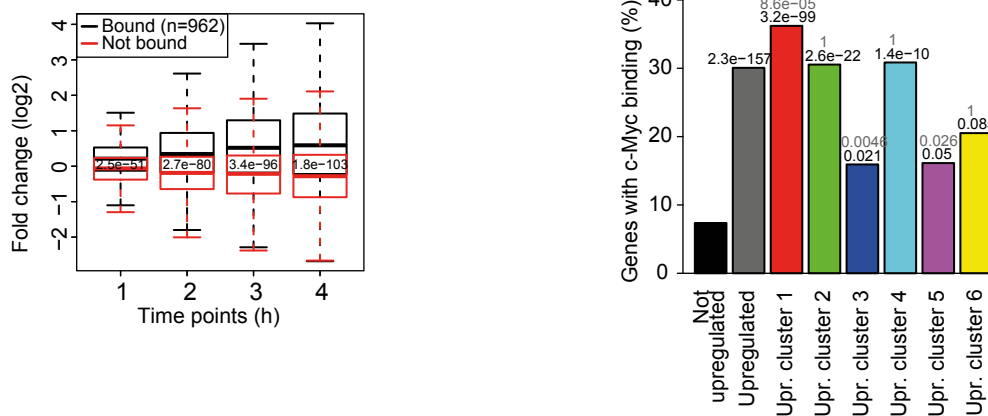


Figure 27: c-Myc is a main regulator of transcriptional upregulation (Lichti, Davari *et al.*, 2017)

Left: comparison of fold changes (\log_2) in *de novo* transcription for genes with c-Myc binding sites (black) within their promoters compared to genes without c-Myc binding sites (red) at each time point (top 1000 binding sites identified in CD8⁺ T cells by ChIP-seq). Boxplots illustrate the distribution of fold changes (\log_2) and p-values (Wilcoxon test, Bonferroni multiple testing correction) indicate the significance of differences in the distributions. Right: Percentage of c-Myc binding sites (as determined in the left figure) within promoters of upregulated genes in general (gray bar) and within all identified clusters of upregulated genes (as defined in Figure 18). P-values comparing the percentage of c-Myc binding to genes not upregulated (black) and upregulated (gray) were obtained using Fischer's exact test (Bonferroni multiple testing correction).

4.2.13 Reduction of cotranscriptional splicing rates early after activation

IGV was used to visualize gene regulation over time. This did not just reveal up- or downregulation of genes but also showed distinct expression patterns for exonic or intronic regions. Surprisingly, many genes showed that the relative frequency of intronic reads increased after 1 h of activation but then decreased again. One example was *IL2*, which clearly visualized elevated levels of intronic reads 1 h after activation (Figure 28A). To investigate this finding on a global scale the fraction of fully spliced transcripts ($\hat{=}$ splicing index) was calculated for each gene (no. of exon-exon junction reads / (no. of exon-exon junction read + no. of exon-intron junction reads)). Genes were grouped into five categories: (1) genes > 4-fold downregulated at 1 h, (2) genes > 4-fold downregulated at 4 h but not at 1 h, (3) genes not regulated at 4 h (4) genes upregulated at 1 h and (5) genes upregulated at 4 h but not at 1 h. Interestingly, all of these genes showed a strong initial drop in splicing rates which was rapidly corrected even beyond levels of non-activated cells (Figure 28B). Although this effect was most pronounced for early upregulated genes, it was consistent, independent of gene regulation.

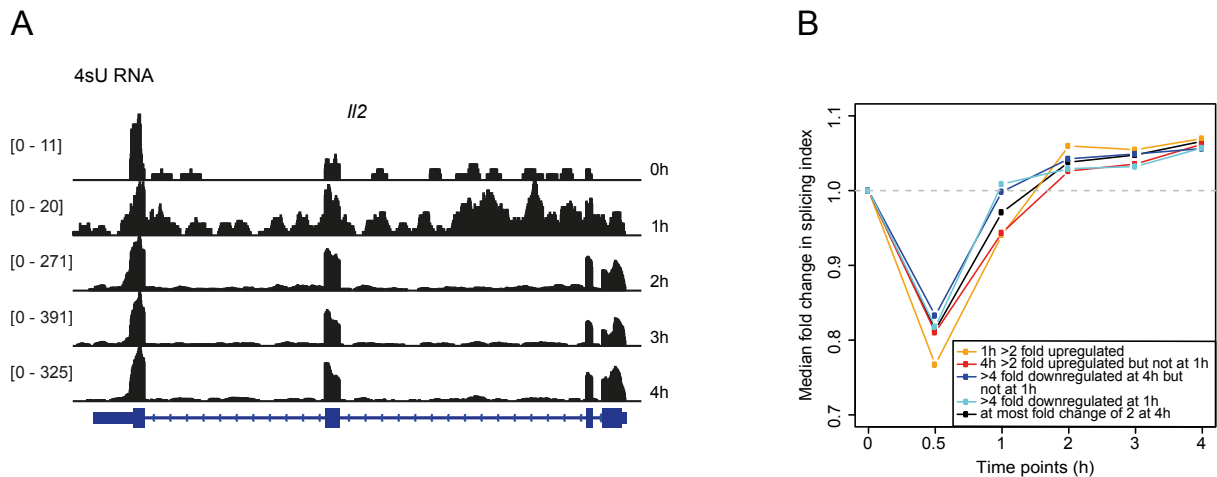


Figure 28: Global reduction in cotranscriptional splicing rates (Lichti, Davari *et al.*, 2017)

(A) Mapped sequencing reads (4sU RNA) for *Il2* indicating increased intron read counts 1 h after activation and reduced intron read counts at later time points. For each time point the range of read counts (y axis) is indicated in square brackets. Gene annotation is indicated below with exons depicted as boxes (smaller boxes are untranslated regions) and introns depicted as lines. (B) Median fold changes in splicing indices over time are displayed for genes upregulated early (≥ 2 -fold upregulated at 1 h; orange) and at later time points (≥ 2 -fold upregulated at 4 h, but not at 1 h; red), genes downregulated early (≥ 4 -fold downregulated at 1 h; cyan) and at later time points (≥ 4 -fold downregulated at 4 h but not at 1 h; blue) as well as non-regulated genes (fold change < 2 after 4 h; black).

To disprove the possible argument that this effect simply reflected an overall increase in *de novo* transcription at the beginning of activation, fold changes in 4sU RNA were quantified. This showed in fact a slight drop in newly transcribed RNA without any changes in rRNA content (Figure 29).

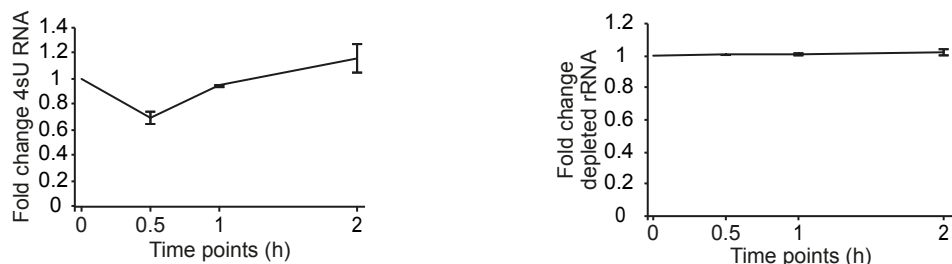


Figure 29: Global reduction in cotranscriptional splicing is not induced by an initial increase in 4sU RNA (Lichti, Davari *et al.*, 2017)

Left: Equal numbers of *in vitro* generated Th1 cells were activated for the indicated time points and 4sU-labeling was performed for the last 0.5 h of each time point. Fold changes in 4sU RNA compared to 0 h were calculated (newly transcribed RNA was quantified via Qubit Fluorometer 2.0 and for each time point related to total biotinylated RNA after precipitation). The mean and standard deviation (error bars) are illustrated for two independent experiments.

4.3 RNA polymerase II ChIP-seq

To further understand the mechanism behind rapid transcriptional regulation upon T cell activation RNAPII ChIP-seq was performed. Besides, this allowed us to verify pausing of RNAPII which has been proposed as an important mechanism for rapid gene activation (Core and Lis, 2008; Gilchrist *et al.*, 2012). ChIP-seq of RNAPII was performed at 0 h, 0.5 h and 2 h upon activation of Th1 cells in two replicates.

4.3.1 Rapid recruitment of RNAPII mediates transcriptional upregulation

To compare data from RNAPII ChIP-seq with 4sU-seq the abundance of RNAPII at the promoter (defined as transcriptional start site (TSS) \pm 500 nt) was quantified analogous to RNA-seq. First, FPKM values of 4sU RNA were compared to the abundance of promoter RNAPII, which could demonstrate a global correlation between all samples (Figure 30A). To determine the correlation between increased recruitment of RNAPII and transcriptional upregulation, fold changes in promoter RNAPII and 4sU RNA were correlated. This analysis showed that upregulation of genes coincides with increased abundance of RNAPII for the respective time point (Figure 30B).

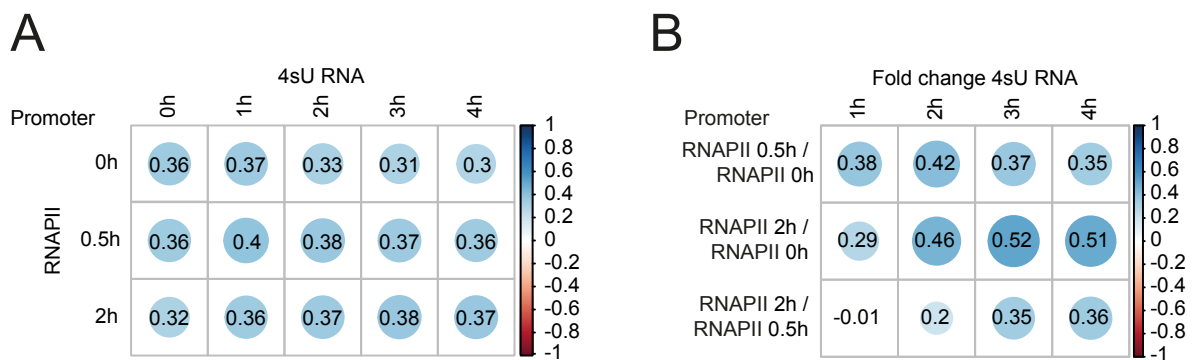


Figure 30: Strong correlation between *de novo* transcription and RNAPII (Lichti, Davari *et al.*, 2017)

(A) Rank correlation of promoter RNAPII abundance to 4sU RNA FPKM levels at each time point. (B) Rank correlation between fold changes in promoter RNAPII abundance between each pair of time points and fold changes in 4sU RNA compared to non-activated cells.

4.3.2 Paused RNAPII is not the main mechanism to allow rapid transcriptional upregulation

Elevated presence of RNAPII at promoters due to temporal pausing of transcription during elongation has been proposed as a possible mechanism for rapid or on demand transcription (Core and Lis, 2008; Gilchrist *et al.*, 2012). While for *Ifng* there was indeed a strong RNAPII signal already visible at the TSS before activation, a rapid intensification of RNAPII over time along with a movement into the gene body could clearly be determined (Figure 31A). To further investigate the role of paused RNAPII as a mechanism for rapid induction of IEGs, fold changes in *de novo* transcription were correlated with fold changes in RNAPII at the promoter, 2 h upon activation. Restricting this analysis to cluster 5 genes, fold changes correlated quite well indicating that rapid transcriptional upregulation of IEGs coincides with rapid upregulation of RNAPII (Figure 31B).

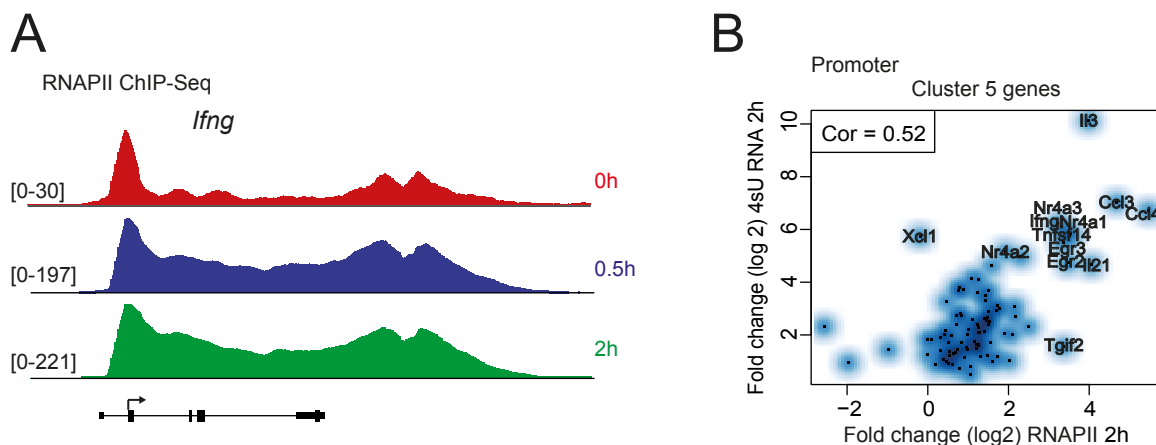


Figure 31: RNAPII of *Ifng* and correlation of cluster 5 genes with *de novo* transcription (Lichti, Davari *et al.*, 2017)

(A) Mapped RNAPII sequencing reads for *Ifng* for Th1 cells at 0 h, 0.5 h and 2 h upon activation. Gene annotation is indicated below, with exons depicted as boxes (smaller boxes depict untranslated regions) and introns depicted as lines. For each sample, the range of read counts is shown in square brackets. (B) Scatterplot comparing log₂ fold changes in promoter RNAPII abundance at 2 h to log₂ fold changes in 4sU RNA at 2 h (compared to non-activated cells, each) for genes of upregulated cluster 5. Rank correlation is indicated.

Besides, for all upregulated genes, FPKM values of promoter RNAPII at 0 h showed a good correlation with FPKM values of 4sU RNA at 0 h (Figure 32).

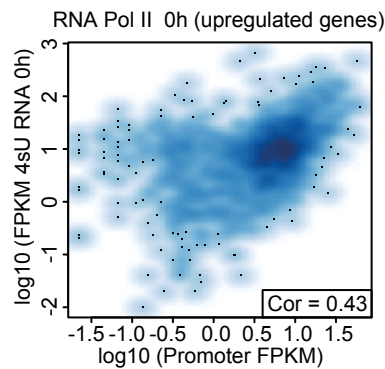


Figure 32: 4sU RNA and RNAPII are well correlated for upregulated genes at 0 h

Scatter plot comparing RNAPII abundance at the promoter (FPKM) at 0 h with 4sU FPKM values at 0 h. Rank correlation is indicated.

To further uncover the potential role that release of paused RNAPII might play for transcriptional upregulation, the change over time in promoter to gene body ratio of RNAPII was calculated (FPKM at the promoter/FPKM at the gene body). This directly reflected dynamics of RNAPII assembly and pause release revealing that there is no global correlation between changes of the RNAPII promoter/gene body ratio and fold changes in *de novo* transcription (Figure 33A). Intriguingly, only 29 genes with a significant RNAPII abundance at the promoter of non-activated cells (FPKM>1), a >2-fold change in *de novo* transcription 4 h upon activation and at least a 30 % reduction of RNAPII promoter/gene body ratio could be identified (data not shown). Indeed, this indicated the presence of paused RNAPII that is released upon activation for these genes (including *Ifng*). Nevertheless, most of these genes already showed elevated FPKM values of 4sU RNA (19/29 with FPKM > 10). This implies that these genes were already transcribed to a certain degree, even in non-activated cells. Although pausing of RNAPII was proposed as a mechanism for rapid transcriptional upregulation, only 9 of the 29 genes belonged to our previously defined clusters of IEGs (cluster 3/5). To determine whether rapidly upregulated genes were indeed not primed for increased presence of RNAPII at the promoter before activation, promoter RNAPII abundance at 0 h was divided by FPKM of 4sU RNA at 0 h, each for non-regulated genes, downregulated genes and all clusters of upregulated genes (Figure 33B). None of the upregulated clusters had significantly increased RNAPII/4sU RNA ratios at 0 h. Thus, rapid *de novo* recruitment of RNAPII is the dominant mechanism to ensure transcriptional upregulation of genes, including IEGs, upon T cell activation.

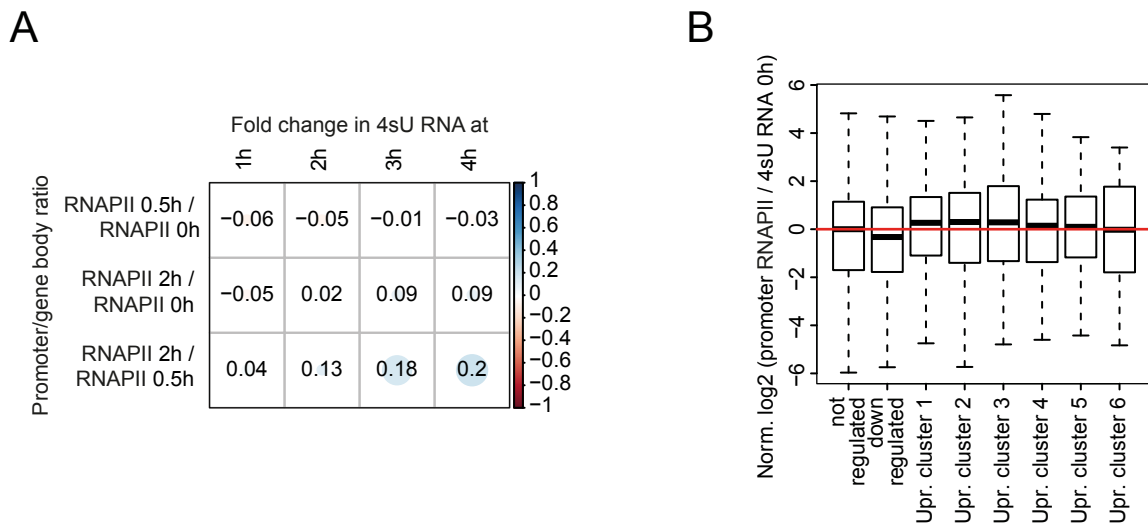


Figure 33: Paused RNAPII is not the key mechanism for transcriptional upregulation (Lichti, Davari *et al.*, 2017)

(A) Rank correlation between fold changes in promoter/gene body ratio for RNAPII compared to fold changes in 4sU RNA at all time points. (B) Ratios of RNAPII abundance to 4sU RNA at 0 h were calculated for non-regulated genes, downregulated genes and genes of the six major upregulated clusters. Distribution of normalized ratios for each group (by dividing by the median ratio for non-regulated genes) is illustrated using boxplots. Positive values indicate higher levels of RNAPII at the promoter than expected from the baseline *de novo* transcription at 0 h compared to non-regulated genes (red horizontal line: median value for non-regulated genes).

4.4 Further analysis of cotranscriptional splicing and rapid recruitment of RNAPII

As already mentioned in chapter 4.2.13 we could discover an increase of the relative frequency of intronic sequencing reads shortly upon activation followed by a subsequent decrease. Although literature agrees that most mRNAs are cotranscriptionally spliced (Bentley, 2014) there are rarely any studies that observed fluctuations like we did. Nevertheless there was a publication by Bhatt *et al.* who also made the same finding for activated macrophages but did not analyze it in more detail (Bhatt *et al.*, 2012). To elucidate this finding, a couple of analyses were performed.

4.4.1 Shift in exon/intron ratio for polyadenylated nuclear RNA and polyadenylated chromatin RNA

Since sequencing of 4sU RNA was performed without poly(A) selection, we wondered whether the observed drop in cotranscriptional splicing also occurs in already

polyadenylated RNA. First we wanted to verify if the observed effect even proves to be true for already polyadenylated RNA from the chromatin. Therefore, cells were activated for 0.5 h and 2 h and subcellular RNA fractionation into cytoplasmic and nuclear RNA, as well as its chromatin fraction, was performed. The purity of subcellular fractionation was confirmed by Western blot using proteins specific for each cellular compartment.

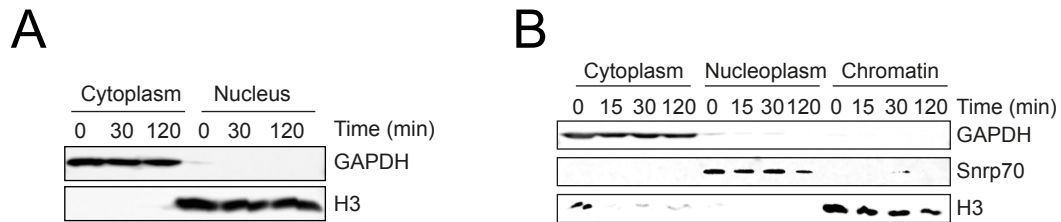


Figure 34: Purity of subcellular fractionation is confirmed by Western Blot (Lichti, Davari *et al.*, 2017)

(A) Confirmation of clean cytoplasm (GAPDH) fractionation versus nucleus (Histon 3 (H3)) fractionation for the different time points in Figure 35B by Western Blot analysis. (B) Confirmation of clean cytoplasm (GAPDH) versus nucleoplasm (Snrp70) and chromatin (H3) fractionation for the different time points in Figure 35C (including a 15 min time point that is not shown).

Primers were designed to identify either spliced (both primers in exonic regions) or unspliced transcripts (one primer in exonic region and one primer in the intronic region) for three highly expressed genes (*Il3*, *Ifng*, *Ccl3*) (Figure 35A). The splicing ratio was calculated by the ratio of spliced to unspliced transcript. Polyadenylated nucleic RNA showed a drop in splicing ratio early upon activation that was later overcome (Figure 35B). Intriguingly, this drop was even visible for the chromatin fraction (Figure 35C).

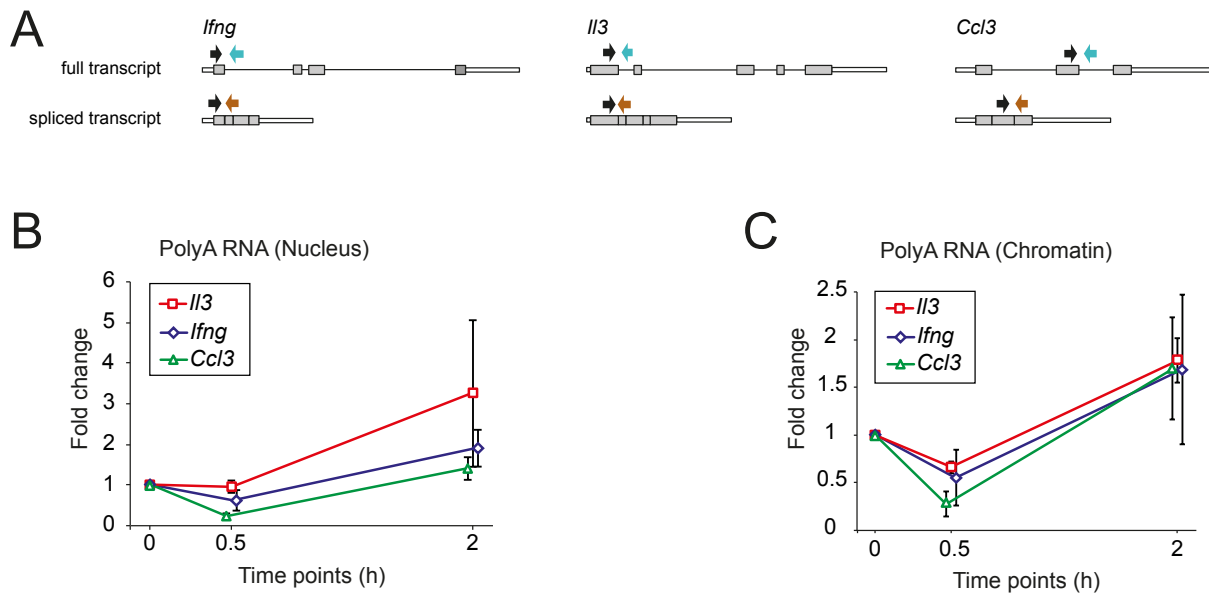


Figure 35: Reduction in cotranscriptional splicing for polyadenylated RNA (Lichti, Davari *et al.*, 2017)

(A) Schematic overview of primer design to study spliced and unspliced transcripts. (B and C) Fold changes in exon/intron ratio determined by qRT-PCR analysis for the polyadenylated whole nucleus fraction (B) and the polyadenylated chromatin fraction (C) for *Il3*, *Ifng* and *Ccl3*. The mean and standard deviation (error bars) are shown for three (B) or five (C) independent experiments.

4.4.2 Phosphorylation states of the CTD of RNAPII correlate with fluctuations in splicing rates

It was already speculated that changes in transcription can dramatically affect cotranscriptional splicing, but also that splicing, in turn, can influence transcription (Bentley, 2014). Since splicing is spatially and temporally linked to transcription, we further characterized RNAPII, a key player in coordinating transcription with splicing. Figure 25 revealed a general upregulation of genes associated with translation. In line with this our data showed that RNAPIII subunits were upregulated, while there was no change in RNAPII subunit expression (data not shown). To determine RNAPII modifications, western analysis of RPB1, the largest subunit of RNAPII was performed. This allowed diminishing the hypophosphorylated IIA form from the hyperphosphorylated IIO form of RNAPII. Upon activation, there was a shift to the IIO form, indicating phosphorylation of the CTD, which is essential for transcriptional elongation (Figure 36A). This shift, observed 2 h upon activation, correlated with the optimization in cotranscriptional splicing. Next we wanted to distinguish transcriptional initiation promoted by Ser5 and transcriptional elongation promoted by Ser2 phosphorylation of the CTD of RNAPII. Interestingly, phosphorylation of

Ser5 peaked at 1 h, while Ser2 phosphorylation increased gradually, becoming the dominant type of phosphorylation 2 h after activation (Figure 36B). Again, this correlated with our findings regarding optimization in cotranscriptional splicing.

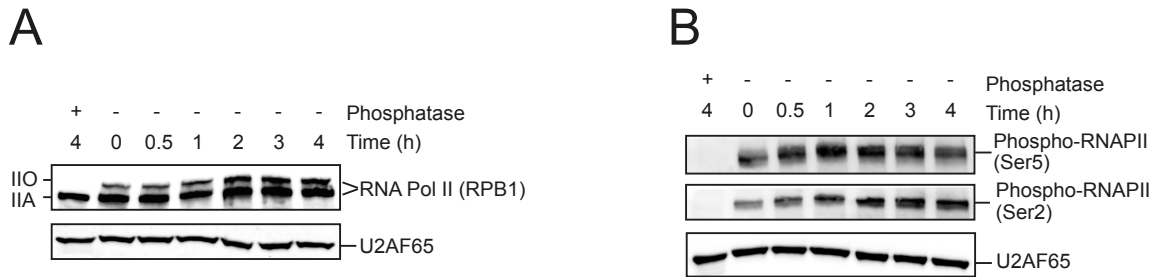


Figure 36: RNAPII phosphorylation states change over time (Lichti, Davari *et al.*, 2017)

Western blot analysis of RNAPII expression using an antibody against RPB1 (indicating hyperphosphorylated IIO and hypophosphorylated IIA form) (A) and Ser5 and Ser2 phosphorylation-specific antibodies (B). The splicing factor U2AF65 was used as loading control.

4.4.3 Changes in splicing rate reflect distance to TSS

Consistent with the role of Ser5 in early RNA processing events (e.g. capping of nascent RNAs), Ser5 phosphorylated RNAPII complexes were shown to be enriched near the TSS (Komarnitsky *et al.*, 2000; Cho *et al.*, 1997). Indeed, changes in splicing rates were most noticeable close to the TSS (Figure 37). Furthermore, decreases in splicing rates close to the TSS were observed until 1 h, whereas at later time points they were slightly increased compared to nonactivated cells. This is consistent with a shift from predominant Ser5 phosphorylation to Ser2 phosphorylation which is most visible close to the TSS.

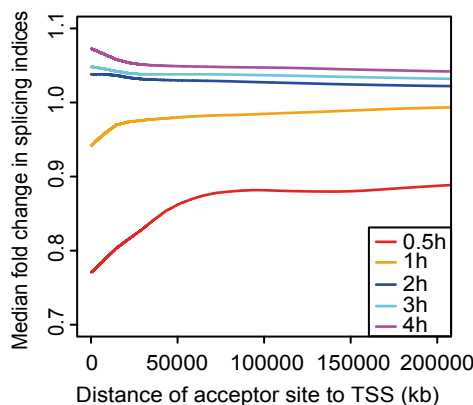


Figure 37: Splicing indices relative to distance to TSS (Lichti, Davari *et al.*, 2017)

Local regression fit is plotted for splicing indices relative to the distance to the TSS for all time points.

4.4.4 Interaction of splicing factors with phosphorylated CTD and activation of pTEFb

Figure 36 revealed that phosphorylation of Ser5 of the RNAPII CTD is the dominant form of phosphorylation until 1 h, when Ser2 phosphorylation takes over. Since the Ser5 phosphorylated form of RNAPII cannot efficiently recruit splicing factors, we wondered if this might explain the drop in cotranscriptional splicing. In turn, it is known that Ser2 phosphorylation is responsible for the recruitment of splicing factors such as U2AF65 (Gu *et al.*, 2013). In line with this, we could show by immunoprecipitating for U2AF65 an increased interaction between this splicing factor and Ser2 phosphorylated RNAPII (Figure 38A). This indicated, that p-Ser2 of the CTD of RNAPII, recruits splicing factors, as indicated for U2AF65, which results in an optimization of cotranscriptional splicing. Ser2 phosphorylation is mediated by the cyclin-dependent kinase pTEFb, which is composed of cyclin-dependent kinase 9 (CDK9) and cyclin T (Peterlin and Price, 2006). Binding of a T family cyclin (CycT1, CycT2a or CycT2b) or CycK is necessary for CDK9 activation (Baumli *et al.*, 2008; Peng *et al.*, 1998). Consequently, we determined whether the observed increase in Ser2 phosphorylation was mediated by activation of pTEFb. Therefore, immunoprecipitation for cyclin T1, the major form of the CDK9/cyclin T complex (Peng *et al.*, 1998) was performed. To distinguish activated pTEFb an antibody that recognized both, phosphorylated CDK9 and total CDK9, was used. Indeed, the longer isoform of CDK9 was massively phosphorylated within the complex no later than 2 h upon activation (Figure 30B), reflecting activation of pTEFb, which likely phosphorylates Ser2 of the CTD of RNAPII coinciding with a global optimization in cotranscriptional splicing processes.

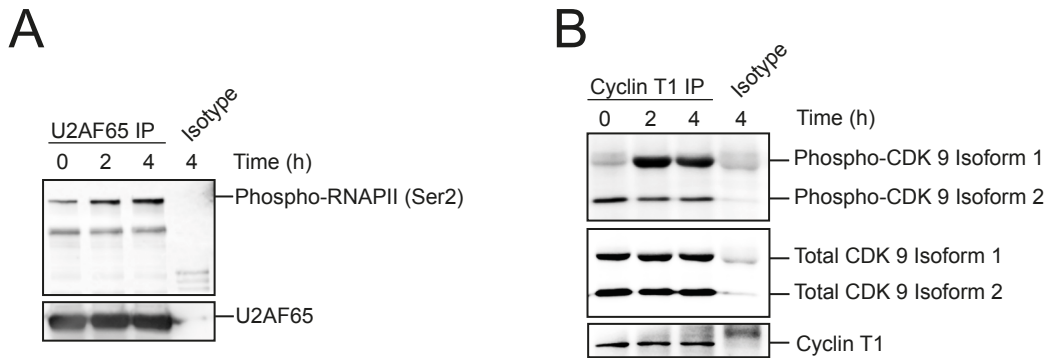


Figure 38: Ser2 phosphorylation of RNAPII mediates recruitment of splicing factors and is activated by pTEFb (Lichti, Davari *et al.*, 2017)

(A) Immunoprecipitation at different time points with antibodies recognizing U2AF65 to detect Ser2 phosphorylated RNAPII. U2AF65 was used as a loading control. (B) Immunoprecipitation with cyclin T1 to detect phosphorylated CDK9 (indicating active elongation complex formations) and total CDK9. Two isoforms of CDK9 could be detected. Cyclin T1 was used as a loading control.

4.5 H3K36me ChIP-seq

Along with RNAPII kinetics, splicing is also coupled with chromatin marks. Recent studies demonstrated, that the histone H3 lysine 36 trimethyl modification (H3K36me₃) is directly influenced by splicing (Kim *et al.*, 2011). Therefore, H3K36me₃ ChIP-seq was performed at 0 h, 0.5 h and 2 h after activation of Th1 cells. A replicate was included and all findings depicted were proven for both replicates.

H3K36me₃ is a mark of active transcription and the H3K36 methyltransferase Set2 associates and travels with RNAPII along the gene (Krogan *et al.*, 2003; Li *et al.*, 2002). Accordingly, it was enriched over gene bodies and marked expressed genes (Figure 39).

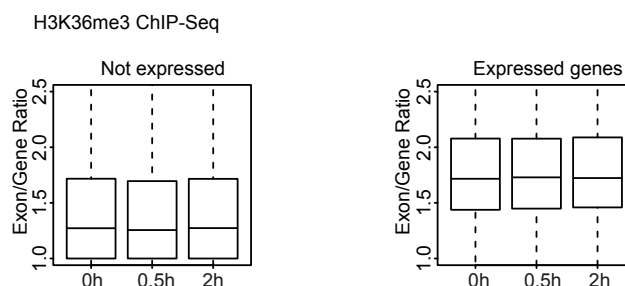


Figure 39: H3K36me₃ marks expressed genes (Lichti, Davari *et al.*, 2017)

Boxplots indicating exon per gene ratio of H3K36me₃ for unexpressed and expressed genes at all time points.

Nevertheless, the relative enrichment of H3K36me3 on exons did not significantly change over time for sets of differently regulated genes (Figure 40).

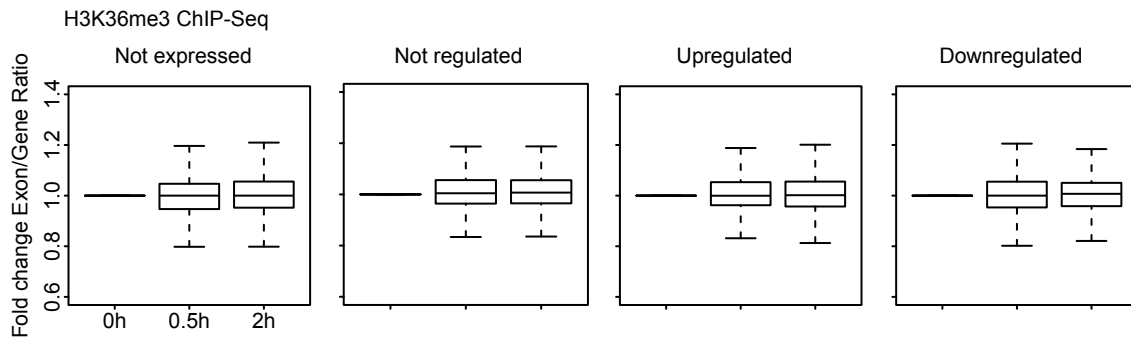


Figure 40: H3K36me3 does not correlate with changes in gene expression (Lichti, Davari *et al.*, 2017)

Boxplots showing fold changes in the exon per gene ratio of H3K36me3 for all time points. Genes were grouped according to their type of regulation.

Besides, we could not determine any correlation between the drop in cotranscriptional splicing and this chromatin mark. This might reflect that modification of H3K36me3 is not as fast and dynamic as RNAPII and therefore has just a minor role for controlling transcription and splicing of activated T cells.

5 Discussion

The results discussed in this chapter have been published to some extent in Cell Reports and Trends in Biochemical Sciences (TIBS) (Lichti, Davari *et al.*, 2017; Lichti *et al.*, in revision). This includes Figure 41 and may include argumentation.

In this study, we combined sequencing methods to simultaneously study total RNA (RNA-seq), *de novo* transcription (4sU-seq), translation (ribosome profiling) as well as RNAPII binding (ChIP-seq). This determined genome-wide temporal dynamics in gene regulation of rapid responding cells. Th1 cells are known for rapid induction of cytokines but the underlying mechanisms were still not sufficiently investigated. Although some mechanisms have been proposed, those studies mainly relied on steady state conditions, cell lines, single mechanisms or unphysiological activation conditions (Scheu *et al.*, 2006; Schott *et al.*, 2014; Chang *et al.*, 2013; Blackinton and Keene, 2016).

5.1 Transcriptional regulation

The experimental setup of our study (Figure 12) allowed us to perform a comprehensive analysis that clearly distinguished transcriptional from translational changes of activated *in vitro* generated Th1 cells over time and correlate it with RNAPII binding and/or recruitment. This depicted a T cell that massively regulates gene transcription with extremely coupled changes in translation (chapter 5.2). Besides, rapid transcriptional upregulation of genes coincided with a rapid increase in RNAPII abundance (chapter 5.5).

A study performed by Bhatt *et al.* indicated that lipid A-activated gene expression in macrophages is primarily regulated at the level of transcriptional initiation (Bhatt *et al.*, 2012), similar to conclusions of LPS-induced transcription and induction of novel cellular functions in dendritic cells (Rabani *et al.*, 2011; Jovanovic *et al.*, 2015) and inducible immune response of macrophages to a bacterial pathogen (Barry *et al.*, 2017), which is all in accordance with our observations in T cells. Unfortunately, no RNAPII ChIP-seq was performed in these studies to verify the connection between transcriptional upregulation and RNAPII. Although a study conducted by Fowler *et al.* suggested RNAPII to be paused at the TSS (chapter 5.4) of BCR activated B cells, RNAPII recruitment was also broadly induced

and they proposed that c-Myc might play an important role during early phases of B cell activation (Fowler *et al.*, 2015). C-Myc was shown to increase overall expression, acting as a universal amplifier of transcription (Nie *et al.*, 2012; Lin *et al.*, 2012). Our study also suggested c-Myc as key transcription factor for the majority of upregulated genes. Assigning genes according to their temporal transcriptional and translational regulation into different hierarchical clusters, STATs and RelA were additionally identified by computational enrichment analysis as main regulators of IEGs (Figure 25). Hence, general transcription factors including c-Myc, STATs and RelA might induce transcriptional regulation, probably in concordance with epigenetic marks and TFIID activity (Kouzin *et al.*, 2013).

Our study provided expression values for 9,420 protein-coding genes over time. Although the magnitude of regulation was significantly higher for upregulated genes, significantly more genes were downregulated (Figure 16). This emphasized that activated T cells focus on a massive transcriptional upregulation of immune response genes. To counteract in terms of energy demands, many genes were shut down, even exceeding numbers of upregulated genes. Noteworthy, hierarchical clustering did not just reveal that most immunological genes were highly upregulated. It also revealed many IEGs that were previously unmentioned in the context of a T cell response. It was further uncovered that ~30 % of all genes were either up- or downregulated (at least 2-fold) 4 h upon activation. These numbers did hardly change when applying more stringent criteria for regulation as described for hierarchical clustering analysis and were accurate for both, *de novo* transcription (4sU RNA) and translation (RP). This further implied that transcription and translation were coupled, which was also proved (Figure 20).

5.2 Coupled changes in transcription and translation

Coupling of transcription and translation has long been proposed to follow the scheme of a forward flow as suggested by the central dogma of molecular biology (Crick, 1970). However, Tebaldi *et al.* showed that for epidermal growth factor treated HeLa cells, transcription and translation were extensively uncoupled (Tebaldi *et al.*, 2012). Based on their finding they extended their analysis on published data claiming that the degree of uncoupling is higher

than for coupling. Intriguingly, they proposed uncoupling as a general mechanism for mammals.

To verify whether changes in transcription and translation were coupled in our study, a correlation analysis of fold changes was performed (Figure 20). This clearly indicated a strong global coupling of changes in transcription and translation. Moreover, no global changes in translation rates could be determined upon activation (Figure 24). Nevertheless, a well-recognized study in NIH3T3 mouse fibroblasts (Schwanhausser *et al.*, 2011) as well as in differentiating mammalian cells (Kristensen *et al.*, 2013) also determined low correlation between protein and mRNA abundance with predominating differences in translation rate. Besides, it was suggested that for mammalian cells $\geq 60\%$ of variance in protein expression could be explained by translation and protein degradation (Li and Biggin, 2015). With improved and more accurate statistical methods as well as including replicates, Jovanovic *et al.* could show for dendritic cells that at steady state mRNA levels explain 68% of the variance in protein expression (Jovanovic *et al.*, 2015). Upon stimulation of cells it increased to $\sim 90\%$, with translation and protein degradation explaining only 4% and 6% of the changes in protein expression, respectively. Especially proteins performing basic cellular functions were predominantly regulated at the level of protein translation or degradation. Despite repression of their transcripts, the levels of many proteins in the translational machinery were upregulated upon stimulation due to increased translation rates. All in all they propose a model in which the induction of novel cellular functions is primarily driven through transcriptional changes (chapter 5.1). (Jovanovic *et al.*, 2015)

When reanalyzing data from Schwanhausser *et al.* (Schwanhausser *et al.*, 2011), measurement errors of the original publication were eliminated showing that mRNA levels do not solely account for 34% of variance in protein levels but at least for 56% (Li *et al.*, 2014). It was further stated that mRNA levels likely explain $\sim 84\%$ of variance in protein levels. These numbers are in accordance with the results of our study, which stress the impact of mRNA abundance on protein outcome during an immune cell response and indicated that $\sim 92\%$ of changes in translation are determined by changes in transcription. But how can the observed differences in coupling amongst mentioned studies be explained? One reason could be, as shown for Schwanhausser *et al.*, wrong statistical models (Li and Biggin, 2015). One might further speculate that differentiating cells and cells that do not

show such a rapid gene response as in immune cells, display a higher degree of uncoupling between the transcriptome and the translome (Tebaldi *et al.*, 2012; Kristensen *et al.*, 2013). This was also shown for dendritic cells at steady state (Jovanovic *et al.*, 2015). In line with this, Kristensen *et al.* observed a high correlation between mRNA and protein, when solely analyzing up- and downregulated genes (Kristensen *et al.*, 2013).

Considering these results, there is growing support for the assumption that upon activation of rapid responding cells, gene regulation is highly coupled and changes in mRNA abundance dominate changes in protein levels, especially for immune response genes. As a consequence cellular programs are less error-prone during the immune response but maintain a rapid forward flow of information, e.g. to fight the pathogen. Support of this notion comes from Barry *et al.* who proposed that selective translation, usually regulated at the level of initiation, would be easily defeated by pathogens which are able to block downstream processes of translation initiation (Barry *et al.*, 2017). Consequently, they indicated mRNA superinduction which describes a massive and sustained production of cytokine transcripts as the main mechanism to overcome the pathogen-mediated global block in protein synthesis, which is a common strategy by many viral and bacterial pathogens (Barry *et al.*, 2017).

5.3 Cotranscriptional splicing

One of the most surprising findings upon activation of Th1 cells was that cotranscriptional splicing rates dropped first but were gradually optimized at later time points (Figure 28). In electron micrography studies of *Drosophila* embryo genes, Beyer and Osheim revealed that RNA could be spliced while still being transcribed (Beyer and Osheim, 1988). This mechanism, termed cotranscriptional splicing, has been accepted to be predominant for most mRNAs (Bentley, 2014). Nevertheless, fluctuations as observed in our study have only been found in lipid-A activated primary macrophages so far (Bhatt *et al.*, 2012). By sequencing subcellular fractions Bhatt *et al.* followed transcription kinetics of individual genes from initiation at the chromatin, release into the nucleoplasm until mRNA export into the cytoplasm. They showed that chromatin-associated transcripts, which are considered to reflect newly transcribed RNA, were incompletely spliced whereas at later time points

introns were lost and this accounted for the majority of genes. In a follow-up paper they showed for a selected set of upregulated genes that intron excision events occur on RNAs that have already been 3'-cleaved and polyadenylated in association with the chromatin (Pandya-Jones *et al.*, 2013). They observed a lag after termination of transcription but before transcript release from the chromatin into the nucleoplasm and suggested this lag to be essential for the completion of splicing and export to the cytoplasm. We performed a similar fractionation assay during activation of Th1 cells and likewise determined (for selected genes) fluctuations in chromatin-associated RNA. Since sequencing of 4sU RNA was performed without previous poly(A) selection, we wondered whether the observed drop in splicing rates likewise occurred in already polyadenylated RNA. Indeed, the drop already occurred in polyadenylated nucleic acid as well as in polyadenylated chromatin-associated RNA and was also followed by an optimization (Figure 35). Although we could not exclude that these transcripts lead to some impairment in protein functionality, unspliced transcripts were very likely not stalled until being spliced. The observed fluctuations seemed rather to be a global mechanism affecting all genes irrespective of their regulation and did not reflect an overall increase in newly transcribed RNA at the beginning of the activation (Figure 29).

Since transcription can affect cotranscriptional splicing and vice versa (Saldi *et al.*, 2016), RNAPII kinetics were correlated with splicing kinetics. Western blot analysis showed that Ser5 phosphorylation of the CTD of RNAPII is noticeably increased at the beginning of T cell activation, while Ser2 phosphorylation is the predominant type 2 h upon activation (Figure 36). This was consistent with an optimization in splicing kinetics and indicated that it needs time until Ser2 phosphorylation of the elongating RNAPII is sufficient, because this modification seems to be necessary for optimal cotranscriptional splicing rates. Since our sequencing data did not reveal any fluctuations in the expression of general splicing factors (data not shown), we suggested that their recruitment had to be optimized. This was shown to be mediated by Ser2 phosphorylation of the CTD (Gu *et al.*, 2013). Indeed, the well-known splicing factor U2AF65, which takes part in the earliest steps of spliceosome assembly (Zamore and Green, 1991), demonstrated an increased interaction with Ser2 phosphorylated CTD over time (Figure 38). In line with that, pTEFb, which is known to preferentially mediate Ser2 phosphorylation (Ni *et al.*, 2004; Peterlin and Price, 2006), was activated over time (Figure 38). Activation of pTEFb might be further associated with c-Myc binding, since

this transcription factor can also bind pTEFb thus, facilitating transcriptional elongation (Rahl *et al.*, 2010).

A study by Hargreaves *et al.* showed that in macrophages GC-rich primary response gene (PRG) promoters were preassociated with Ser5-phosphorylated RNAPII, even prior to LPS activation (Hargreaves *et al.*, 2009). However, they revealed that transcription was not paused and Ser5 phosphorylation at PRGs generated full-length but unspliced transcripts that were quickly degraded because transcription could not be coupled with RNA processing unless activation took place. It has to be considered that this was only shown for a small number of 25 GC-rich PRGs, which experienced further recruitment of RNAPII upon activation. They further demonstrated that p-TEFb engagement is essential to induce PRG expression (Hargreaves *et al.*, 2009). Nevertheless, this again reveals that transcriptional and cotranscriptional splicing processes are directly linked but especially exceptions occurring in this interaction are not yet sufficiently investigated. It would be furthermore interesting to know whether the observed fluctuations in cotranscriptional splicing are a necessary regulatory mechanism or just a result of a massive *de novo* recruitment of RNAPII.

5.4 Global pausing of RNAPII is not the main mechanism to keep genes responsive

Pausing of RNAPII is widely argued as main mechanism to keep genes highly responsive, especially when they need to be expressed rapidly (Jonkers and Lis, 2015). This means that RNAPII is already bound to the promoter and pauses in the early transcriptional elongation state, when it is stably associated with the nascent RNA until gene expression takes place (Adelman and Lis, 2012). It was obvious to speculate that rapidly upregulated genes, especially cytokines from our study might benefit from this mechanism. RNAPII ChIP-seq clearly demonstrated that fold changes in newly transcribed RNA, which were highly correlated with fold changes in translation, correlated with fold changes in RNAPII abundance at the promoter (Figure 30). However, distinct RNAPII peaks at the TSS of genes were also detected before activation. Yet, our experimental setup allowed us to compare genes with promoter RNAPII peaks at the TSS of non-activated cells to FPKM values of newly transcribed RNA of the respective gene. We observed that most genes with a distinct RNAPII peak at the TSS already showed *de novo* transcriptional activity even for unregulated

genes (data not shown). In general, FPKM values of promoter RNAPII correlated well with FPKM values of *de novo* transcription even before activation (data not shown). Besides, we only identified 29 genes that are potentially induced by a paused RNAPII, indicating that at least for T cells on time *de novo* recruitment of RNAPII is the dominant mechanism to ensure a rapid transcriptional gene response.

A significant genome-wide increase in RNAPII recruitment was also observed in B cells, albeit just upon activation via the BCR and not via LPS (Fowler *et al.*, 2015). Furthermore, they suggest that RNAPII is paused before activation, since the transition from transcriptional initiation to elongation was less for BCR induced B cells. Although RNAPII pausing in immune cells is widely discussed in literature, there are some drawbacks of those studies. RNAPII pausing was either shown for a small amount of genes (Hargreaves *et al.*, 2009), genes already showed constitutive expression (Hargreaves *et al.*, 2009) or no significant change in promoter to gene body ratio could be detected (Kouzine *et al.*, 2013). Furthermore, most of these studies just suggest pausing RNAPII as a mechanism without proving it and additionally proposed RNAPII recruitment to be in action (chapter 5.5) (Fowler *et al.*, 2015).

In human embryonic stem cells, for example, approximately 30 % of genes experienced transcription initiation without any evidence of further elongation and transcript detection, suggesting post-initiation regulation to be the control mechanism (Guenther *et al.*, 2007). Further analysis in primary human hepatocytes and a B cell line confirmed these observations and the authors reasoned that the lack of transcript accumulation might be due to two general mechanisms. First, transcriptional pausing, poor processivity or abortive initiation and second, posttranscriptional degradation. Interestingly, they also suggested that transcript levels are difficult to detect (Guenther *et al.*, 2007). Apparently, this lack in sensitivity could explain their observations. In line with this, a global analysis of the human transcriptome by Sultan *et al.* identified virtually no hypophosphorylated RNAPII near promoters of silent genes detected by RNA-seq (Sultan *et al.*, 2008), suggesting that nearly all genes that are bound by RNAPII produce full-length transcripts (Core *et al.*, 2008) albeit often just detectable with high sensitivity methods.

Supposing that RNAPII pausing nevertheless appears, but not as a genome-wide mechanism, it still remains an open question, when it occurs and which genes are affected. Since one main feature of paused RNAPII is to retain the windows of opportunity for regulation and coordination of transcriptional regulation, it seems that at least for T cells, and maybe also for immune cells in general, transcriptional processes during activation are tightly regulated, once started. Although pausing of RNAPII might be a mechanism to keep single genes responsive, rapid upregulation of RNAPII seemed to be the genome-wide mechanism for gene response, also for the majority of IEGs (Figure 31) (chapter 5.5).

5.5 Rapid recruitment of RNAPII dictates transcriptional changes

Our study clearly revealed that fold changes in RNAPII promoter abundance correlated with fold changes in *de novo* transcription and determined that rapid *de novo* recruitment of RNAPII primarily mediated transcriptional changes (Figure 30). This particularly applied for IEGs, which showed hardly any RNAPII peaks prior to activation. Although some studies proposed pausing of RNAPII as the main mechanism to keep genes, especially IEGs, highly responsive (Jonkers and Lis, 2015), most of these studies agree that additional recruitment of RNAPII is necessary and contributes to gene expression (Fowler *et al.*, 2015; Hargreaves *et al.*, 2009). Our analysis did not just demonstrate that additional RNAPII recruitment is necessary, but determined that it primarily mediates transcriptional changes in activated T cells, especially for IEGs (Figure 31). Transcriptional features characterizing these genes might facilitate this, since PRGs from murine macrophages and human T cells were shown to be primed for rapid activation by the enriched presence of CpG dinucleotides (CpG islands) (Ramirez-Carrozzi *et al.*, 2009; Hargreaves *et al.*, 2009). This might prevent the formation of stable nucleosomes, and consequently exhibit open chromatin to facilitate transcriptional activation (Singh, 2009). Nevertheless, this was solely noticed for a limited number of PRGs using microarrays and was not confirmed in our study, although constitutively active chromatin was preferentially determined at LPS-induced CpG island promoters (Ramirez-Carrozzi *et al.*, 2009). Consistently, Bhatt *et al.* achieved the conclusion that CpG content of a promoter per se neither dictates basal gene transcription nor responsiveness to LPS (Bhatt *et al.*, 2012; Sen and Fugmann, 2012). In B cells, CpG islands were slightly higher correlated with gene expression, than areas without CpG (Fowler *et al.*,

2015). This suggests that CpG content may facilitate transcriptional upregulation but is not a prerequisite. Induced abundance of RNAPII was also shown for activated B cells (Fowler *et al.*, 2015). Interestingly, this induction was most pronounced for activation via the B cell receptor (BCR) but hardly visible upon LPS activation and no preference for CpG associated promoter gene expression was detected for either response. LPS activated macrophages did also show *de novo* recruitment of RNAPII for induced genes, although RNAPII was suggested to be already preassociated (Hargreaves *et al.*, 2009).

5.6 The emerging picture of a global immune response

Previously mentioned studies, which performed comprehensive gene analysis of activated macrophages, dendritic cells, B cells, T cells as well as pathogen-infected macrophages demonstrated that the majority of functional changes during immune activation is controlled at the level of transcription (Bhatt *et al.*, 2012; Jovanovic *et al.*, 2015; Fowler *et al.*, 2015; Lichti, Davari *et al.*, 2017; Barry *et al.*, 2017). To be more precise, RNAPII recruitment drives changes during B cell and T cell activation (Fowler *et al.*, 2015; Lichti, Davari *et al.*, 2017) and most likely for all rapid responding immune cells. Along with global switches in phosphorylation states of RNAPII we observed a temporary switch in cotranscriptional splicing (Lichti, Davari *et al.*, 2017), which was also examined upon macrophage activation (Bhatt *et al.*, 2012).

A study that received considerable attention claimed that *Ifng* was posttranscriptionally regulated during the switch of T effector cells to aerobic glycolysis upon activation (Chang *et al.*, 2013). Although this was highly questioned and epigenetic causes might drive these changes (Peng *et al.*, 2016) posttranscriptional gene control was even proposed as a principal mechanism in immune responses (Piccirillo *et al.*, 2014). However, comprehensive studies investigating different levels of gene regulation were still lacking at that time. A crucial question remains: Which context allows immune function to be dominantly shaped at the level of posttranscriptional control. Therefore, the question arises whether posttranscriptional control acts in synergy during the immune response, potentially as a fine-tuning mechanism, or whether it might be generally disabled but becomes reactivated for the resolution of the response. Micro RNAs (miRNAs) are a family of small RNAs that

silence gene expression at the posttranscriptional level, predominantly through binding the 3' UTR of their mRNA targets (Jonas and Izaurralde, 2015). Remarkably, posttranscriptional control by miRNAs was decreased in activated and differentiating T cells (Bronevetsky *et al.*, 2013). Downregulation of miRNAs was also shown for activated B cells (Fowler *et al.*, 2015). Furthermore, this downregulation was more elevated upon BCR activation (Fowler *et al.*, 2015), which coincided with an intensified gene response compared to LPS activation. One might speculate that downregulation of miRNAs is a necessary step to ensure a proper immune response. Moreover, it was shown in monocytes, B cells and T cells that upon activation mRNAs tend to have shorter 3' UTRs (Sandberg *et al.*, 2008) efficiently reducing possible posttranscriptional control events due to a loss of key regulatory elements such as miRNA target sites and AU-rich elements (AREs). The prominent CCCH-type zinc finger proteins tristetraprolin (TTP, encoded by *Zfp36*), Roquin-1 (Rc3h1) and Regnase-1 (Zc3h12a/Mcpip1) are well-known regulators of inflammatory genes. Despite different ways to target mRNA decay they share a common feature, namely maintenance of cellular function and shut down of immune response. While TTP promotes decay by binding to AREs in the 3' UTR of its target mRNAs, Roquin-1 and Regnase-1 recognize stem-loop motifs in 3' UTRs (Fu and Blackshear, 2017). These evolutionarily closely related proteins act similarly (or even in concert as demonstrated for Regnase-1 and Roquin-1) and are degraded upon activation as shown for different stimuli and immune cells (Mino *et al.*, 2015; Jeltsch *et al.*, 2014; Iwasaki *et al.*, 2011). Besides, TTP was shown to be induced biphasic upon macrophage activation, which means that after strong induction, it is rapidly degraded until a second phase of expression started at later time points (Tchen *et al.*, 2004). All three proteins recognize their own mRNA (Fu and Blackshear, 2017), which enables reappearance after the initial response, while during activation other processes seem to be in progress. Indeed, our study showed significantly high turnover rates for highly expressed genes (including most IEGs), likely to facilitate shut down of these genes after the immune response. Whereas during the response translation rates do not change, principally for all genes, emphasizing that on a global scale, translational regulation only plays a minor role. It might be possible that these genes additionally contain elevated levels of AREs, thus, they are more subject to ARE-mediated decay to ensure immune resolution as shown for *Tnf* (Kontoyiannis *et al.*, 1999).

To delineate the whole picture of gene regulatory mechanisms during the life of an immune cell, the question of regulation before the activation still remains. At this resting steady state, programs that maintain cell lineage identity must play a major role. One example are Roquin-1 and Regnase-1, which posttranscriptionally regulated important immunological genes including transcription factors and co-stimulators like *Nfkbid*, *c-Rel*, and *Icos* (Fu and Blakeshear, 2017). Consistently, *Roquin-1*- and *Regnase-1*-deficient mice displayed alterations in T effector differentiation programs (Fu and Blakeshear, 2017). The TTP family member proteins ZFP36L1 and ZFP36L2 were proven to ensure the maintenance of the marginal B cell state and to prevent a premature differentiation into follicular B cells (Galloway *et al.*, 2016). Additionally, mice in which T cells lacked all mature miRNAs displayed impaired T helper differentiation programs (Jeker and Bluestone, 2013). Besides, splicing mechanisms and translational programs seemed to be distinct between different types of resting immune cells (Schaub and Glasmacher, 2017; Bjur *et al.*, 2013).

Setting our study in context proposes a scenario for immune cells, in which functional changes during activation are driven by transcriptional networks, whereas cell lineage identity and subsequent immune resolution are ensured by posttranscriptional mechanisms (Figure 41).

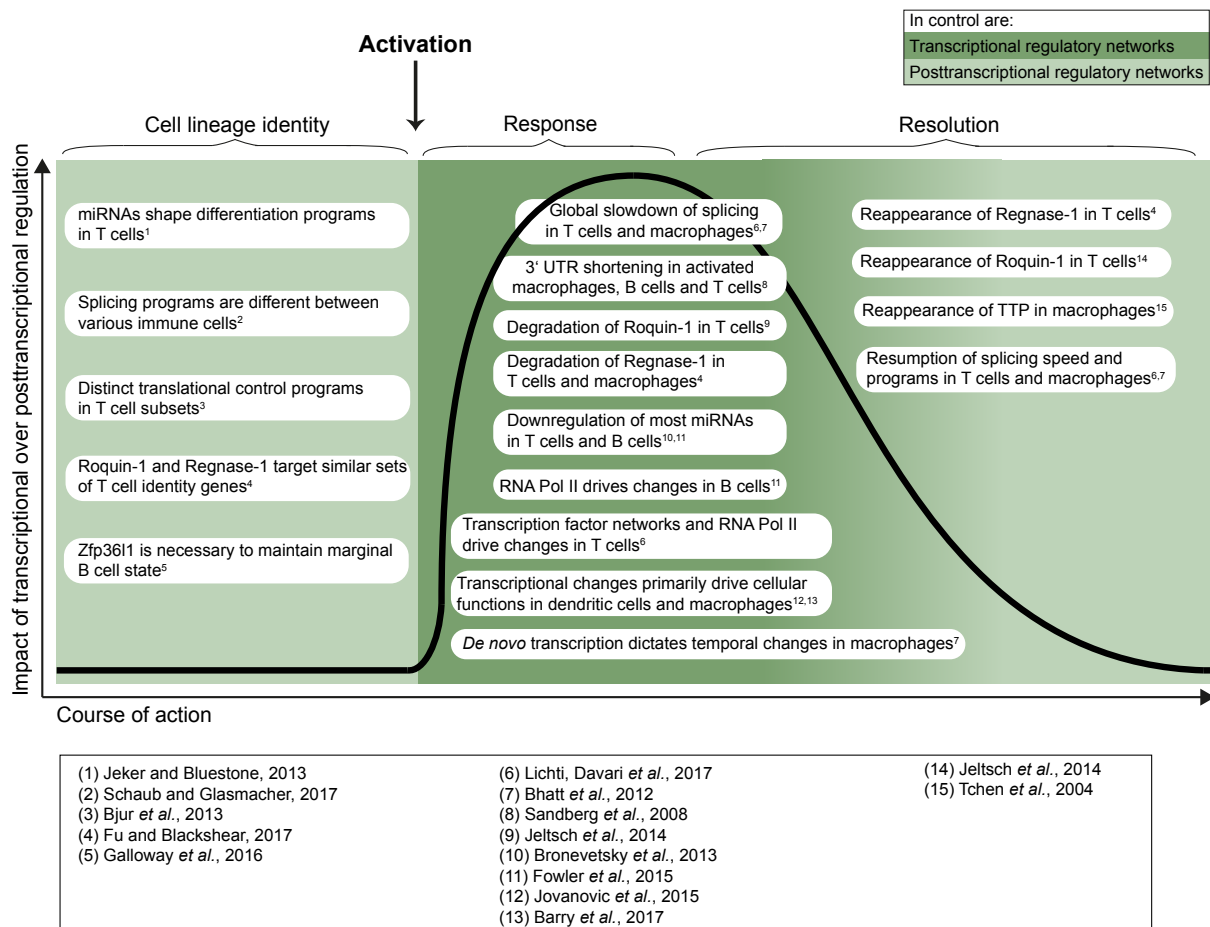


Figure 41: Alternating functional programs in immune cells (modified from Lichti *et al.*)

Schematic drawing of a general model that emerges for gene regulatory networks in immune cells. Reviewed literature is shown that supports the hypothesis that transcriptional networks (dark green) alternate with posttranscriptional networks (green) to dominantly shape gene expression for immune activation versus resolution and lineage identity, respectively. References are given below.

6 Conclusion

By now, a myriad of studies described mechanisms responsible and necessary to ensure immune responses. To unmask the underlying molecular mechanisms during a T cell response, we performed a dynamic genome-wide study in *in vitro* generated Th1 cells. Combining 4sU-seq, RNA-seq, ribosome profiling and RNAPII ChIP-seq allowed us to track transcriptional and translational changes, as well as alterations in RNAPII binding.

This holistic approach delineated all potential layers of RNA regulation to uncover the principal molecular mechanisms that occur genome-wide during the immune response of a T cell. Rapid *de novo* recruitment of RNAPII primarily mediated transcriptional changes, which were highly coupled to translational changes. Cotranscriptional splicing rates showed a genome-wide temporary slowdown that was subsequently optimized and correlated with increasing Ser2 phosphorylation of the RNAPII CTD and activation of the pTEFb.

The data depicted in this study initiated many debates amongst immunologists, defining the role of transcriptional and posttranscriptional regulation during the immune response. While at the beginning of this thesis just a few genome-wide studies in immune cells were published, meanwhile our study, in context with others, sheds light on the genome-wide principles of gene regulation in immune cells. This let us propose a model of transcriptional and posttranscriptional control for immune cells showing that posttranscriptional regulation might be generally dismantled during the immune response, but comes to play when ensuring subsequent immune resolution and to maintain cell lineage identity.

7 Contributions and Acknowledgments

First of all I would especially like to thank Dr. Elke Glasmacher for her engagement and passion to push and publish the project. I am grateful for her unique assistance as well as her suggestions and ideas that helped to shape the project.

Thanks for performing GFP transfection together with Dr. Kathrin Davari during the review of our paper.

A special thanks applies to Dr. Kathrin Davari who worked with me on this project. Thanks for being a great source of inspiration that helped managing my thesis. She performed Ribosome Profiling for the preliminary test and the main experiment. I would further like to thank her for performing ChIP and subcellular fractionation assays. She also performed Western Blots shown in Figure 34 and Figure 36 as well as immunoprecipitation shown in Figure 38.

I would also like to thank Dr. Franziska Greulich, who helped all the time I had a question concerning bioinformatics. Thanks for all your advice and meaningful discussions during my thesis. She also helped us with ChIP-seq and performed library preparation for RNAPII and H3K36me3 ChIP samples.

Prof. Dr. Caroline Friedel performed mapping of all sequencing results as well as analysis described in chapter (3.9.1 – 3.9.3). She helped us interpreting the results and suggested further analyses. I am very grateful that she created Figure 13, 16, 18-22, 24-26, 28 (right), 30, 31 (right), 32-33, 37 and 39-40. Without her help, the project would not have been possible.

I would further like to thank Prof. Matthias Heinig for performing additional bioinformatics analysis. This included Figure 27.

Contributions
and
Acknowledgments

A special thanks also applies to Elisabeth Graf and her help and assistance in establishing library preparation and sequencing. Sandy Loesecke also helped in library preparation, thanks for that.

I would also like to thank Thomas Schwarzmayr, who performed mapping of the first sequencing results, which contributed to Figure 8. And thanks for helping me to learn how to analyze sequencing data.

Thanks to all members of the AG Glasmacher. It was always a pleasure working with you. I also have to thank you for all your help, discussions, scientific input and support during the last years. Christine Wolf helped performing Western Blots and immunoprecipitation. Christian Gallus performed Western Blot for Figure 5. Thanks to Matthias von Gamm for mouse colony maintenance and proofreading my thesis.

Dirk Eick, Andrew Flatley and Elisabeth Kremmer provided RNAPII and T cell antibodies.

Finally I would like to thank my family and especially Magda for unlimited support during the time of my thesis.

8 Literature

- ADELMAN, K. & LIS, J. T. 2012. Promoter-proximal pausing of RNA polymerase II: emerging roles in metazoans. *Nat Rev Genet*, 13, 720-31.
- AFKARIAN, M., SEDY, J. R., YANG, J., JACOBSON, N. G., CEREB, N., YANG, S. Y., *et al.* 2002. T-bet is a STAT1-induced regulator of IL-12R expression in naive CD4⁺ T cells. *Nat Immunol*, 3, 549-57.
- ALBERTS, B. 2015. *Molecular biology of the cell*, New York, NY [u.a.], Garland Science.
- BARBORIC, M., LENASI, T., CHEN, H., JOHANSEN, E. B., GUO, S. & PETERLIN, B. M. 2009. 7SK snRNP/P-TEFb couples transcription elongation with alternative splicing and is essential for vertebrate development. *Proc Natl Acad Sci U S A*, 106, 7798-803.
- BARRON-CASELLA, E. & CORDEN, J. L. 1992. Conservation of the mammalian RNA polymerase II largest-subunit C-terminal domain. *J Mol Evol*, 35, 405-10.
- BARRY, K. C., INGOLIA, N. T. & VANCE, R. E. 2017. Global analysis of gene expression reveals mRNA superinduction is required for the inducible immune response to a bacterial pathogen. *Elife*, 6.
- BAUMLI, S., LOLLI, G., LOWE, E. D., TROIANI, S., RUSCONI, L., BULLOCK, A. N., *et al.* 2008. The structure of P-TEFb (CDK9/cyclin T1), its complex with flavopiridol and regulation by phosphorylation. *EMBO J*, 27, 1907-18.
- BENTLEY, D. L. 2014. Coupling mRNA processing with transcription in time and space. *Nat Rev Genet*, 15, 163-75.
- BENTLEY, D. R., BALASUBRAMANIAN, S., SWERDLOW, H. P., SMITH, G. P., MILTON, J., BROWN, C. G., *et al.* 2008. Accurate whole human genome sequencing using reversible terminator chemistry. *Nature*, 456, 53-9.
- BEYER, A. L. & OSHEIM, Y. N. 1988. Splice site selection, rate of splicing, and alternative splicing on nascent transcripts. *Genes Dev*, 2, 754-65.
- BHATT, D. M., PANDYA-JONES, A., TONG, A. J., BAROZZI, I., LISSNER, M. M., NATOLI, G., *et al.* 2012. Transcript dynamics of proinflammatory genes revealed by sequence analysis of subcellular RNA fractions. *Cell*, 150, 279-90.
- BIRSE, C. E., LEE, B. A., HANSEN, K. & PROUDFOOT, N. J. 1997. Transcriptional termination signals for RNA polymerase II in fission yeast. *EMBO J*, 16, 3633-43.
- BJUR, E., LARSSON, O., YURCHENKO, E., ZHENG, L., GANDIN, V., TOPISIROVIC, I., *et al.* 2013. Distinct translational control in CD4⁺ T cell subsets. *PLoS Genet*, 9, e1003494.
- BLACKINTON, J. G. & KEENE, J. D. 2016. Functional coordination and HuR-mediated regulation of mRNA stability during T cell activation. *Nucleic Acids Res*, 44, 426-36.
- BLECHER-GONEN, R., BARNETT-ITZHAKI, Z., JAITIN, D., AMANN-ZALCENSTEIN, D., LARA-ASTIASO, D. & AMIT, I. 2013. High-throughput chromatin immunoprecipitation for genome-wide mapping of in vivo protein-DNA interactions and epigenomic states. *Nat Protoc*, 8, 539-54.
- BONFERT, T., KIRNER, E., CSABA, G., ZIMMER, R. & FRIEDEL, C. C. 2015. ContextMap 2: fast and accurate context-based RNA-seq mapping. *BMC Bioinformatics*, 16, 122.
- BONIFACE, K., BLUMENSCHNIG, W. M., BROVONT-PORTH, K., MCGEACHY, M. J., BASHAM, B., DESAI, B., *et al.* 2010. Human Th17 cells comprise heterogeneous subsets including IFN-gamma-producing cells with distinct properties from the Th1 lineage. *J Immunol*, 185, 679-87.

- BRONEVETSKY, Y., VILLARINO, A. V., EISLEY, C. J., BARBEAU, R., BARCZAK, A. J., HEINZ, G. A., *et al.* 2013. T cell activation induces proteasomal degradation of Argonaute and rapid remodeling of the microRNA repertoire. *J Exp Med*, 210, 417-32.
- BURATOWSKI, S. 2009. Progression through the RNA polymerase II CTD cycle. *Mol Cell*, 36, 541-6.
- BURGER, K., MUHL, B., KELLNER, M., ROHRMOSER, M., GRUBER-EBER, A., WINDHAGER, L., *et al.* 2013. 4-thiouridine inhibits rRNA synthesis and causes a nucleolar stress response. *RNA Biol*, 10, 1623-30.
- CAUDRON-HERGER, M., COOK, P. R., RIPPE, K. & PAPANTONIS, A. 2015. Dissecting the nascent human transcriptome by analysing the RNA content of transcription factories. *Nucleic Acids Res*, 43, e95.
- CHAN, P. K., QI, Y., AMLEY, J. & KOLLER, C. A. 1996. Quantitation of the nucleophosmin/B23-translocation using imaging analysis. *Cancer Lett*, 100, 191-7.
- CHANG, C. H., CURTIS, J. D., MAGGI, L. B., JR., FAUBERT, B., VILLARINO, A. V., O'SULLIVAN, D., *et al.* 2013. Posttranscriptional control of T cell effector function by aerobic glycolysis. *Cell*, 153, 1239-51.
- CHEN, E. Y., TAN, C. M., KOU, Y., DUAN, Q., WANG, Z., MEIRELLES, G. V., *et al.* 2013. Enrichr: interactive and collaborative HTML5 gene list enrichment analysis tool. *BMC Bioinformatics*, 14, 128.
- CHO, E. J., TAKAGI, T., MOORE, C. R. & BURATOWSKI, S. 1997. mRNA capping enzyme is recruited to the transcription complex by phosphorylation of the RNA polymerase II carboxy-terminal domain. *Genes Dev*, 11, 3319-26.
- CHOU, C., PINTO, A. K., CURTIS, J. D., PERSAUD, S. P., CELLA, M., LIN, C. C., *et al.* 2014. c-Myc-induced transcription factor AP4 is required for host protection mediated by CD8+ T cells. *Nat Immunol*, 15, 884-93.
- CHURCHMAN, L. S. & WEISSMAN, J. S. 2012. Native elongating transcript sequencing (NET-seq). *Curr Protoc Mol Biol*, Chapter 4, Unit 4 14 1-17.
- COOPER, G. M. & HAUSMAN, R. E. 2013. *The cell: a molecular approach*, Sunderland, Mass., Sinauer Associates.
- CORDEN, J. L. 1990. Tails of RNA polymerase II. *Trends Biochem Sci*, 15, 383-7.
- CORE, L. J. & LIS, J. T. 2008. Transcription regulation through promoter-proximal pausing of RNA polymerase II. *Science*, 319, 1791-2.
- CORE, L. J., WATERFALL, J. J. & LIS, J. T. 2008. Nascent RNA sequencing reveals widespread pausing and divergent initiation at human promoters. *Science*, 322, 1845-8.
- CRICK, F. 1970. Central dogma of molecular biology. *Nature*, 227, 561-3.
- CRICK, F. H. 1958. On protein synthesis. *Symp Soc Exp Biol*, 12, 138-63.
- DAHMUS, M. E. 1996. Reversible phosphorylation of the C-terminal domain of RNA polymerase II. *J Biol Chem*, 271, 19009-12.
- DAVARI, K., LICHTI, J., FRIEDEL, C. C. & GLASMACHER, E. in revision. Real-time analysis of transcription factor binding, transcription, translation and turnover to display global events during cellular activation. *J Vis Exp*.
- DAVARI, K., LICHTI, J., GALLUS, C., GREULICH, F., UHLENHAUT, N. H., HEINIG, M., *et al.* 2017. Rapid Genome-wide Recruitment of RNA Polymerase II Drives Transcription, Splicing, and Translation Events during T Cell Responses. *Cell Rep*, 19, 643-654.
- DJURETIC, I. M., LEVANON, D., NEGREANU, V., GRONER, Y., RAO, A. & ANSEL, K. M. 2007. Transcription factors T-bet and Runx3 cooperate to activate Ifng and silence Il4 in T helper type 1 cells. *Nat Immunol*, 8, 145-53.

- DOLKEN, L., RUZSICS, Z., RADLE, B., FRIEDEL, C. C., ZIMMER, R., MAGES, J., *et al.* 2008. High-resolution gene expression profiling for simultaneous kinetic parameter analysis of RNA synthesis and decay. *RNA*, 14, 1959-72.
- DRANOFF, G. 2004. Cytokines in cancer pathogenesis and cancer therapy. *Nat Rev Cancer*, 4, 11-22.
- EID, J., FEHR, A., GRAY, J., LUONG, K., LYLE, J., OTTO, G., *et al.* 2009. Real-time DNA sequencing from single polymerase molecules. *Science*, 323, 133-8.
- EISENBERG, E. & LEVANON, E. Y. 2013. Human housekeeping genes, revisited. *Trends Genet*, 29, 569-74.
- FOWLER, T., GARRUSS, A. S., GHOSH, A., DE, S., BECKER, K. G., WOOD, W. H., *et al.* 2015. Divergence of transcriptional landscape occurs early in B cell activation. *Epigenetics Chromatin*, 8, 20.
- FRIEDEL, C. C. & DOLKEN, L. 2009. Metabolic tagging and purification of nascent RNA: implications for transcriptomics. *Mol Biosyst*, 5, 1271-8.
- FU, M. & BLACKSHEAR, P. J. 2017. RNA-binding proteins in immune regulation: a focus on CCCH zinc finger proteins. *Nat Rev Immunol*, 17, 130-143.
- GALLOWAY, A., SAVELIEV, A., LUKASIAK, S., HODSON, D. J., BOLLAND, D., BALMANN, K., *et al.* 2016. RNA-binding proteins ZFP36L1 and ZFP36L2 promote cell quiescence. *Science*, 352, 453-9.
- GARCIA-MARTINEZ, J., ARANDA, A. & PEREZ-ORTIN, J. E. 2004. Genomic run-on evaluates transcription rates for all yeast genes and identifies gene regulatory mechanisms. *Mol Cell*, 15, 303-13.
- GILCHRIST, D. A., FROMM, G., DOS SANTOS, G., PHAM, L. N., MCDANIEL, I. E., BURKHOLDER, A., *et al.* 2012. Regulating the regulators: the pervasive effects of Pol II pausing on stimulus-responsive gene networks. *Genes Dev*, 26, 933-44.
- GILMOUR, D. S. & LIS, J. T. 1984. Detecting protein-DNA interactions in vivo: distribution of RNA polymerase on specific bacterial genes. *Proc Natl Acad Sci U S A*, 81, 4275-9.
- GORER, P. A. 1950. Studies in antibody response of mice to tumour inoculation. *Br J Cancer*, 4, 372-9.
- GREGORY, S. G., BARLOW, K. F., MCLAY, K. E., KAUL, R., SWARBRECK, D., DUNHAM, A., *et al.* 2006. The DNA sequence and biological annotation of human chromosome 1. *Nature*, 441, 315-21.
- GU, B., EICK, D. & BENSUAUDE, O. 2013. CTD serine-2 plays a critical role in splicing and termination factor recruitment to RNA polymerase II in vivo. *Nucleic Acids Res*, 41, 1591-603.
- GUENTHER, M. G., LEVINE, S. S., BOYER, L. A., JAENISCH, R. & YOUNG, R. A. 2007. A chromatin landmark and transcription initiation at most promoters in human cells. *Cell*, 130, 77-88.
- GUO, H., INGOLIA, N. T., WEISSMAN, J. S. & BARTEL, D. P. 2010. Mammalian microRNAs predominantly act to decrease target mRNA levels. *Nature*, 466, 835-40.
- HARGREAVES, D. C., HORNG, T. & MEDZHITOV, R. 2009. Control of inducible gene expression by signal-dependent transcriptional elongation. *Cell*, 138, 129-45.
- HASHIMOTO, S., TAKAHASHI, Y., TOMITA, Y., HAYAMA, T., SAWADA, S., HORIE, T., *et al.* 1991. Mechanism of calcium ionophore and phorbol ester-induced T-cell activation. Accessory cell requirement for T-cell activation. *Scand J Immunol*, 33, 393-403.
- HEGAZY, A. N., PEINE, M., HELMSTETTER, C., PANSE, I., FROHLICH, A., BERGTHALER, A., *et al.* 2010. Interferons direct Th2 cell reprogramming to generate a stable GATA-3(+)T-bet(+) cell subset with combined Th2 and Th1 cell functions. *Immunity*, 32, 116-28.

- HEINZ, S., BENNER, C., SPANN, N., BERTOLINO, E., LIN, Y. C., LASLO, P., *et al.* 2010. Simple combinations of lineage-determining transcription factors prime cis-regulatory elements required for macrophage and B cell identities. *Mol Cell*, 38, 576-89.
- HUANG DA, W., SHERMAN, B. T. & LEMPICKI, R. A. 2009. Systematic and integrative analysis of large gene lists using DAVID bioinformatics resources. *Nat Protoc*, 4, 44-57.
- HUBER, W., CAREY, V. J., GENTLEMAN, R., ANDERS, S., CARLSON, M., CARVALHO, B. S., *et al.* 2015. Orchestrating high-throughput genomic analysis with Bioconductor. *Nat Methods*, 12, 115-21.
- INGOLIA, N. T., BRAR, G. A., ROUSKIN, S., MCGEACHY, A. M. & WEISSMAN, J. S. 2012. The ribosome profiling strategy for monitoring translation in vivo by deep sequencing of ribosome-protected mRNA fragments. *Nat Protoc*, 7, 1534-50.
- INGOLIA, N. T., GHAEMMAGHAMI, S., NEWMAN, J. R. & WEISSMAN, J. S. 2009. Genome-wide analysis in vivo of translation with nucleotide resolution using ribosome profiling. *Science*, 324, 218-23.
- IWASAKI, H., TAKEUCHI, O., TERAGUCHI, S., MATSUSHITA, K., UEHATA, T., KUNIYOSHI, K., *et al.* 2011. The IkappaB kinase complex regulates the stability of cytokine-encoding mRNA induced by TLR-IL-1R by controlling degradation of regnase-1. *Nat Immunol*, 12, 1167-75.
- JANEWAY, C., TRAVERS, P., WALPORT, M. & SHLOMCHIK, M. 2005. *Immunobiology, the immune system in health and disease*, New York, NY [u.a.], Garland Science.
- JEKER, L. T. & BLUESTONE, J. A. 2013. MicroRNA regulation of T-cell differentiation and function. *Immunol Rev*, 253, 65-81.
- JELTSCH, K. M., HU, D., BRENNER, S., ZOLLER, J., HEINZ, G. A., NAGEL, D., *et al.* 2014. Cleavage of roquin and regnase-1 by the paracaspase MALT1 releases their cooperatively repressed targets to promote T(H)17 differentiation. *Nat Immunol*, 15, 1079-89.
- JOHNSON, D. S., MORTAZAVI, A., MYERS, R. M. & WOLD, B. 2007. Genome-wide mapping of in vivo protein-DNA interactions. *Science*, 316, 1497-502.
- JONAS, S. & IZAURRALDE, E. 2015. Towards a molecular understanding of microRNA-mediated gene silencing. *Nat Rev Genet*, 16, 421-33.
- JONKERS, I. & LIS, J. T. 2015. Getting up to speed with transcription elongation by RNA polymerase II. *Nat Rev Mol Cell Biol*, 16, 167-77.
- JOVANOVIĆ, M., ROONEY, M. S., MERTINS, P., PRZYBYLSKI, D., CHEVRIER, N., SATIJA, R., *et al.* 2015. Immunogenetics. Dynamic profiling of the protein life cycle in response to pathogens. *Science*, 347, 1259038.
- KENT, W. J., SUGNET, C. W., FUREY, T. S., ROSKIN, K. M., PRINGLE, T. H., ZAHLER, A. M., *et al.* 2002. The human genome browser at UCSC. *Genome Res*, 12, 996-1006.
- KENZELMANN, M., MAERTENS, S., HERGENHAHN, M., KUEFFER, S., HOTZ-WAGENBLATT, A., LI, L., *et al.* 2007. Microarray analysis of newly synthesized RNA in cells and animals. *Proc Natl Acad Sci U S A*, 104, 6164-9.
- KIM, S., KIM, H., FONG, N., ERICKSON, B. & BENTLEY, D. L. 2011. Pre-mRNA splicing is a determinant of histone H3K36 methylation. *Proc Natl Acad Sci U S A*, 108, 13564-9.
- KIMBALL, S. R. 1999. Eukaryotic initiation factor eIF2. *Int J Biochem Cell Biol*, 31, 25-9.
- KOMARNITSKY, P., CHO, E. J. & BURATOWSKI, S. 2000. Different phosphorylated forms of RNA polymerase II and associated mRNA processing factors during transcription. *Genes Dev*, 14, 2452-60.

- KONTOYIANNIS, D., PASPARAKIS, M., PIZARRO, T. T., COMINELLI, F. & KOLLIAS, G. 1999. Impaired on/off regulation of TNF biosynthesis in mice lacking TNF AU-rich elements: implications for joint and gut-associated immunopathologies. *Immunity*, 10, 387-98.
- KOUZINE, F., WOJTOWICZ, D., YAMANE, A., RESCH, W., KIEFFER-KWON, K. R., BUNDLE, R., *et al.* 2013. Global regulation of promoter melting in naive lymphocytes. *Cell*, 153, 988-99.
- KRISTENSEN, A. R., GSPONER, J. & FOSTER, L. J. 2013. Protein synthesis rate is the predominant regulator of protein expression during differentiation. *Mol Syst Biol*, 9, 689.
- KROGAN, N. J., KIM, M., TONG, A., GOLSHANI, A., CAGNEY, G., CANADIEN, V., *et al.* 2003. Methylation of histone H3 by Set2 in *Saccharomyces cerevisiae* is linked to transcriptional elongation by RNA polymerase II. *Mol Cell Biol*, 23, 4207-18.
- KURKI, S., PELTONEN, K., LATONEN, L., KIVIHARJU, T. M., OJALA, P. M., MEEK, D., *et al.* 2004. Nucleolar protein NPM interacts with HDM2 and protects tumor suppressor protein p53 from HDM2-mediated degradation. *Cancer Cell*, 5, 465-75.
- LACHMANN, A., XU, H., KRISHNAN, J., BERGER, S. I., MAZLOOM, A. R. & MA'AYAN, A. 2010. ChEA: transcription factor regulation inferred from integrating genome-wide ChIP-X experiments. *Bioinformatics*, 26, 2438-44.
- LAITY, J. H., LEE, B. M. & WRIGHT, P. E. 2001. Zinc finger proteins: new insights into structural and functional diversity. *Curr Opin Struct Biol*, 11, 39-46.
- LAZAREVIC, V., CHEN, X., SHIM, J. H., HWANG, E. S., JANG, E., BOLM, A. N., *et al.* 2011. T-bet represses T(H)17 differentiation by preventing Runx1-mediated activation of the gene encoding RORgammat. *Nat Immunol*, 12, 96-104.
- LAZAREVIC, V., GLIMCHER, L. H. & LORD, G. M. 2013. T-bet: a bridge between innate and adaptive immunity. *Nat Rev Immunol*, 13, 777-89.
- LECOEUR, H., LEDRU, E., PREVOST, M. C. & GOUGEON, M. L. 1997. Strategies for phenotyping apoptotic peripheral human lymphocytes comparing ISNT, annexin-V and 7-AAD cytofluorometric staining methods. *J Immunol Methods*, 209, 111-23.
- LEVIN, J. Z., YASSOUR, M., ADICONIS, X., NUSBAUM, C., THOMPSON, D. A., FRIEDMAN, N., *et al.* 2010. Comprehensive comparative analysis of strand-specific RNA sequencing methods. *Nat Methods*, 7, 709-15.
- LI, H. & DURBIN, R. 2009. Fast and accurate short read alignment with Burrows-Wheeler transform. *Bioinformatics*, 25, 1754-60.
- LI, J., MOAZED, D. & GYGI, S. P. 2002. Association of the histone methyltransferase Set2 with RNA polymerase II plays a role in transcription elongation. *J Biol Chem*, 277, 49383-8.
- LI, J. J., BICKEL, P. J. & BIGGIN, M. D. 2014. System wide analyses have underestimated protein abundances and the importance of transcription in mammals. *PeerJ*, 2, e270.
- LI, J. J. & BIGGIN, M. D. 2015. Gene expression. Statistics requantitates the central dogma. *Science*, 347, 1066-7.
- LICHTI, J., GALLUS, C. & GLASMACHER, E. in revision. Immune responses - transcriptional & post-transcriptional networks pass the baton. *Trends Biochem Sci*.
- LIN, C. Y., LOVEN, J., RAHL, P. B., PARANAL, R. M., BURGE, C. B., BRADNER, J. E., *et al.* 2012. Transcriptional amplification in tumor cells with elevated c-Myc. *Cell*, 151, 56-67.
- LIN, S., COUTINHO-MANSFIELD, G., WANG, D., PANDIT, S. & FU, X. D. 2008. The splicing factor SC35 has an active role in transcriptional elongation. *Nat Struct Mol Biol*, 15, 819-26.

- LIPSETT, M. N. 1965. The isolation of 4-thiouridylic acid from the soluble ribonucleic acid of *Escherichia coli*. *J Biol Chem*, 240, 3975-8.
- MAHONY, S. & PUGH, B. F. 2015. Protein-DNA binding in high-resolution. *Crit Rev Biochem Mol Biol*, 50, 269-83.
- MANLEY, J. L. & TACKE, R. 1996. SR proteins and splicing control. *Genes Dev*, 10, 1569-79.
- MARTIN, M. 2011. Cutadapt removes adapter sequences from high-throughput sequencing reads. *EMBnet.journal*, 17, 10-12.
- MAXAM, A. M. & GILBERT, W. 1977. A new method for sequencing DNA. *Proc Natl Acad Sci USA*, 74, 560-4.
- MELVIN, W. T., MILNE, H. B., SLATER, A. A., ALLEN, H. J. & KEIR, H. M. 1978. Incorporation of 6-thioguanosine and 4-thiouridine into RNA. Application to isolation of newly synthesised RNA by affinity chromatography. *Eur J Biochem*, 92, 373-9.
- MINO, T., MURAKAWA, Y., FUKAO, A., VANDENBON, A., WESSELS, H. H., ORI, D., *et al.* 2015. Regnase-1 and Roquin Regulate a Common Element in Inflammatory mRNAs by Spatiotemporally Distinct Mechanisms. *Cell*, 161, 1058-1073.
- MURPHY, K. M. & REINER, S. L. 2002. The lineage decisions of helper T cells. *Nat Rev Immunol*, 2, 933-44.
- NI, Z., SCHWARTZ, B. E., WERNER, J., SUAREZ, J. R. & LIS, J. T. 2004. Coordination of transcription, RNA processing, and surveillance by P-TEFb kinase on heat shock genes. *Mol Cell*, 13, 55-65.
- NIE, Z., HU, G., WEI, G., CUI, K., YAMANE, A., RESCH, W., *et al.* 2012. c-Myc is a universal amplifier of expressed genes in lymphocytes and embryonic stem cells. *Cell*, 151, 68-79.
- O'SHEA, J. J. & PAUL, W. E. 2010. Mechanisms underlying lineage commitment and plasticity of helper CD4⁺ T cells. *Science*, 327, 1098-102.
- OZSOLAK, F., PLATT, A. R., JONES, D. R., REIFENBERGER, J. G., SASS, L. E., MCINERNEY, P., *et al.* 2009. Direct RNA sequencing. *Nature*, 461, 814-8.
- PANDYA-JONES, A., BHATT, D. M., LIN, C. H., TONG, A. J., SMALE, S. T. & BLACK, D. L. 2013. Splicing kinetics and transcript release from the chromatin compartment limit the rate of Lipid A-induced gene expression. *RNA*, 19, 811-27.
- PENG, J., ZHU, Y., MILTON, J. T. & PRICE, D. H. 1998. Identification of multiple cyclin subunits of human P-TEFb. *Genes Dev*, 12, 755-62.
- PENG, M., YIN, N., CHHANGAWALA, S., XU, K., LESLIE, C. S. & LI, M. O. 2016. Aerobic glycolysis promotes T helper 1 cell differentiation through an epigenetic mechanism. *Science*, 354, 481-484.
- PETERLIN, B. M. & PRICE, D. H. 2006. Controlling the elongation phase of transcription with P-TEFb. *Mol Cell*, 23, 297-305.
- PICCIRILLO, C. A., BJUR, E., TOPISIROVIC, I., SONENBERG, N. & LARSSON, O. 2014. Translational control of immune responses: from transcripts to translomes. *Nat Immunol*, 15, 503-11.
- RABANI, M., LEVIN, J. Z., FAN, L., ADICONIS, X., RAYCHOWDHURY, R., GARBER, M., *et al.* 2011. Metabolic labeling of RNA uncovers principles of RNA production and degradation dynamics in mammalian cells. *Nat Biotechnol*, 29, 436-42.
- RABANI, M., RAYCHOWDHURY, R., JOVANOVIC, M., ROONEY, M., STUMPO, D. J., PAULI, A., *et al.* 2014. High-resolution sequencing and modeling identifies distinct dynamic RNA regulatory strategies. *Cell*, 159, 1698-710.
- RADLE, B., RUTKOWSKI, A. J., RUZSICS, Z., FRIEDEL, C. C., KOSZINOWSKI, U. H. & DOLKEN, L. 2013. Metabolic labeling of newly transcribed RNA for high resolution

- gene expression profiling of RNA synthesis, processing and decay in cell culture. *J Vis Exp*.
- RAHL, P. B., LIN, C. Y., SEILA, A. C., FLYNN, R. A., MCCUINE, S., BURGE, C. B., *et al.* 2010. c-Myc regulates transcriptional pause release. *Cell*, 141, 432-45.
- RAMIREZ-CARROZZI, V. R., BRAAS, D., BHATT, D. M., CHENG, C. S., HONG, C., DOTY, K. R., *et al.* 2009. A unifying model for the selective regulation of inducible transcription by CpG islands and nucleosome remodeling. *Cell*, 138, 114-28.
- REINER, S. L. & LOCKSLEY, R. M. 1995. The regulation of immunity to *Leishmania major*. *Annu Rev Immunol*, 13, 151-77.
- REN, B., ROBERT, F., WYRICK, J. J., APARICIO, O., JENNINGS, E. G., SIMON, I., *et al.* 2000. Genome-wide location and function of DNA binding proteins. *Science*, 290, 2306-9.
- ROBINSON, J. T., THORVALDSDOTTIR, H., WINCKLER, W., GUTTMAN, M., LANDER, E. S., GETZ, G., *et al.* 2011. Integrative genomics viewer. *Nat Biotechnol*, 29, 24-6.
- ROTHBERG, J. M., HINZ, W., REARICK, T. M., SCHULTZ, J., MILESKI, W., DAVEY, M., *et al.* 2011. An integrated semiconductor device enabling non-optical genome sequencing. *Nature*, 475, 348-52.
- SALDI, T., CORTAZAR, M. A., SHERIDAN, R. M. & BENTLEY, D. L. 2016. Coupling of RNA Polymerase II Transcription Elongation with Pre-mRNA Splicing. *J Mol Biol*, 428, 2623-2635.
- SANDBERG, R., NEILSON, J. R., SARMA, A., SHARP, P. A. & BURGE, C. B. 2008. Proliferating cells express mRNAs with shortened 3' untranslated regions and fewer microRNA target sites. *Science*, 320, 1643-7.
- SANGER, F., NICKLEN, S. & COULSON, A. R. 1977. DNA sequencing with chain-terminating inhibitors. *Proc Natl Acad Sci U S A*, 74, 5463-7.
- SCHAUB, A. & GLASMACHER, E. 2017. Splicing in immune cells-mechanistic insights and emerging topics. *Int Immunol*, 29, 173-181.
- SCHEU, S., STETSON, D. B., REINHARDT, R. L., LEBER, J. H., MOHRS, M. & LOCKSLEY, R. M. 2006. Activation of the integrated stress response during T helper cell differentiation. *Nat Immunol*, 7, 644-51.
- SCHMID, I., UITTENBOGAART, C. H. & GIORGI, J. V. 1994. Sensitive method for measuring apoptosis and cell surface phenotype in human thymocytes by flow cytometry. *Cytometry*, 15, 12-20.
- SCHNEIDER-POETSCH, T., JU, J., EYLER, D. E., DANG, Y., BHAT, S., MERRICK, W. C., *et al.* 2010. Inhibition of eukaryotic translation elongation by cycloheximide and lactimidomycin. *Nat Chem Biol*, 6, 209-217.
- SCHOTT, J., REITTER, S., PHILIPP, J., HANEKE, K., SCHAFER, H. & STOECKLIN, G. 2014. Translational regulation of specific mRNAs controls feedback inhibition and survival during macrophage activation. *PLoS Genet*, 10, e1004368.
- SCHROEDER, A., MUELLER, O., STOCKER, S., SALOWSKY, R., LEIBER, M., GASSMANN, M., *et al.* 2006. The RIN: an RNA integrity number for assigning integrity values to RNA measurements. *BMC Mol Biol*, 7, 3.
- SCHWALB, B., MICHEL, M., ZACHER, B., FRUHAUF, K., DEMEL, C., TRESCH, A., *et al.* 2016. TT-seq maps the human transient transcriptome. *Science*, 352, 1225-8.
- SCHWANHAUSSER, B., BUSSE, D., LI, N., DITTMAR, G., SCHUCHHARDT, J., WOLF, J., *et al.* 2011. Global quantification of mammalian gene expression control. *Nature*, 473, 337-42.
- SCHWANHAUSSER, B., BUSSE, D., LI, N., DITTMAR, G., SCHUCHHARDT, J., WOLF, J., *et al.* 2013. Corrigendum: Global quantification of mammalian gene expression control. *Nature*, 495, 126-7.

- SEN, R. & FUGMANN, S. D. 2012. Transcription, splicing, and release: are we there yet? *Cell*, 150, 241-3.
- SINGH, H. 2009. Teeing up transcription on CpG islands. *Cell*, 138, 14-6.
- SULTAN, M., SCHULZ, M. H., RICHARD, H., MAGEN, A., KLINGENHOFF, A., SCHERF, M., *et al.* 2008. A global view of gene activity and alternative splicing by deep sequencing of the human transcriptome. *Science*, 321, 956-60.
- SZABO, S. J., KIM, S. T., COSTA, G. L., ZHANG, X., FATHMAN, C. G. & GLIMCHER, L. H. 2000. A novel transcription factor, T-bet, directs Th1 lineage commitment. *Cell*, 100, 655-69.
- TARN, W. Y. & STEITZ, J. A. 1997. Pre-mRNA splicing: the discovery of a new spliceosome doubles the challenge. *Trends Biochem Sci*, 22, 132-7.
- TCHEN, C. R., BROOK, M., SAKLATVALA, J. & CLARK, A. R. 2004. The stability of tristetraprolin mRNA is regulated by mitogen-activated protein kinase p38 and by tristetraprolin itself. *J Biol Chem*, 279, 32393-400.
- TEAM, R. D. C. 2016. R: A Language and Environment for Statistical Computing. *Vienna, Austria : the R Foundation for Statistical Computing*.
- TEBALDI, T., RE, A., VIERO, G., PEGORETTI, I., PASSERINI, A., BLANZIERI, E., *et al.* 2012. Widespread uncoupling between transcriptome and translatoome variations after a stimulus in mammalian cells. *BMC Genomics*, 13, 220.
- THASTRUP, O., CULLEN, P. J., DROBAK, B. K., HANLEY, M. R. & DAWSON, A. P. 1990. Thapsigargin, a tumor promoter, discharges intracellular Ca²⁺ stores by specific inhibition of the endoplasmic reticulum Ca²⁺(+)-ATPase. *Proc Natl Acad Sci U S A*, 87, 2466-70.
- THIERFELDER, W. E., VAN DEURSEN, J. M., YAMAMOTO, K., TRIPP, R. A., SARAWAR, S. R., CARSON, R. T., *et al.* 1996. Requirement for Stat4 in interleukin-12-mediated responses of natural killer and T cells. *Nature*, 382, 171-4.
- THIEU, V. T., YU, Q., CHANG, H. C., YEH, N., NGUYEN, E. T., SEHRA, S., *et al.* 2008. Signal transducer and activator of transcription 4 is required for the transcription factor T-bet to promote T helper 1 cell-fate determination. *Immunity*, 29, 679-90.
- TRAPNELL, C., PACHTER, L. & SALZBERG, S. L. 2009. TopHat: discovering splice junctions with RNA-Seq. *Bioinformatics*, 25, 1105-11.
- WANG, Z., GERSTEIN, M. & SNYDER, M. 2009. RNA-Seq: a revolutionary tool for transcriptomics. *Nat Rev Genet*, 10, 57-63.
- WINDHAGER, L., BONFERT, T., BURGER, K., RUZSICS, Z., KREBS, S., KAUFMANN, S., *et al.* 2012. Ultrashort and progressive 4sU-tagging reveals key characteristics of RNA processing at nucleotide resolution. *Genome Res*, 22, 2031-42.
- ZAMORE, P. D. & GREEN, M. R. 1991. Biochemical characterization of U2 snRNP auxiliary factor: an essential pre-mRNA splicing factor with a novel intranuclear distribution. *EMBO J*, 10, 207-14.
- ZHANG, J. & CORDEN, J. L. 1991. Identification of phosphorylation sites in the repetitive carboxyl-terminal domain of the mouse RNA polymerase II largest subunit. *J Biol Chem*, 266, 2290-6.
- ZHANG, Y., LIU, T., MEYER, C. A., ECKHOUTE, J., JOHNSON, D. S., BERNSTEIN, B. E., *et al.* 2008. Model-based analysis of ChIP-Seq (MACS). *Genome Biol*, 9, R137.
- ZIMMERMANN, M. & MEYER, N. 2011. Annexin V/7-AAD staining in keratinocytes. *Methods Mol Biol*, 740, 57-63.

9 Supplements

9.1 List of tables

Table 1 Anti-mouse antibodies and cytokines for T cell differentiation	20
Table 2 Western Blot antibodies	20
Table 3 ChIP antibodies	20
Table 4 FACS antibodies	21
Table 5 Primers for detection of gene expression	21
Table 6 Primers for splicing	21
Table 7 Primers for detection of downregulated genes	22
Table 8 Primers for ChIP	22
Table 9 Chemicals	23
Table 10 Kits	24
Table 11 Composition of buffers, solutions and media	25
Table 12 Devices	27
Table 13 Software	27

9.2 List of figures

Figure 1: The innate and adaptive immune response (modified from Dranoff, 2004)	7
Figure 2: The central dogma of molecular biology (from today's view)	10
Figure 3: Work-flow for 4sU-labeling	15
Figure 4: Work flow for Ribosome Profiling	17
Figure 5: Verification of optimal 4sU-labeling conditions without perturbing cell physiology (Lichti, Davari <i>et al.</i> , 2017)	44
Figure 6: RNA integrity of 4sU labeled RNA (Lichti, Davari <i>et al.</i> , in revision)	46
Figure 7: Recovery of <i>Hprt</i> and <i>18S rRNA</i> in newly transcribed RNA samples	47
Figure 8: Differences in exonic/intronic rate and mapping statistics for sequenced samples ..	48
Figure 9: PAGE purification of RPFs	49
Figure 10: Amplified Ribosome Profiling library	49
Figure 11: Mapped reads for <i>Ifng</i> of the preliminary test	50
Figure 12: Experimental setup (Lichti, Davari <i>et al.</i> , 2017)	51
Figure 13: Replicates are highly correlated (Lichti, Davari <i>et al.</i> , 2017)	52
Figure 14: Analysis of <i>Ifng</i> expression over time (Lichti, Davari <i>et al.</i> , 2017)	53
Figure 15: Most upregulated genes (Top 15)	54
Figure 16: Gene regulation differs in speed and magnitude for up- and downregulated genes	55
Figure 17: Validation of downregulated genes via GFP plasmid (Lichti, Davari <i>et al.</i> , 2017) ..	56
Figure 18: Gene response for upregulated genes differ in time and magnitude on the transcriptional and translational level (Lichti, Davari <i>et al.</i> , 2017)	57
Figure 19: Gene response for downregulated genes differs in time and magnitude on the transcriptional and translational level (in part from Lichti, Davari <i>et al.</i> , 2017)	58
Figure 20: Global correlation analysis shows highly coupled changes in transcription and translation (Lichti, Davari <i>et al.</i> , 2017)	59
Figure 21: Changes in translation are mainly determined by changes in total RNA (Lichti, Davari <i>et al.</i> , 2017)	60
Figure 22: Turnover rates determine correlation between transcription and translation (Lichti, Davari <i>et al.</i> , 2017)	61
Figure 23: Functional characteristics of gene groups with different turnover rates	62
Figure 24: Global translation rates do not change (Lichti, Davari <i>et al.</i> , 2017)	63
Figure 25: Increased expression of the translational but not of the transcriptional machinery (Lichti, Davari <i>et al.</i> , 2017)	64
Figure 26: Enriched transcription factor targets (modified from Lichti, Davari <i>et al.</i> , 2017) ..	65
Figure 27: c-Myc is a main regulator of transcriptional upregulation (Lichti, Davari <i>et al.</i> , 2017)	66
Figure 28: Global reduction in cotranscriptional splicing rates (Lichti, Davari <i>et al.</i> , 2017) ..	67
Figure 29: Global reduction in cotranscriptional splicing is not induced by an initial increase in 4sU RNA (Lichti, Davari <i>et al.</i> , 2017)	67

Figure 30: Strong correlation between <i>de novo</i> transcription and RNAPII (Lichti, Davari <i>et al.</i> , 2017)	68
Figure 31: RNAPII of <i>Ifng</i> and correlation of cluster 5 genes with <i>de novo</i> transcription (Lichti, Davari <i>et al.</i> , 2017)	69
Figure 32: 4sU RNA and RNAPII are well correlated for upregulated genes at 0 h.....	70
Figure 33: Paused RNAPII is not the key mechanism for transcriptional upregulation (Lichti, Davari <i>et al.</i> , 2017)	71
Figure 34 Purity of subcellular fractionation is confirmed by Western Blot (Lichti, Davari <i>et al.</i> , 2017)	72
Figure 35: Reduction in cotranscriptional splicing for polyadenylated RNA (Lichti, Davari <i>et al.</i> , 2017)	73
Figure 36: RNAPII phosphorylation states change over time (Lichti, Davari <i>et al.</i> , 2017)	74
Figure 37: Splicing indices relative to distance to TSS (Lichti, Davari <i>et al.</i> , 2017)	74
Figure 38: Ser2 phosphorylation of RNAPII mediates recruitment of splicing factors and is activated by pTEFb (Lichti, Davari <i>et al.</i> , 2017)	76
Figure 39: H3K36me3 marks expressed genes (Lichti, Davari <i>et al.</i> , 2017).....	76
Figure 40: H3K36me3 does not correlate with changes in gene expression (Lichti, Davari <i>et al.</i> , 2017)	77
Figure 41: Alternating functional programs in immune cells (modified from Lichti <i>et al.</i>) ...	89

9.3 List of abbreviations

4sU	4-thiouridine
7-AAD.....	7-aminoactinomycine D
APC.....	antigen-presenting cell
AREs.....	AU-rich elements
BCR.....	B cell receptor
CD4.....	cluster of differentiation
CDK.....	cyclin-dependent kinase
ChIP.....	chromatin immunoprecipitation
CTD.....	carboxy-terminal domain
DTT.....	dithiothreitol
eIF2 α	eukaryotic translation initiation factor 2 α
ER.....	endoplasmic reticulum
FBS.....	fetal bovine serum
FPKM.....	fragments per kilobase of transcript per million mapped reads
GAPDH.....	glyceraldehyde-3-phosphate dehydrogenase
GFP.....	green fluorescent protein
GO.....	gene ontology
GRO-seq.....	global run-on sequencing
IEG.....	immediate early gene
IFN.....	interferon
IGV.....	integrative genomics viewer
JoVE.....	Journal of Visualized Experiments
Lowess.....	Locally weighted scatterplot smoothing
LPS.....	lipopolysaccharide
MHCII.....	major histocompatibility complex II
miRNAs.....	Micro RNAs
mRNA.....	messenger RNA
NET-seq.....	native elongating transcript sequencing
NKT cell.....	natural killer T cell
OVA.....	ovalbumin

PAMPs	pathogen associated molecular patterns
PBS	phosphate-buffered saline
PFA	paraformaldehyde
PIR	protein information resource
PLG	phase lock gel
PMA	phorbol myristate acetate
PRG	primary response gene
PRR	pattern recognition receptor
PS	phosphatidylserine
pTEFb	positive transcriptional elongation factor b
PVDF	polyvinylidene fluoride
RIN	RNA integrity number
RNA	ribonucleic acid
RNAPII	RNA polymerase II
RP	ribosome profiling
RPF	ribosome protected fragment
rRNA	ribosomal RNA
RT	room temperature
snRNP	small nuclear ribonucleoprotein
SP-PIR	Swiss-Prot protein information resource
SPRI	solid phase reversible immobilization
STAT	signal transducer and activator of transcription
T-bet	T-box transcription factor
TCR	T-cell receptor
TF	transcription factor
Tfh	follicular T helper
Th cell	T helper cell
Th1	type 1 helper
TIBS	Trends in Biochemical Sciences
TSS	transcriptional start site
TTP	tristetraprolin
TT-seq	transient transcriptome sequencing

10 Publications

Data and figures of the present dissertation were in part published in the following publications. The accession numbers for the 4sU-seq, total RNA-seq and RP data reported in chapter 4.2 is GEO: GSE83351 and for ChIP-seq data reported in chapter 4.3 is GEO: GSE94698.

LICHTI, J.[#], DAVARI, K.[#], GALLUS, C., GREULICH, F., UHLENHAUT, N. H., HEINIG, M., FRIEDEL, C. C., GLASMACHER, E. “Rapid Genome-wide Recruitment of RNA Polymerase II Drives Transcription, Splicing, and Translation Events during T Cell Responses”. *Cell Rep* (2017), 19, 643-654.

[#] authors contributed equally

LICHTI, J.[#], DAVARI, K.[#], FRIEDEL, C. C. & GLASMACHER, E. “Real-time analysis of transcription factor binding, transcription, translation and turnover to display global events during cellular activation”. *J Vis Exp* (in review)

[#] authors contributed equally

LICHTI, J., GALLUS, C. & GLASMACHER, E. “Immune responses - transcriptional & post-transcriptional networks pass the baton”. *Trends Biochem Sci* (in review)

11 Erklärung

Ich erkläre an Eides statt, dass ich die bei der Fakultät für Medizin der TUM zur Promotionsprüfung vorgelegte Arbeit mit dem Titel *Global gene regulation in immune cells* am HelmholtzZentrum München, Institut for Diabetes and Obesity unter der Anleitung und Betreuung durch Dr. Elke Glasmacher ohne sonstige Hilfe erstellt und bei der Abfassung nur die gemäß § 6 Abs. 6 und 7 Satz 2 angegebenen Hilfsmittel benutzt habe.

Ich habe keine Organisation eingeschaltet, die gegen Entgelt Betreuerinnen und Betreuer für die Anfertigung von Dissertationen sucht, oder die mir obliegenden Pflichten hinsichtlich der Prüfungsleistungen für mich ganz oder teilweise erledigt.

Ich habe die Dissertation in dieser oder ähnlicher Form in keinem anderen Prüfungsverfahren als Prüfungsleistung vorgelegt.

Die vollständige Dissertation wurde in _____ veröffentlicht. Die promotionsführende Einrichtung _____ hat der Vorveröffentlichung zugestimmt.

Ich habe den angestrebten Doktorgrad noch nicht erworben und bin nicht in einem früheren Promotionsverfahren für den angestrebten Doktorgrad endgültig gescheitert.

Ich habe bereits am
bei der Fakultät für
der Hochschule
unter Vorlage einer Dissertation mit dem Thema
die Zulassung zur Promotion beantragt mit dem Ergebnis:

Die öffentlich zugängliche Promotionsordnung der TUM ist mir bekannt, insbesondere habe ich die Bedeutung von § 28 (Nichtigkeit der Promotion) und § 29 (Entzug des Doktorgrades) zur Kenntnis genommen. Ich bin mir der Konsequenzen einer falschen Eidesstattlichen Erklärung bewusst.

Mit der Aufnahme meiner personenbezogenen Daten in die Alumni-Datei bei der TUM bin ich

einverstanden, nicht einverstanden.

Ort, Datum

Johannes Lichti

12 Lebenslauf

Ausbildung

Seit 02/2014	<p>Promotion</p> <p>HelmholtzZentrum München - Garching, Deutschland</p> <p>Institut für Diabetes und Adipositas; AG Molekulare Immunologie</p> <p>Techniken: molekulare Methoden, Zellkultur, NGS, RNA-Arbeit</p>
05/2012 – 05/2013	<p>Diplomarbeit</p> <p>Technische Universität Wien, Österreich</p> <p>Institut für Verfahrenstechnik, Umwelttechnik und Biowissenschaften; AG Gentechnik</p> <p>Titel: „Identification of <i>cis</i>-elements in the <i>cbh1</i> promoter of <i>Trichoderma reesei</i>“</p> <p>Techniken: <i>in vivo</i> footprinting, PCR, Kultivierung</p> <p>Note: 1,0</p>
10/2010 – 05/2013	<p>Masterstudium Technische Chemie – Biotechnologie und Bioanalytik</p> <p>Technische Universität Wien, Österreich</p> <p>Prüfungsfächer: Molekularbiologie und Genetik (Hauptfach) Umweltchemie (Nebenfach) Phytochemie (Nebenfach) Notenschnitt: 1,4</p>
10/2007 – 10/2010	<p>Bachelor of Science Ernährungswissenschaften</p> <p>Universität Wien, Österreich</p> <p>Titel der Arbeit: Nutritive Einflussfaktoren auf den Fettsäurestoffwechsel im Ausdauersportbereich</p> <p>Institut für medizinische Chemie, Universität Wien</p>
09/1997 – 06/2006	<p>Allgemeine Hochschulreife</p> <p>Franz-Marc-Gymnasium, Markt Schwaben, Deutschland</p>
09/1992 – 07/1996	<p>Grundschule, Markt Schwaben, Deutschland</p>